C.C.W. van der Post

Building a sample chamber for measuring the reflectivity and transparency of detector materials at VUV wavelengths

TU Delft

Building a sample chamber for measuring the reflectivity and transparency of detector materials at VUV wavelengths

By

C.C.W. van der Post

in partial fulfilment of the requirements for the degree of

Master of Science

in Applied Physics

at the Delft University of Technology,
to be defended publicly on **April 28th, 2022**

Supervisor:	dr. ir. T. Pollmann	NIKHEF
Thesis committee:	dr. ir. D. Schaart	TU Delft
	dr. E. van der Kolk	TU Delft
	dr. ir. H. Schut	TU Delft

TU Delft

Preface

A wonderful experimental setup is being built at NIKHEF to characterize the optical properties in the vacuum ultraviolet region, of liquid xenon dark matter detector materials. I was able to partially design and build this setup from the ground up.

And with my background in applied physics, physics for instrumentation, the project was a perfect fit. I was able to both investigate the theoretical background and do literature research, as well as hands on build the experiment and solder cables together. The practical nature of this project made that I enjoyed the whole journey.

my hope is that my findings building this experimental setup in the vacuum ultraviolet region help future projects in the field, so they do not need to make the same mistakes I did and have some designs on which they can build the next generation of detectors.

I am very grateful to Dr. Tina Pollmann and Dr. Dennis Schaart for supervising me the way they did. Where I had space to explore and test my abilities, with the right questions at the right time to put me back on track when I would deviate to much in my process.

Also, I would like to thank the members of the VUV group, Marjolein Nuland-Troost, Vikas Gupta and Emily Brooks for helping me. They were helping me with programming software and assembling the experiments. But also, were willing to help me writing by giving feedback on the thesis.

Lastly, I would like to thank Marrit Beijloos who endured all the emotions of setbacks as well as euphoric moments. You were there when I needed an emotional outlet.

C.C.W. van der Post
Amsterdam, April 2022

Abstract

The Vacuum Ultraviolet experiment is built at NIKHEF to support the larger experiments in their search for dark matter. This support consists of research into the optical properties of detector materials. By building an optical characterization experiment for scintillation light in the VUV region. Getting a better understanding of what is happing inside the detector and how the materials behave, can be used as an advantage to the measurement and eventually lead to the next generation of detectors. During my time at NIKHEF I partially designed, fully build, and commissioned parts of the experiment. The design part consists mostly of holders for samples of detector materials and sensors, as well as support for the experiment itself. The built part involves the assembly of all the parts to their correct specifications and improve parts of the design when components are not compatible. Parts one can think of is a deuterium lamp which will generate the spectrum in the vacuum Ultraviolet region of $178\,[\mathrm{nm}]$, the monochromator which will filter the spectrum to one specific wavelength in the spectrum, and a sample chamber where samples of detector materials will be placed for measurements. Lastly, the commissioning where all the different components are tested on their function and if designed and fabricated parts work as needed. Most important will be the quality of the vacuum and the ability to send a measurable signal across the vacuum border.

Contents

1 Introduction

1.1 Dark matter

1.1.1 The presumption of dark matter existence

Dark matter, the elusive particle that has taunted scientists since 1933. In 1933 Fritz Zwicky found a disparity between what he saw and what he calculated. When calculating the mass of galaxies in the Coma cluster. Using the Virial theorem, which states that the potential energy over time is equal to the kinetic energy of a self-gravitating system, to calculate apparent velocities. From these apparent velocities he found a mass for the cluster. However, this calculated mass was much higher than the mass inferred by the luminosity of the Coma cluster. He therefore hypostasized the existence of non-luminous matter [1].

Years later, in 1978, Vera Rubin et al. measured again evidence for the existence of non-luminous matter. While studying the rotation velocity in the Andromeda Galaxy with some reasonable simplifications the group of Rubin could determine the mass distribution of the galaxy. Comparing these calculations to their spectroscopic observations did not give the same result.

Due to the inconsistency between observed and calculated velocities Rubins group proposed, an increasing distribution of mass which is proportional to the galaxy radius and consists of non-luminous matter located in a halo surrounding the galaxy [2].

The evidence supporting the existence of non-luminous matter, which we now believe is mostly Dark Matter, becomes more serious when gravitational lensing is used. Gravitational lensing is predicted by Albert Einstein and is an effect where the light deviates from its direct course due to a massive object's presence. In practise this means the image of a deep space object will be deformed when looked at it with a massive object in between, see Figure 1-1.

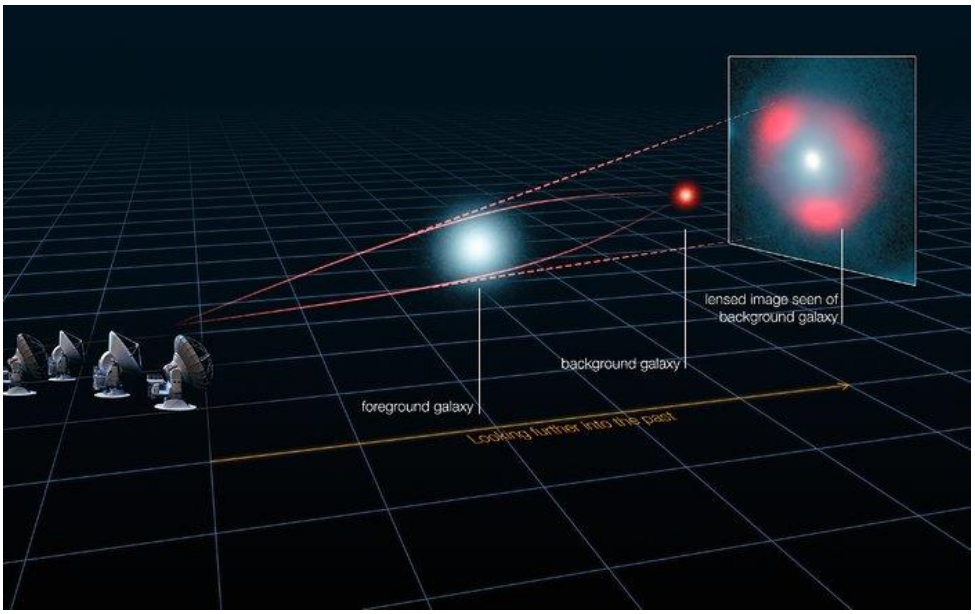

Figure 1-1: This schematic image represents how light from a distant galaxy is distorted by the gravitational effects of a nearer foreground galaxy, which acts like a lens and makes the distant source appear distorted [3].

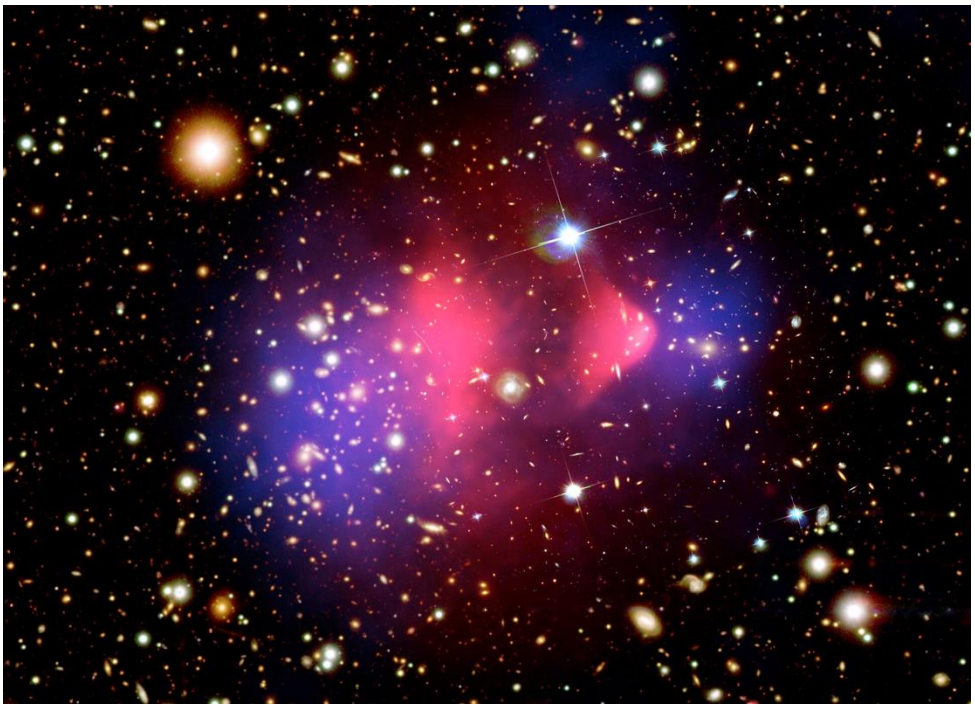

Figure 1-2: Image of the Bullet cluster (1E 0657-56). The optical image is from the Magellan and Hubble Space Telescope. The normal matter is shown by the Chandra X-ray image (pink). Gravitational lensing reveals the mass of the cluster is dominated by dark matter (blue) [4].

The gravitational lensing was used on the bullet galaxy cluster, see Figure 1-2. The cluster is divided up in two clear regions, the normal matter which is detected using X-ray shown in pink, and dark matter detected using the gravitational lensing shown in blue. The division of mass could not be explained by Newtonian gravity [5]. Therefore, this is evidence supporting the existence of Dark Matter.

Studies into the universe and its geometry have been done since men looked up into the sky. In 1964 two astronomers Arno Penzias and Robert Wilson a type of background radiation known today as the cosmic microwave background radiation (CMB) and is one of the most powerful ways of studying the universe. Using the light of CMB we can look back in time to 380.000 years after the Big Bang. This light contains traces of information about the beginning of the universe, which helps us understand the history [6].

Multiple telescopes and satellites are used to analyse the CMB, one of which is the satellite Planck. The data collected by Planck shows from all the matter in the universe 84% is dark matter, and 26% of everything we have in the universe is dark matter [7].

1.1.2 Dark matter candidates

Since the idea of dark matter made its entrance into the scientific community, different hypotheses, and ideas about what this dark matter would look like were made. There are ideas of baryonic dark matter as well as non-baryonic dark matter, in this thesis we will focus on the non-baryonic candidates. Some observational evidence has already set some of the properties of dark matter. It must be dense and massive, otherwise it would not explain the missing mass in galaxies. Dark matter must be non-relativistic, sometimes called cold, and does not possess any electrical, or colour charge. Furthermore, if dark matter is around since the early universe, it must be stable, non-luminous, and only gravitational and weakly interaction with a small interaction cross-section.

Among these candidates we have Standard model neutrinos, a particle which has been known to exist. But unfortunately, it exists not abundantly enough to be a candidate for dark matter. Sterile neutrinos, a candidate because of its cosmological abundance. But still a hypothetical particle where being dark matter could be ruled out due to their light mass. Axions, a strong candidate it is very light, has weak interaction with normal matter and therefore not in equilibrium with the early universe. Their existence is based on assumptions regarding the production mechanism. Nevertheless, it has an acceptable range where it supports the constraints. WIMPs (**W**eakly **I**nteractive **M**assive **P**articles) this is also a strong candidate which has become experimentally motivated. The idea is a particle with a mass of a few GeV which can interact with very dense particles [7]. From these candidates the focus lies mostly on the WIMP because it is the candidate looked for by the experiments the VUV experiment will support.

1.1.3 Detection of dark matter

1.1.3.1 *Indirect detection*

With indirect detection the search for dark matter is based around the self-annihilation of dark matter particles into particles from the Standard Model. When events with missing transferred momentum and energy are observed this could infer the presence of a dark matter particle. There are two ways of this indirect detection, the first being accelerators and looking at particle collisions, second is looking at the gravitational accumulation of dark matter particles in astrophysical objects. Such objects can be stars, galaxies, and even our Sun.

The search for indirect signals has some favourable sources such as, the galactic centre and halo, close galaxy cluster, or dwarf galaxies. An increased dark matter density in said favourable sources, enhanced self-annihilation, scattering and decay into standard model particles, can therefore produce and measurable particle flux [8].

When these processes take place in our Sun, Earth base detectors such as SuperKamiokande [9] and AMANDA [10]. Further stars and galaxies will be studied with telescopes such as AMS [11], CELESTE [12] and PAMELA [13].

1.1.3.2 *Direct detection*

The basis of all the direct detection experiments is identifying nuclear recoils by the collision between dark matter and a detector's target nuclei. These collisions are elastic scattering, and if WIMPs with masses of $(10-1000)\,[\mathrm{Gev/c^2}]$ elastically scatter it would produce nuclear recoils in the range of $(1-100)\,[\mathrm{keV}]$ [14]. Unambiguously identifying such low-energy interaction requires a detailed knowledge on signal signature, particle physics and nuclear physics modelling.

Dark matter interactions result in a differential recoil spectrum written in equation (1).

$$\frac{dR}{dE}(E,t) = \frac{\rho_0}{m_\chi \cdot m_A} \cdot \int v \cdot f(\overline{\boldsymbol{v}},t) \cdot \frac{d\sigma}{dE}(E,v)\, d^3v \qquad (1)$$

Where the dark matter mass is given by m_χ and $\frac{d\sigma}{dE}(E,v)$ the differential cross-section. The WIMP cross-section σ and m_χ are the two parameters observed in a dark matter experiment. v is the dark matter velocity defined in the rest frame of the detector and the mass of the nucleus is given by m_A. Local dark matter density is ρ_0 and the WIMP velocity distribution in the detectors reference frame is $f(\overline{\boldsymbol{v}},t)$. Based on equation (1) detection strategies can exploit the energy, time, or direction dependencies of the signal.

The energy of a nuclear recoil can be converted to three different particles, Photons (scintillation), Electrons (ionization), and Phonons (heat). Unfortunately, these are not the only particles in the detector, in the case of WIMP detection $\alpha, \beta\ or\ \gamma$ particles also scatter on the target nuclei leaving electric recoil. To discriminate sufficiently between electric and nuclear recoil two signals are recorded, the first process is excitation leading to scintillation, the second is ionization, see Figure 1-4.

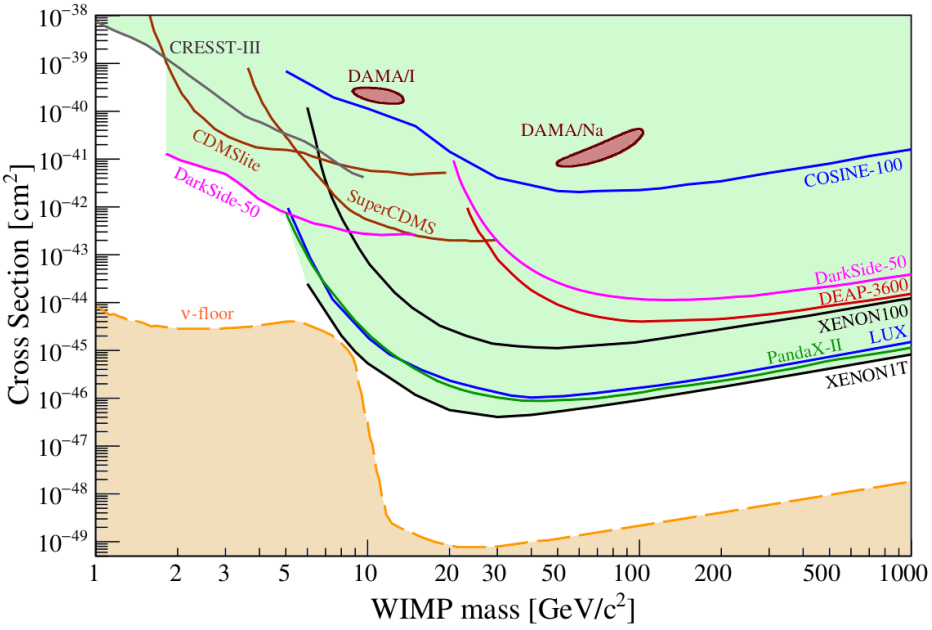

Figure 1-3: Comparison between the excluded regions calculated from some of direct detectors of spin-independent cross section for WIMPS and nucleon, 2019. The space above the lines is excluded at a 90% confidence level [15]. *In the low part of the graph, the "neutrinos floor" is due to the irreducible background from coherent neutrino-nucleus scattering* [16]. *The results for DAMA are the observed annual modulation in the scattering on iodine (I) and sodium (Na), respectively. They are fully included in the other experiments exclusion regions* [17].

No WIMP particles are identified so far, every time a detector becomes more sensitive it can exclude certain regions where the WIMP cannot exist. Figure 1-3 shows these exclusion regions which show the contains on the WIMP-nucleus cross-section. In this thesis we will focus on what happens as a result of the excitation and scintillation process and how the photons created in these processes interact with detector materials.

1.2 Dark matter search with liquid xenon

1.2.1 The properties of liquid Xenon

As discussed in the previous section 1.1.3 the scattering strongly depends on the properties of the target material. Two candidates for target materials are argon and xenon. Both noble gasses are used in experiments trying to detect dark matter. The main differences between these two gasses are: atomic mass number ($argon: A = 40, xenon: A = 131$) [18], and density ($liquid\ Argon: 1.4\ [\mathrm{g/cm^3}], liquid\ xenon: 3.1\ [\mathrm{g/cm^3}]$) [19], [20]. Both gasses have their advantages, for example argon is abundantly available on Earth, and xenon has better stopping power due to its higher density. In this thesis I will focus on xenon because of the XENON1T experiment to which NIKHEF is affiliated in the Laboratori nazionali del gran sasso (LNGS).

When the xenon is colliding with a WIMP, it either excites (Xe*), or ionizes (Xe^+) [19]. The photons that emerge when the xenon deexcites back to the ground state, has a wavelength of $177.6\ [\mathrm{nm}]$ and is called scintillation light.

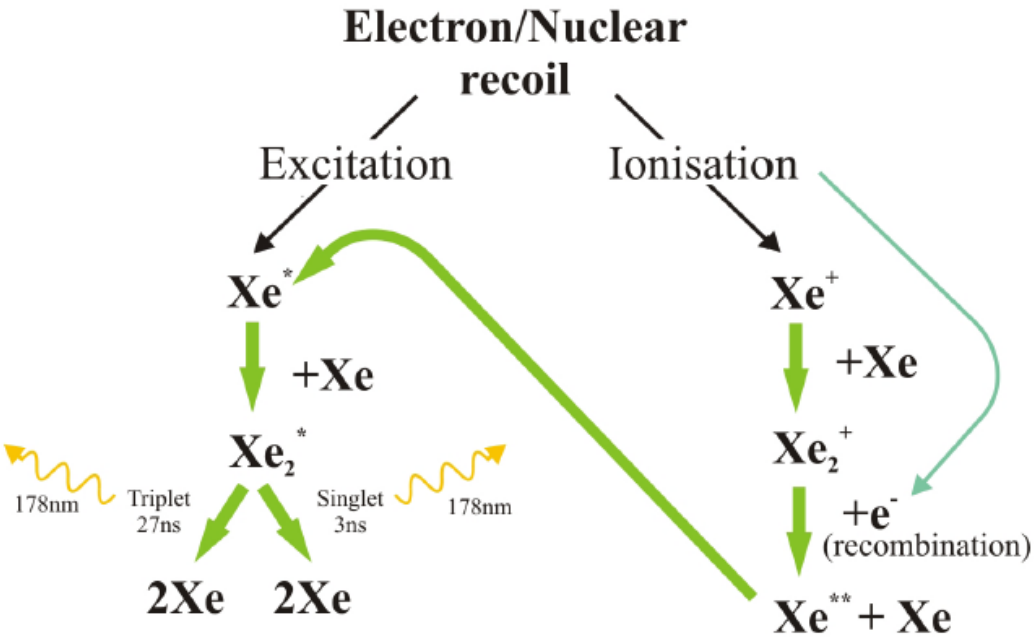

Figure 1-4: The basic sequence of the scintillation process of liquid xenon (LXe). The initial ionization or excitation is produced by an ionizing particle traversing the LXe [21].

The process of Xe^* decaying back to the ground state is described by equation (2).

$$\begin{aligned} Xe^* + Xe &\rightarrow Xe_2^* \\ Xe_2^* &\rightarrow 2Xe + hv \end{aligned} \tag{2}$$

The produced photons are not reabsorbed by the xenon, thus allowing the scintillation light to be detected. The Xe^+ gets recombined following equation (3).

$$\begin{aligned} Xe^+ + Xe &\rightarrow Xe_2^+ \\ Xe_2^+ + e^- &\rightarrow Xe^{**} + Xe \\ Xe^{**} &\rightarrow Xe^* + heat \end{aligned} \tag{3}$$

The Xe^* from equation (3), decays again via by equation (2). Leaving no ionized or excited xenon.

1.2.2 Liquid xenon based dark matter detectors

There are multiple dark matter experiments scattered around the world studying the detection of the WIMP. There are all based on the principle of direct detection as discussed in 1.1.3.2. All detectors discussed in this chapter will be dual-phase Time Projection Chambers (TPC). The Particle and Astrophysical Xenon Detector (PandaX) is located in China Jinping Underground Laboratory (CJPL) and is from all the experiments it occupies the deepest underground laboratory in the world [22]. Till a few years ago we also had the Large Underground Xenon experiment (LUX) at the Sanford Underground Laboratory (SURF) [23] and ZonEd Proportional scintillation in Liquid Noble gases (ZEPLIN) at the Boulby Underground Laboratory [24] but they joint forces in the LZ dark matter experiment at SURF. The XENONnT [25] experiment at LNGS is the last in this list of xenon-based detectors. All previously mentioned detectors work on the same principle but due to the NIKHEF dark matter ties to XENONnT the explanations will be based on that detector.

The XENONnT experiment is located $1400\ [\mathrm{m}]$ underground to shield the detector from cosmic rays. The experiment has three layers of detectors. It is enclosed by a cylindrical tank, $10.2\ [\mathrm{m}]$ high and a diameter of $9.6\ [\mathrm{m}]$, filled with Gd-loaded water. The tank is equipped with photomultiplier tubes and acts as a water Cherenkov muon veto. The second detector is a neutron veto and is contained within but optically separated from the muon veto volume. And finally as mentioned before the xenon dual-phase time projection chamber, filled with $5.9\ \mathrm{tonne}$ of liquid and gaseous xenon, located at the centre of the neutron veto system [25].

Different particles enter the detector, and their interaction is depending on their type, it either interacts with an electron of the xenon atom (electronic recoil) or with the nucleus of the xenon (nuclear recoil). Both interactions lead scintillation signals in the detector. The first scintillation signal (S1) is produced via excitation, the second signal (S2) is generated by the electrons released by ionization that drift up to the liquid-gaseous interface using an electric field and get accelerated by a stronger second field in the gaseous xenon where they produce a time-delayed scintillation signal. A schematic view of this process can be seen in Figure 1-5.

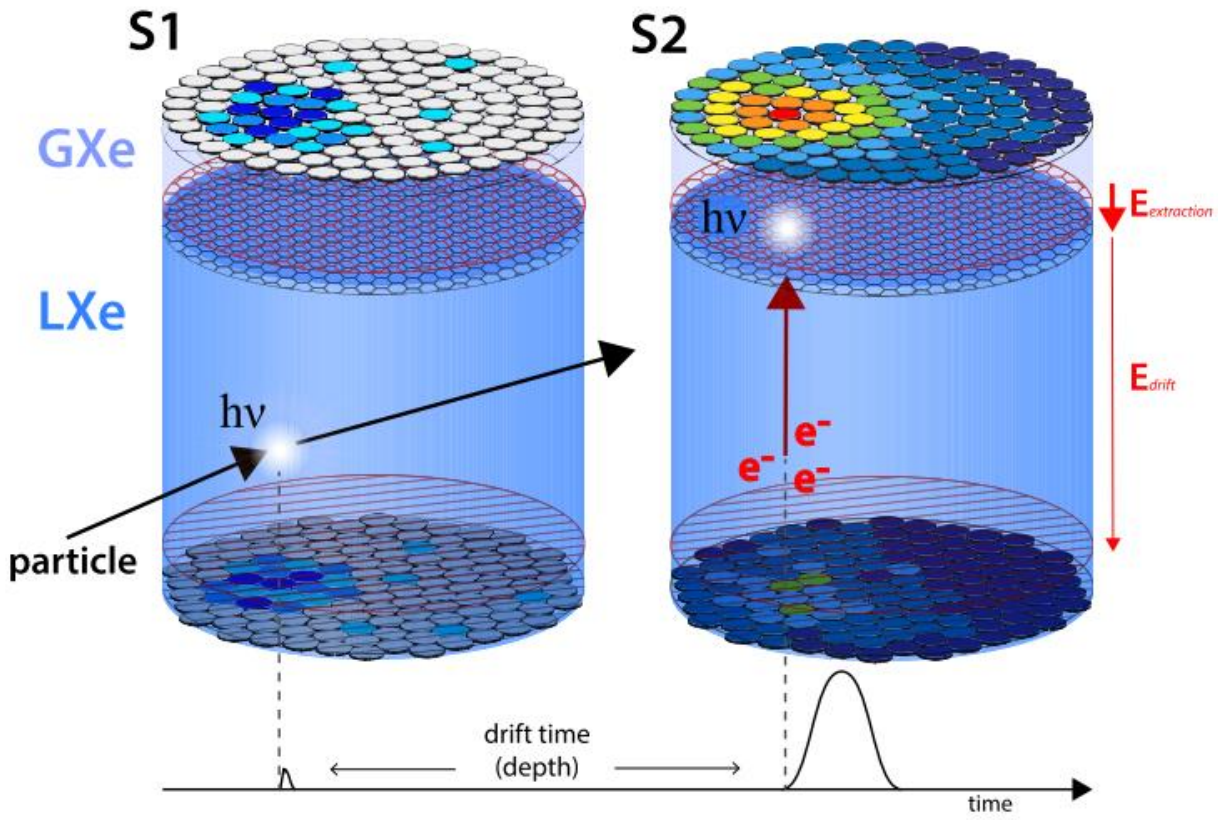

Figure 1-5: Schematic view of the working principle of a dual-phase TPC. The S1 signal is observed by both the top and bottom PMT arrays. The ionization electros are drifted from the interaction point to the LXe/GXe interface using a uniform electric field. The S2 signal is formed via proportional scintillation triggered by the electrons extracted in the GXe. The localized pattern of the S2 signal in the top PMT array is used to reconstruct the position in the (x, y) plane. The time delay between S1 and S2 gives the z-coordinate. The energy is reconstructed from the combination of both signals [26].

Dark matter has a small interaction cross-section, therefore in the WIMP search, having more than one scatter inside the detector is excluded. Because multiple scatter events are assumed to come from electronic recoil or background nuclear events.

Improving the sensitivity is among other things the result of reducing the background as much as possible. The background is reduced by improving the purity of the xenon inventory, as well as reducing muon-induced and radiogenic neutrons coming from the TPC walls by only using a fiducial volume of 4 tons inside the TPC. All is enclosed by a large water tack for extra shielding. A 3D CAD drawing of the XENONnT setup can be seen in Figure 1-6.

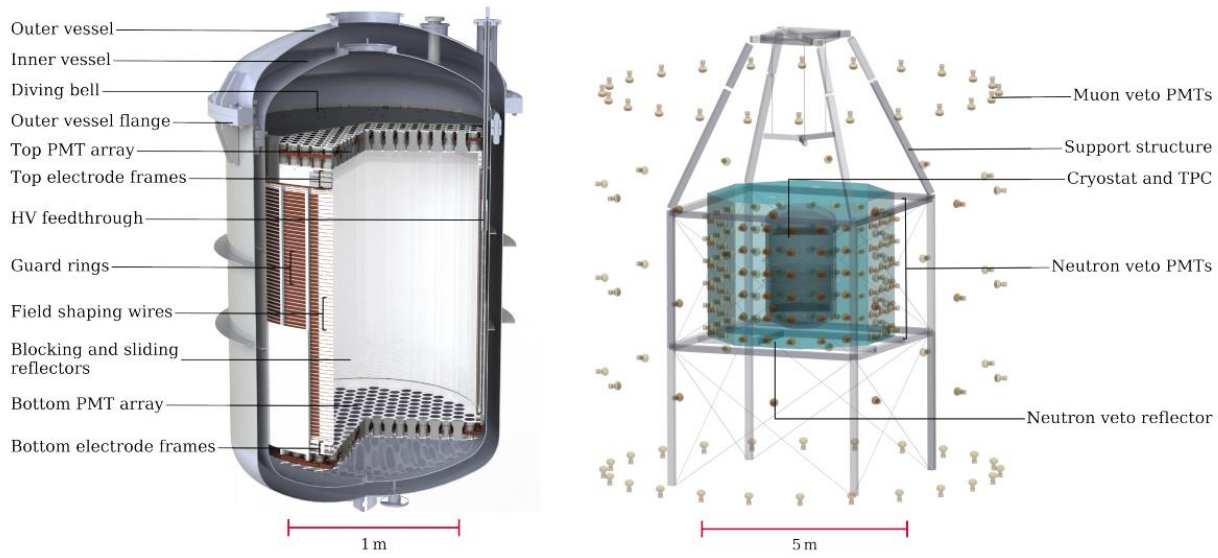

Figure 1-6: On the left the XENONnT inner cryostat with the TPC inside. On the right a rendering of the three nested detectors, including muon and neutron veto. The water tank which encloses the complete setup is omitted to make the image clearer [25].

The inner TPC vessel is lined with Polytetrafluoroethylene (PTFE) it is found to be reflective at wavelengths above $280\,[\mathrm{nm}]$. The VUV experimental setup will look at the optical properties of PTFE below this wavelength closer to the $178\,[\mathrm{nm}]$ produced by scintillation. This will give a better idea about future upgrades of these detectors.

1.3 The Vacuum UV optical characterization chamber

Measuring dark matter is done using detectors as described in section 1.1.3. The Vacuum UV (VUV) setup will look at processes happening in liquid xenon detectors mentioned in section 1.2.2, and specifically at the scintillation process. The photons being released in the scintillation, can scatter in any random direction. This also means there is the probability photons get released in a direction which is not towards a detector. And to be able to know how the detector materials either absorbs, transmits, or reflects the photons the VUV experiment will be built.

The VUV experiment will be setup in such a way, that the scintillation light from the xenon can be reproduced without any xenon present. Furthermore, we want to be able to place samples of detector materials within the beam of light. And be able to manipulate the sample to see how it behaves in transmission and reflection.

1.3.1 Requirements for the experimental setup

1.3.1.1 *Sample chamber requirements*

1. Being modular for additions in the future
2. Oxygen free environment
3. Rotationally manipulate the sample and the detectors from outside the sample chamber
4. Ease of access for placing and replacing of samples
5. Ability to configure the chamber for full intensity calibration measurement
6. Ability to measure reflectivity and transmissivity of a sample
7. With material selection outgassing must be considered

1.3.1.2 *Sample holder*

8. A sample can be placed without touching the front or back of the sample
9. The sample holder can hold two samples
10. The sample can be cooled in future experiments

1.3.2 The scope of this research

During this thesis project I will design, build, and commission a vacuum UV optical characterization experimental setup. I will investigate if the specifications to which the VUV experiment is designed before me are correct. This means compare the workings and methods of previously build experiments to our own, and test if changes have any consequences for the workings of the experiment.

When we use prefabricated vacuum components, these components will have specifications. And in some cases of our experiment, it is possible we venture onto the border of what these components are made to do. So, I need to investigate if the standard vacuum components will fulfil the specifications for our system. And if not, we need to investigate what is missing decide what we do need from that component and make custom components to adhere to the specifications.

In doing experiments we need to record data, in the VUV experiment the bottle neck will mostly be positioning of said system. We need the temperature of the sample and the light that passes through or reflects of the sample using a photon sensor. The challenge we do have to study is how to place the different sensors without compromising on requirements or reducing the quality of the characterization measurement. Here I will also investigate a data acquisition system, where I will focus on what we need and the electronics.

And finally, all the components will be assembled and the experimental setup. To make sure all the components work as intended we will commission all the different parts to see if they work as was designed.

2 VUV experimental setup

2.1 Setup

In the VUV experimental setup, we want to investigate the transmission or reflection of light on a sample. To do so the different components in the experiment must have different orientations for the two different experiments. Thus, we need a design where the sample can be manipulated from a transmission position to a reflection position. As well as the light sensors being moved to capture the transmitted or reflected light. The lights sensors will also need to be moved so we can measure the diffuse reflection as a function of the angle with respect to the sample. See Figure 2-1 for the different orientations needed in the experimental setup.

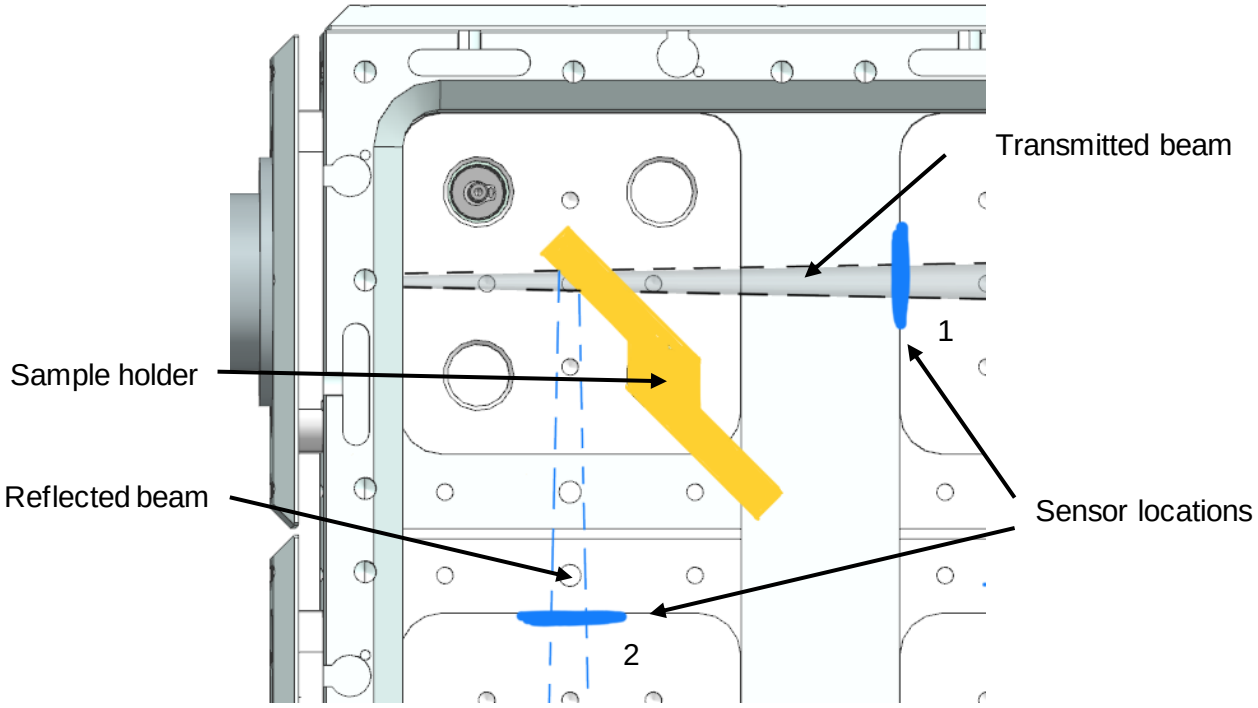

Figure 2-1: With a sample holder either transmitting or reflecting the light. There are multiple points where sensors are needed (Blue). Sensor location 2 needs to be free in rotation to adjust for different angles of incidence.

All the parts of the experimental setup have been selected such that the photons emerging in the liquid xenon can be created without needing the liquid xenon for scintillation. In Figure 2-2 an overview of the experimental setups design is shown. Later in this chapter all the different parts will be explained in more detail.

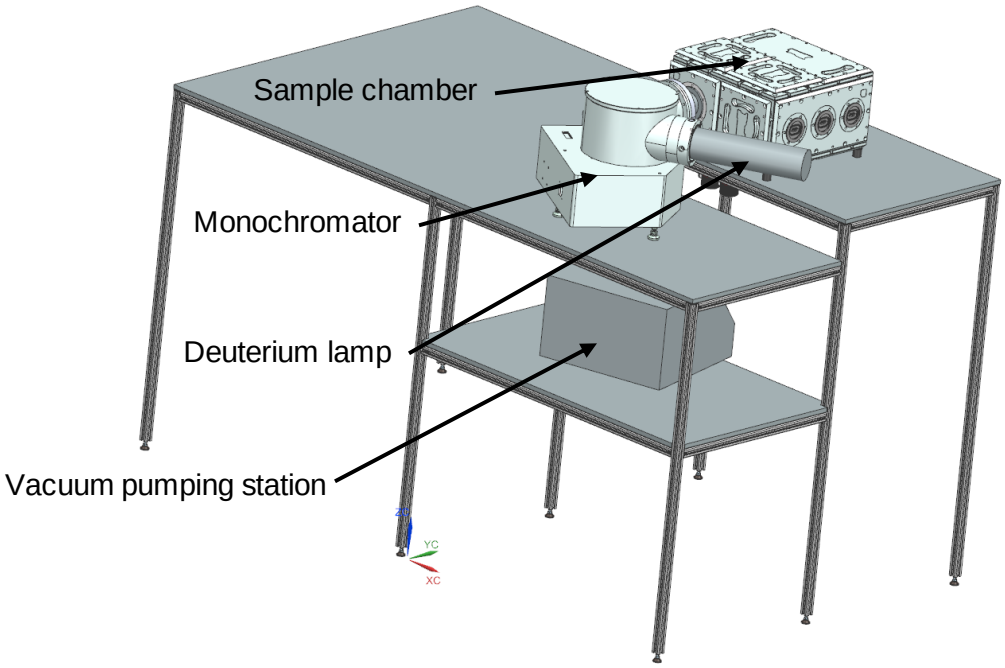

Figure 2-2: The complete design of the VUV experiment, with all its components. This digital CAD drawing was made to see the proportions of the different components relative to each other and a setup table.

At the end of this chapter all the different components and methods will have been chosen. Leading to an experimental setup as seen in Figure 2-3.

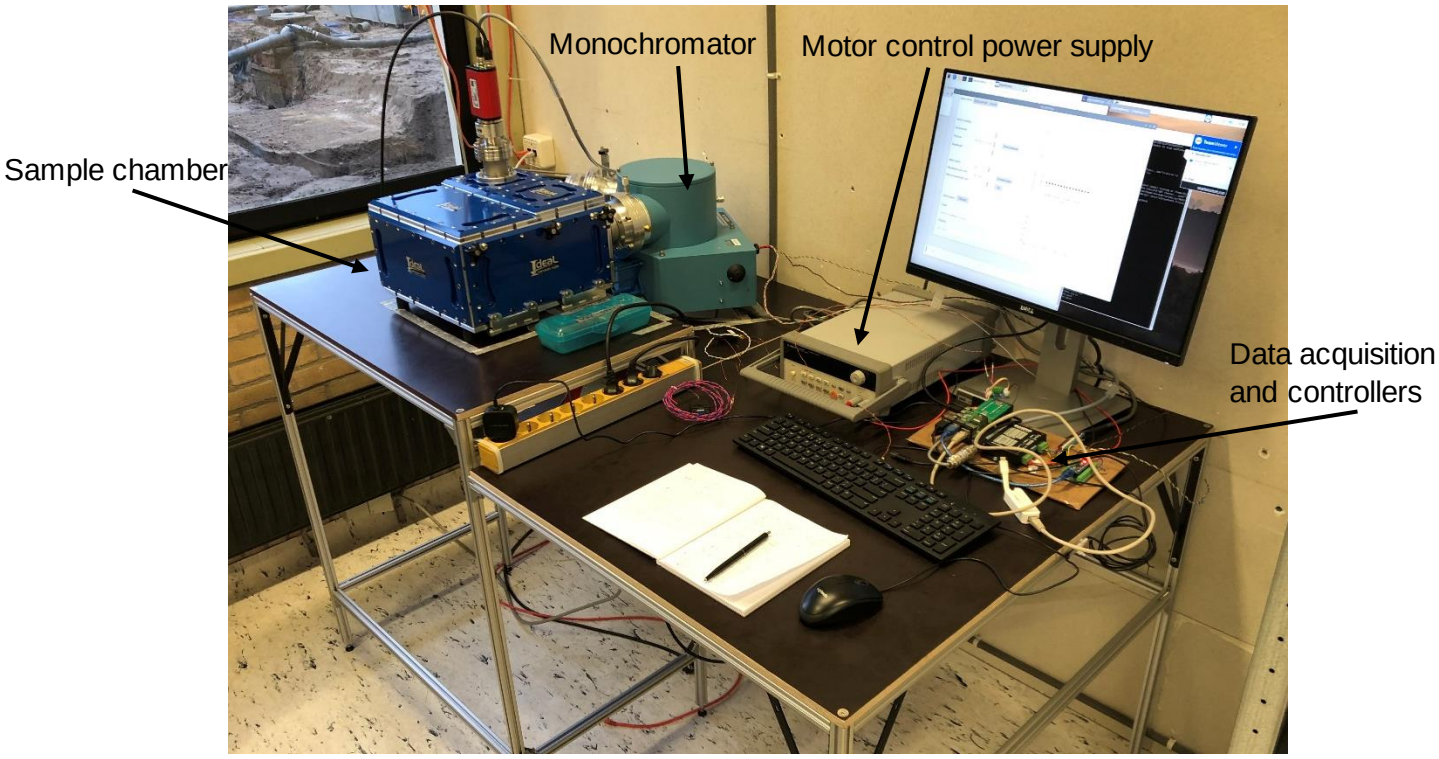

Figure 2-3: The experimental setup for the VUV experiment assembled.

2.2 Light source and monochromator

To measure the optical properties of detector materials in a comparable environment as in the xenon-based experiments, there is the need for a source able to generate light at the same wavelength as the scintillation light from xenon. This is an uncommon product, due to its restrictions. For example, the photons at the scintillation wavelengths of $170\ [\mathrm{nm}]$, easily get absorbed by a lot of different media. Glass being one of the most used materials in lamps is one of those media. Hamamatsu is one of the companies making equipment for generating and detecting photons in wavelengths beyond the visible spectrum. Their deuterium lamp model L11798, see Figure 2-4, emits light with a spectrum ranging from $115\ [\mathrm{nm}]$ to $400\ [\mathrm{nm}]$. And the special magnesium fluoride window makes sure that the wavelengths we need passes through into the experiment [27].

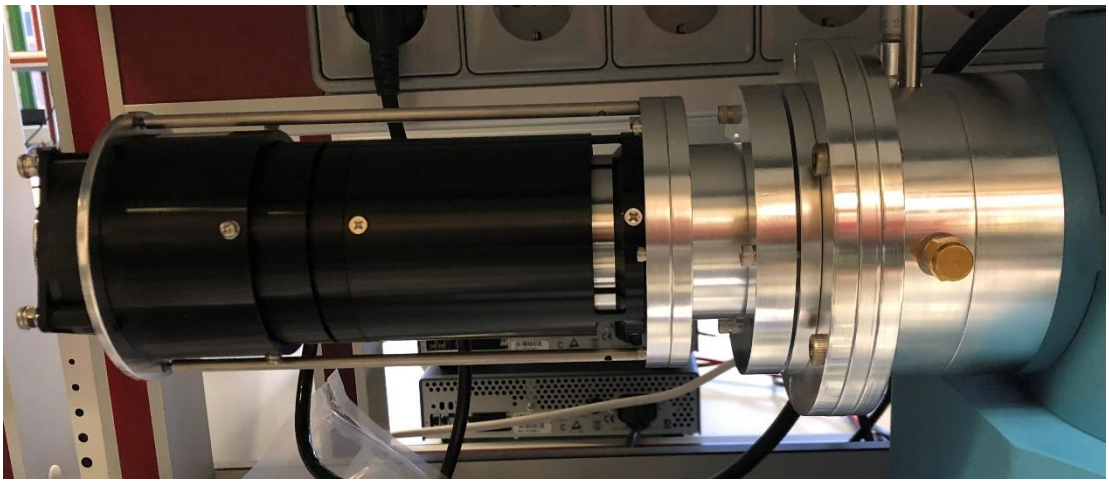

Figure 2-4: Hamamatsu Deuterium lamp, shown connected to the monochromator.

Because the deuterium lamp is emitting a spectrum of light while the experiment requires one specific wavelength, a monochromator is used to filter the spectrum down to one specific wavelength, see Figure 2-5 for an outside view. For this filtering a McPhersons monochromator uses a specifically designed grating mirror within a highly light absorbent region, see Figure 2-7 for the inside and the light absorbing coating. The design of the monochromator is such that no extra design is needed, this because the focal points of the system lie in the entrance and exit slit, see Figure 2-6 for the optical path.

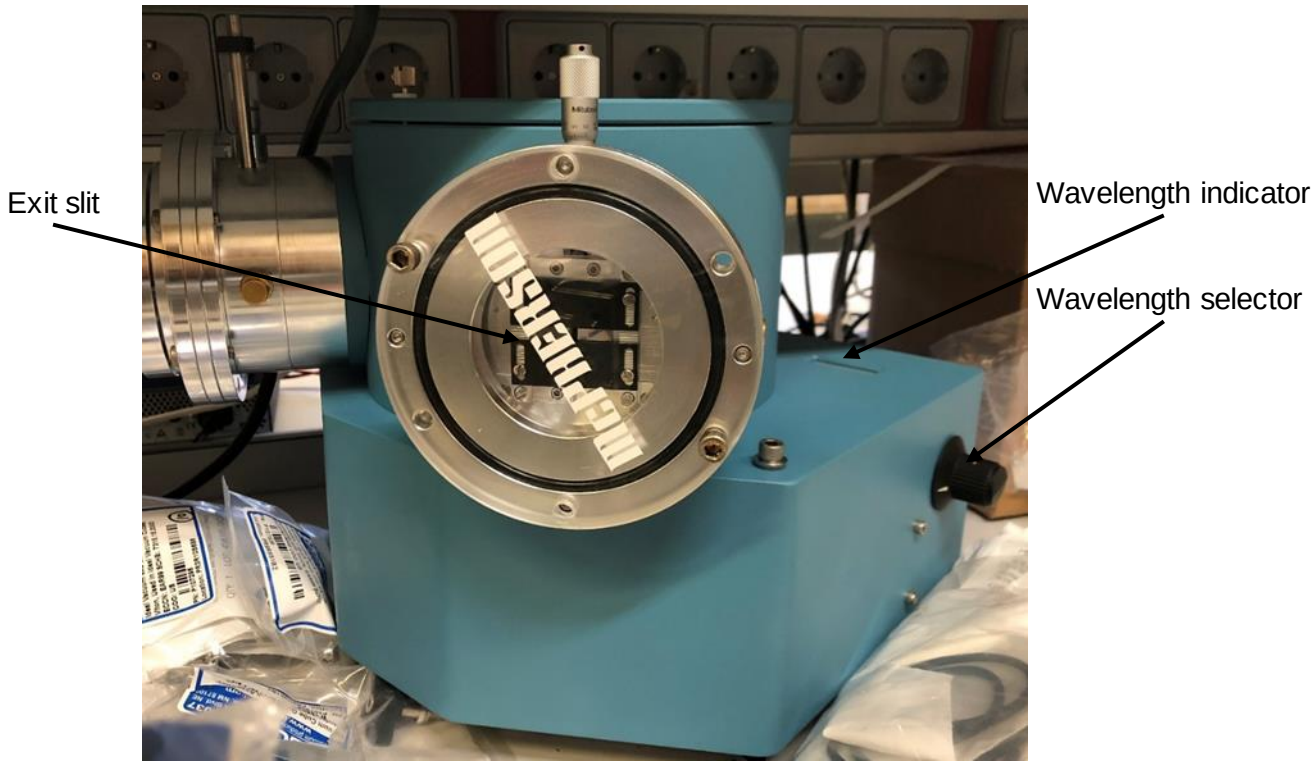

Figure 2-5: McPherson monochromator, exterior view with slits visible.

No filter is perfect, so also with this monochromator. Even though the mirror is designed to pass one specific wavelength, see Figure 2-8 for the reflective grating. Not one specific wavelength passes through, but a more gaussian looking shape around the chosen wavelength. To make the sides of the bell shape narrower, the slit size can be changed. This has the consequence of making the intensity lower and size of the beam smaller. But leaving a more accurate wavelength. The wavelength can be selected down to an accuracy of $0.1\,[\mathrm{nm}]$ [28]. The selection of a wavelength can be done using the knob on the side or using the build in stepper motor. The selected wavelength can be always seen using the build in counter, which displace the wavelength in Ångström.

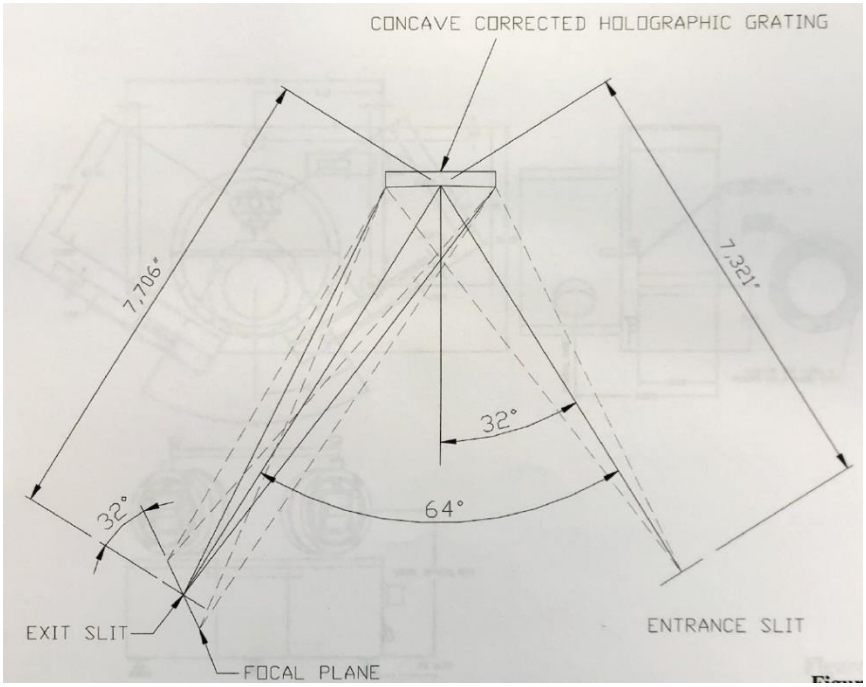

Figure 2-6: Optical diagram of the McPherson monochromator, showing the image at the entrance slit is reflected on the exit slit image taken from [29].

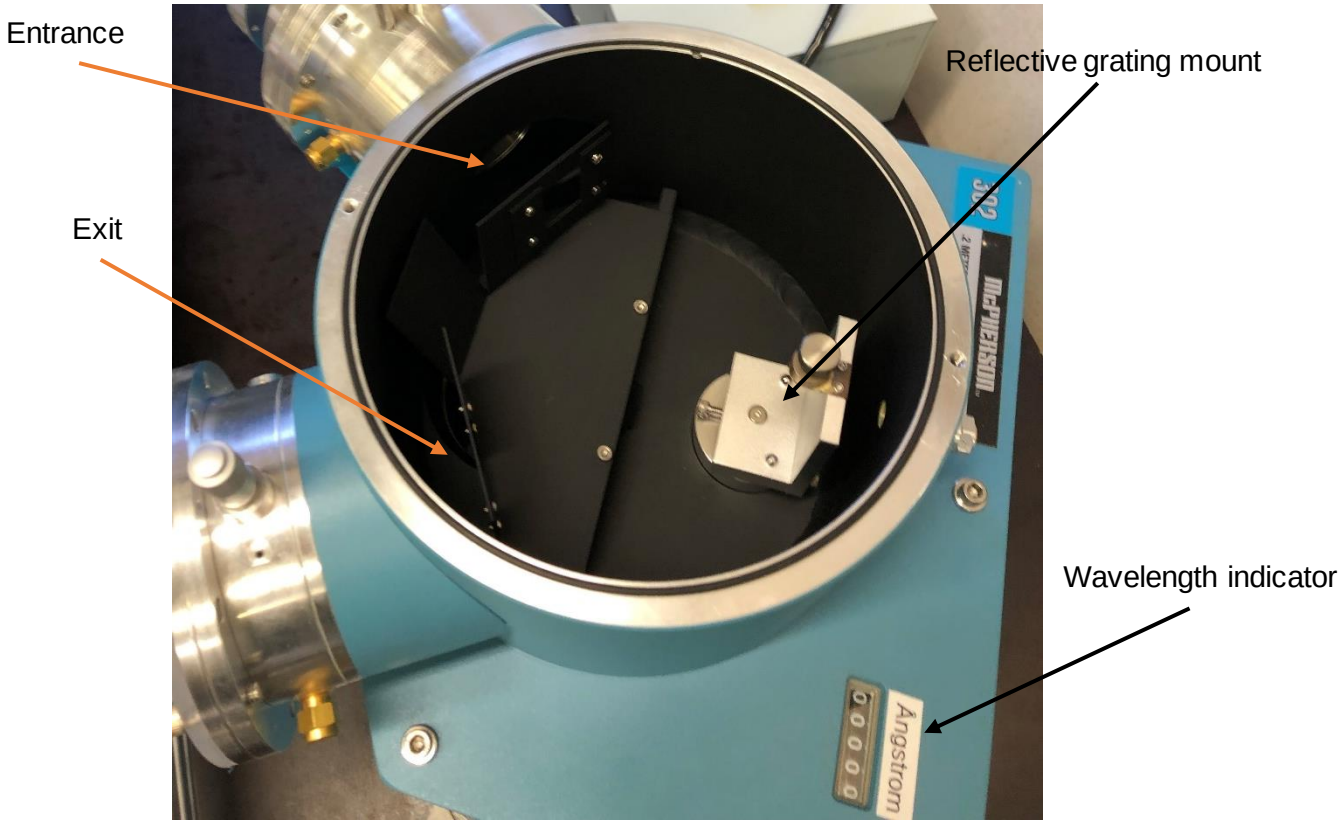

Figure 2-7: Monochromator inside view, with the reflective grating removed.

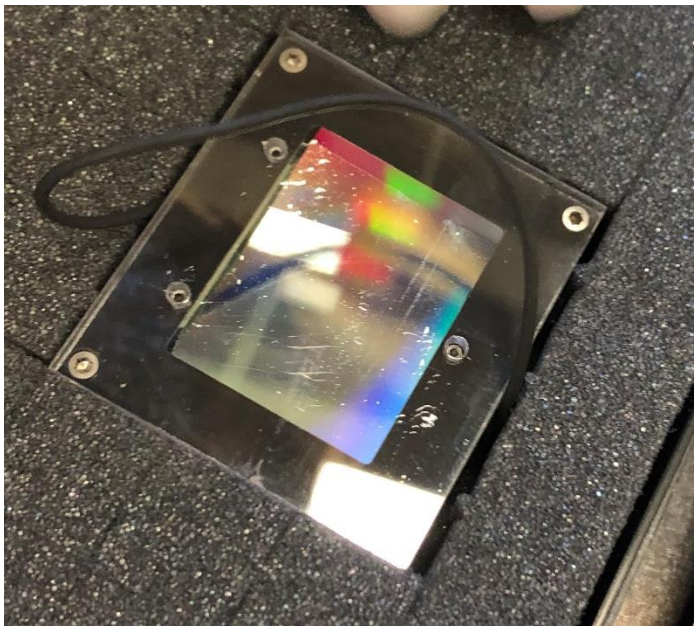

Figure 2-8: Reflective grating covered by protective plexiglass in its storage container. This is one of the most delicate parts of this setup. It can lose its very precise reflective properties if any material settles on its surface.

2.3 Sample chamber

The sample chamber will be the part where all the sample measurements will take place. And because of possible change in the scope of the experimental setup, the need for a modular setup was favoured. To begin with, the setup needs to be able to measure transmission and reflection properties of a sample. As mentioned in 2.2, lots of materials absorb the photons at the required wavelength of about $170\ [\mathrm{nm}]$, next to glass, oxygen also falls into this category.

Therefore, a sample chamber without any oxygen present, is a must. The two options for this setup would be a nitrogen environment or a vacuum environment. The nitrogen environment has the advantage that because of the atmospheric pressure, outgassing is limited. But using nitrogen brings along the need for a rest gas analyser to make sure the purity of N_2 is maintained throughout the characterization measurement. Instead of filling the chamber with non-oxygen particles, getting rid of all the oxygen by pumping a vacuum works equally well. Although, with creating a vacuum outgassing needs to be considered.

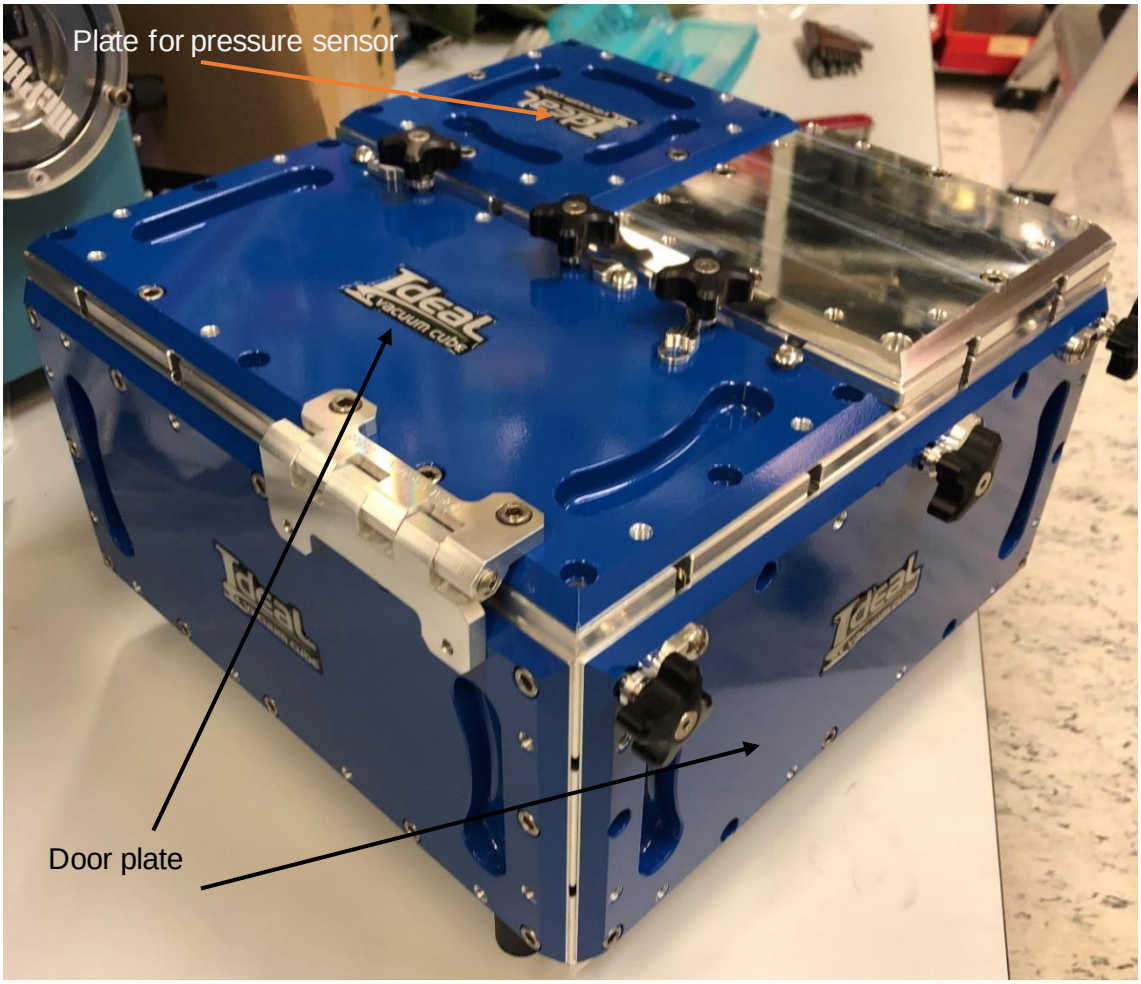

Figure 2-9: The Ideal vacuum 12"x12"x6" modular vacuum chamber

Outgassing is a phenomenon that happens when the space in which a material is placed has a low pressure, such that particles from within that material can diffuse into the environment. This phenomenon happens often with vacuum environments because there are not many particles in the environment thus making it easier for materials to diffuse into the environment.

As seen in Figure 2-9, the vacuum chamber is built from all sorts of different plates with different shapes and sizes. This modular characteristic is a welcome ability to make the sample chamber fulfil all the different requirements. The modular nature of the chamber brings with it the need for rubber seals. The rubber seals and the light absorbent paint of the monochromator are a possible outgassing source. Choosing all other materials we introduce into the chamber carefully, minimizes the possibility for more outgassing. The company Ideal vacuum fabricates modular vacuum chambers to supply the need of flexibility [30].

2.4 Vacuum pumping station

To get the vacuum in the Ideal vacuum sample chamber, we need a pump that can pump a vacuum of the order $1 \cdot 10^{-5}$ [mbar] in a volume of 14.2 [L]. We want a small station that would fit under a table and would not take too long reaching our target pressure.

The Pfeiffer Vacuum HiCube 80 Eco DN63 (PM183255AT) is the pump we will use in this experiment. This HiCube 80 is a pumping station with a backing and turbopump already build into one unit. The unit has the dimensions $301.8\ x\ 301\ x\ 362.3$ [mm], making it the ideal size for under the table placement. It can pump down to $1 \cdot 10^{-7}$ [mbar] and has a pump-down time of 557 [s] for a chamber of 10 [L] [31].

Figure 2-10: The Pfeiffer vacuum HiCube 80 pumping station. With the MVP 015-2 backing pump and HiPace 80 turbopump. Controlled by the TC110 electronic drive unit [31].

The pump has vibration springs keeping the experimental setup as free as possible from the vibrations of the pumps.

2.5 Sensors

In the experiment we want to register three parameters, the pressure of the sample chamber, the temperature of the sample, the light reflection off or passing through the sample. With these three parameters we can confirm the quality of the characterization measurement, low pressure so many photons make it onto the sample, temperature to see how this influences the reflectivity or transmission of the sample, and of course the light sensor itself. The light sensor will also be influenced by the temperature resulting in dark counts, mentioned later on in this section.

For measuring the pressure, we use a Pfeiffer MPT 200 AR, see Figure 2-11. This sensor connects to the vacuum station mentioned in 2.4. We place the sensor close to the position of the sample, so we can measure how good the vacuum is. The quality of the vacuum is important because the vacuum UV light is easily absorbed by oxygen, we therefore need to make sure the pressure close to the sample is of the order $1 \cdot 10^{-5}$ [mbar].

Figure 2-11: Pfeiffer vacuum pressure sensor MPT 200 AR DN40 [32].

The pressure sensor has an operating temperature between $5\,℃$ and $60\,℃$, so we need to make sure it will stay thermally isolated from any cold sources. This will be an extra requirement for the complete system. In the range we want to perform experiments the precision of this senor is $\pm 25\%$ [32], which means $0.25 \cdot 10^{-5}$ [mbar]. This is sufficient for our experiment.

The temperature we want to measure at different positions, and we will use PT100 sensors to do so. We will use two different models of temperature sensor. A Heraeus 1PT100 KN1510, ceramic Wire Wound Pt RTD probe sensor (332206914) [33], see Figure 2-12 left. This sensor has an operating range of $-196\,℃$ to $660\,℃$ sufficient for our future flash cooling with liquid nitrogen. And this sensor will be probed into the sample holder block. And a TE Platinum Thin Film temperature element (PTFC101B1G0) [34], see Figure 2-12 right, with an operating range of $-200\,℃$ to $600\,℃$, which is also sufficient. This last sensor is chosen because of its Thin Film characteristic and will be used in between the sample holder and the sample, more on this will be explained in 3.3.

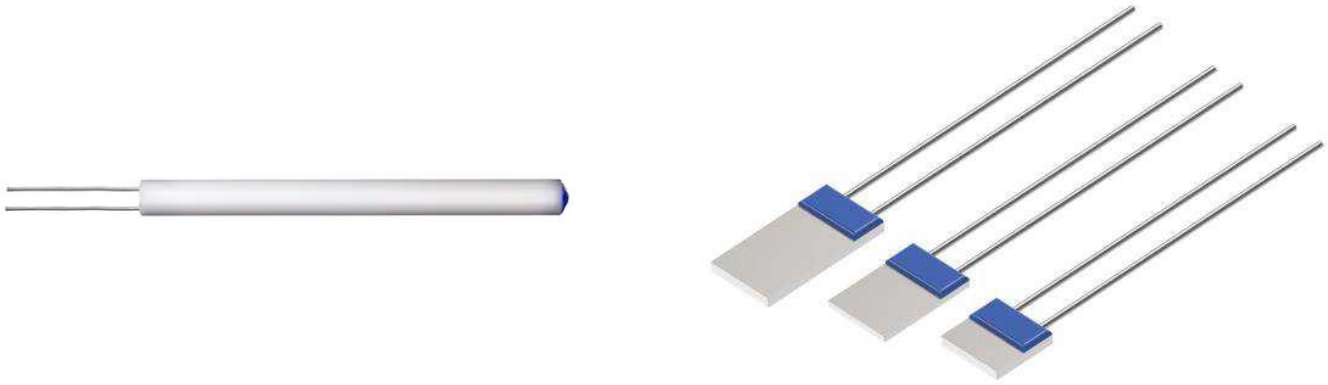

Figure 2-12: The two different temperature sensors, on the left the Heraeus probe sensor [33] *which will be used to measure the temperature of the sample holder, and on the right the TE Platinum Tin Film sensor* [34] *which will be used to measure the temperature directly from the sample*

The final sensor we need to discuss is the Silicon Photodetector (SiPM) used to measure the reflected or transmitted light. We will use a 4th generation Vacuum Ultraviolet Multi-Pixel Photon Counter (VUV-MPPC) S13370 from Hamamatsu photonics [35]. This sensor is specifically made to measure light down to a wavelength of $120\,[\mathrm{nm}]$. These sensors are specially made for detecting scintillation light produced by liquid Xenon or liquid Argon. As we can see in figure, the 4th generation has really improved from the 3rd generation at the wavelength of liquid Xenon.

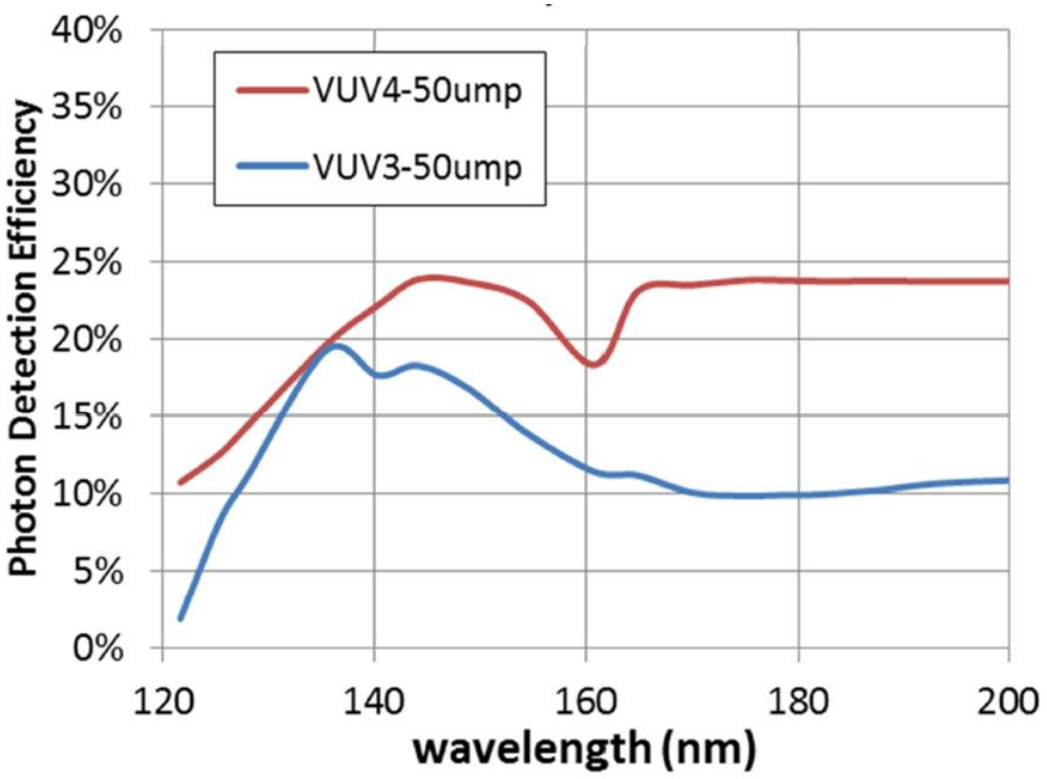

Figure 2-13: In this figure the photon detection efficiency is plotted against the wavelength. This image shows the improved performance of detecting scintillation light of liquid xenon at a wavelength of $178\,[nm]$ [35].

Due to the knowledge of the beam size within the sample chamber, explained more in 3.1, we wanted the large sensor in an array of $3\ x\ 3$ sensors. This would have been a custom-made sensor with a photosensitive area of $18\ x\ 18\ [\mathrm{mm}]$. Unfortunately, this was an absurdly expensive option and therefore choose to order nine loose $6\ x\ 6\ [\mathrm{mm}]$ sensors of the model 6050CN. These were not available in the time we had for the project and resorted to borrowing sensors from colleagues in the Dark matter group. They had ordered the exact same sensors we needed but only in the $3\ x\ 3\ [\mathrm{mm}]$ 3050CN model. Concerning time this was sufficiently large to test the light within the sample chamber as well as performing a test measurement for proof of concept for the measurement setup.

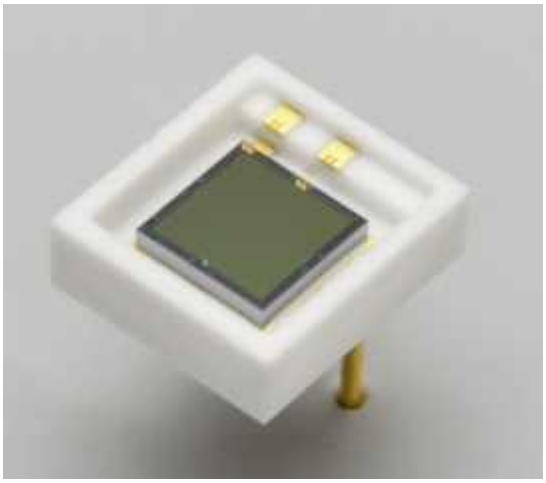

Figure 2-14: The Hamamatsu S13370-3050CN VUV-MPPC. This is the sensor we used in all the test and experiments during this project [35].

The sensors we want to use and which we used during this project have the same specifications, see Figure 2-14 for the 3050CN model. Sensitive in the range of $120\ \mathrm{to}\ 900\ [\mathrm{nm}]$, with an efficiency of 35%. The operating voltage of the sensor is at $56\ [\mathrm{V}]$ (breaks down at $53\ [\mathrm{V}]$) with a current of $0.47\ [\mu\mathrm{A}]$ and with a dark count of $1\ \mathrm{to}\ 3\ [\mathrm{Mcps}]$ [35].

These VUV-MPPC's are photosensitive diodes and will be connected in reversed bias. This means that the sensor will only become sensitive if enough bias voltage is supplied, see Figure 2-15.

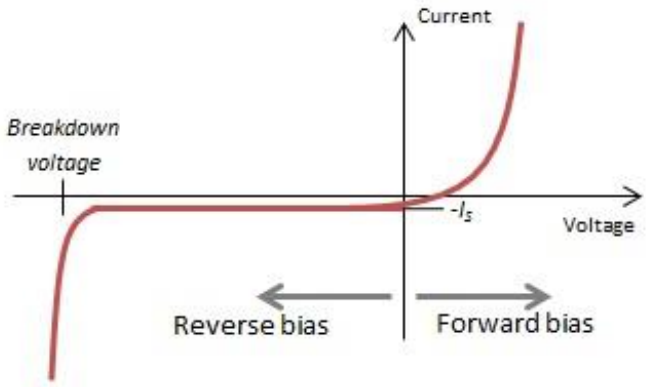

Figure 2-15: Voltage vs Current diagram of a diode, showing the characteristic shape it has in forward or reverse bias [36].

Because our sensors are connected reverse bias, they become so sensitive that not only a photon can knock out an electron creating a photon electric (PE) signal, but the electrons are so energetic they sometimes vibrate out themselves looking like a PE signal. When an electron gets released without a photon and creates a PE signal this is called a dark count. The only way to reduce dark count is to reduce the temperature of the sensor slowing down the electrons reducing the chance one gets released without a photon. This phenomenon is why we want to test the intensity of the light, because the dark count is always a one PE signal. So, we prefer a signal of at least 2 PE making it easier to filter out the dark count. See Figure 2-16 for the shape of a signal pulse as per factory design

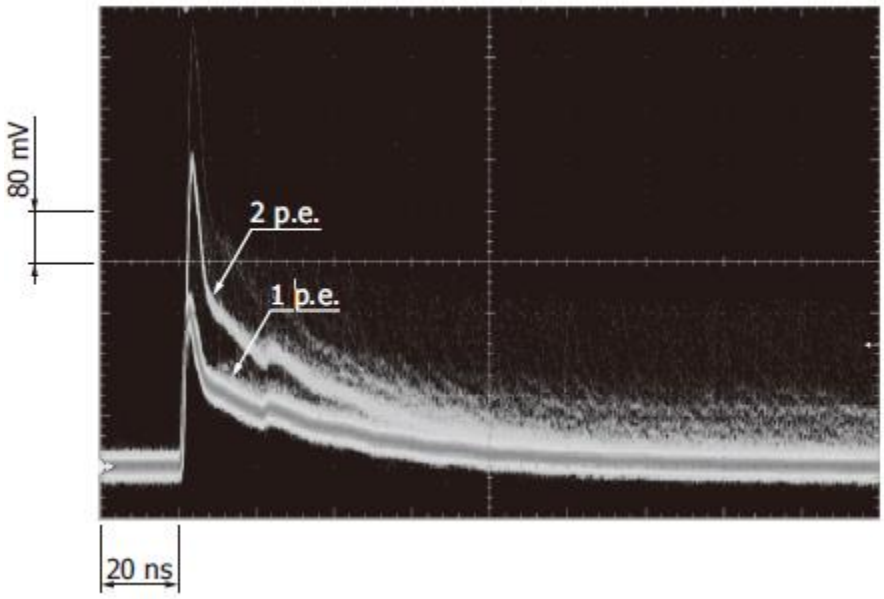

Figure 2-16: Screenshot of the oscilloscope showing the pulse waveform of a 1 PE and 2 PE signal using a linear amplifier [37].

2.6 Feedthroughs

Having a sample which we can manipulate in the experiment without too much effort increases the number of characterization measurements one can take in one vacuum run. And the one parameter we need to be able to manipulate for the experiment, is the angle of incidence of the light to the sample. We therefore need a feedthrough trough which we can rotationally manipulate the sample to a precision of $5°$. We also need enough rotational freedom to change from $0°$ incidence (transmission) to around $30°$ incidence (reflection). We also need to rotationally manipulate the light sensors, to measure the light at various diffuse reflection positions. With the Pfeiffer magnetically coupled rotary feedthrough DN16 (420MRM016) [38] we will have that rotational freedom, see Figure 2-17.

Figure 2-17: Pfeiffer vacuum magnetically coupled rotary feedthrough DN16 [38].

With this rotary feedthrough we have the rotational freedom to put to samples on the holder and rotate it, to be able to change sample while doing a characterization measurement. With the operating temperature lying between $-10\,℃ \text{ and } 50\,℃$ we need to thermally isolate the feedthrough from the sample holder, this will be discussed in 3.2. And therefore, we get the design requirement of thermally isolating the cooled sample from the chamber.

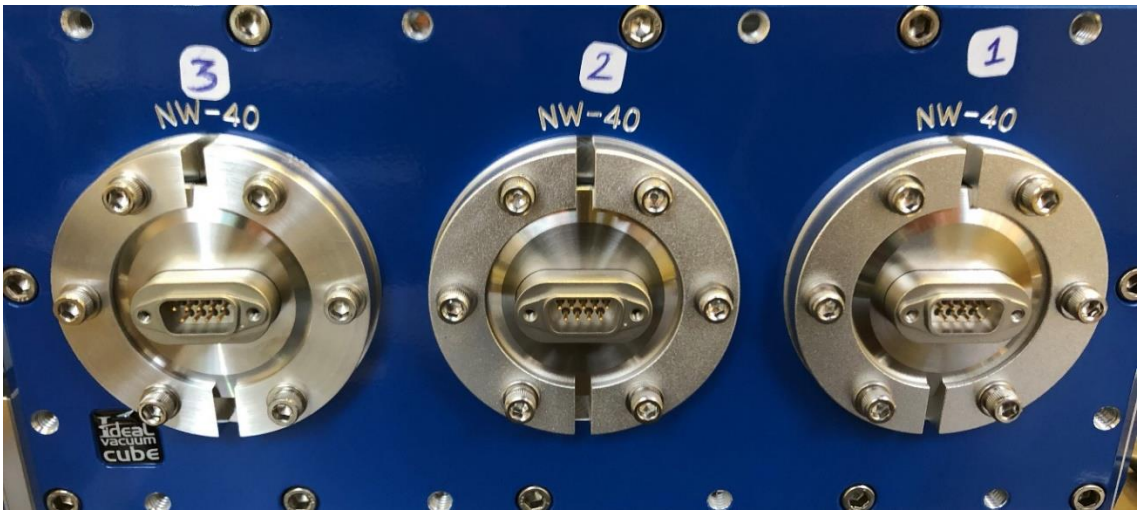

Figure 2-18: Electrical feedthroughs as seen from the outside of the sample chamber.

We will need another feedthrough to get the signals generated by the different sensors within the sample chamber out. We expect to use nine SiPMs each having two wires, and three temperature sensors also having two wires each. We therefore need to feed through 24 individual wires. Besides the number of wires, the feedthrough also needs to handle the $56\ [\mathrm{V}]$ bias voltage and a current of $0.47\ [\mu A]$ needed for the SiPMs. Having the NW-40/DN40 holes in our sample chamber we decided upon the Pfeiffer D-sub feedthrough, flanged, DN40 (120XSD040-9) [39]. Which has a maximum voltage of $500\ [\mathrm{V}]$ at $5\ [\mathrm{A}]$ and gave us 27 individual wire feedthroughs with the ease of the standardized D-sub pins, see Figure 2-18.

The electrical feedthrough used is shown in from the outside Figure 2-18 and in Figure 2-19 from the inside. On the outside of the feedthrough, we use these larger labelled connector as seen in Figure 2-20, these are easy to fabricate and connect to different electronics. On the vacuum side of the feedthrough, we use a Kapton wire with female D-sub pin soldered to them. On the inside we use individual pins oppose to a larger connector to keep the number of different materials we introduce into the vacuum at a minimum. This way we want to control possible outgassing which may damage parts of the monochromator.

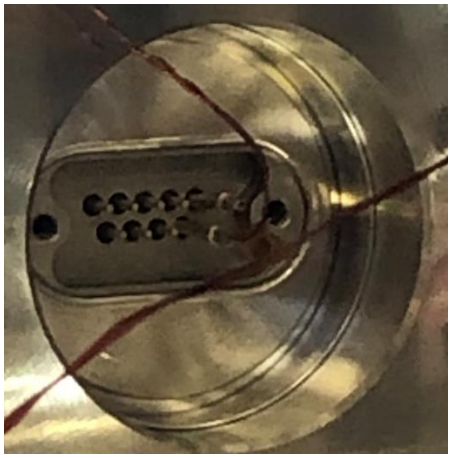

Figure 2-19: Electrical feedthrough as seen from the inside of the sample chamber, already with some wires connected.

Figure 2-20: Cabling used on the outside of the sample chamber, a connecter is used for ease of connection and neatness.

3 Designing and Commissioning

Completing the experimental setup, a holder for the sample, holder for the SiPMs, and placement locations for temperature sensors are needed. These need to be designed in accordance with the requirements mentioned in 1.3.1.2 as well as the space available in the vacuum chamber. When design becomes reality the workability of the pieces needs to be checked and where necessary modified.

3.1 The beam inside the sample chamber

For designing the sample holder, the beam width and trajectory must be known accurately. Using this information, both the placement and size of the sample can be determined using ray tracing. The optical information is fed into a script drawing the ray trajectories of the most extreme paths of light. This method led to Figure 3-1 shows how the light traverses a schematic representation of the optical system. From this schematic beam, together with position of entry and size of the sample chamber, restrictions for the sample holder can be set.

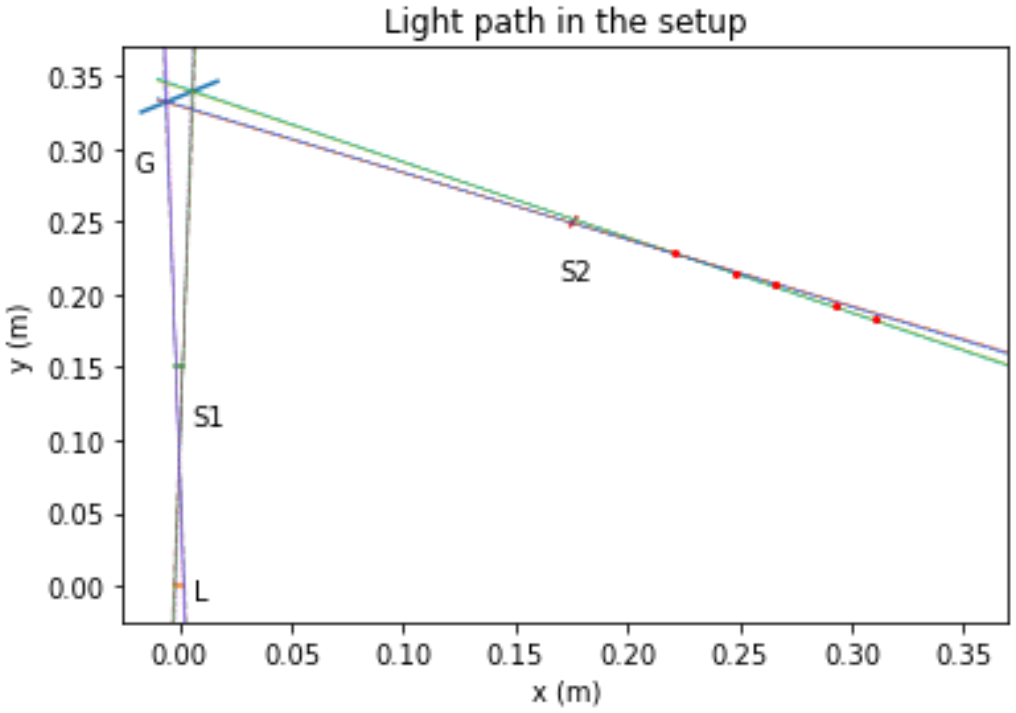

Figure 3-1: The path of light originating in the deuterium lamp (L) in a schematic representation of the experimental setup. The light will enter the monochromator via the entrance slit (S1) and is reflected of the grating (G) towards the exit slit (S2). In the graph different points are marked, which indicate the distance to the exit slit (S2). Measurements were performed at these distances to correspond with the above shown calculations.

The path of light is looked at from its extremes. From these maximum values the width of the beam can be calculated at the pre-determined points, $50\,[\mathrm{mm}]$, $80\,[\mathrm{mm}]$, $100\,[\mathrm{mm}]$, $130\,[\mathrm{mm}]$,and $150\,[\mathrm{mm}]$. Which are then compared to measurements done on the setup, the results of which can be found in Figure 3-3. These measurements and calculations are most important for our design process. Because we are limited by the size of the light sensor, section 2.5, we need to know the size of the beam so we can optimize the light sensor placement for the experiments.

The beam size measurement was done by placing paper in the path of the beam and tracing the cross-section area, measuring the size of that cross section resulted in the data shown in Figure 3-3. These measurements were done before we had the vacuum chamber and realised that installed in the chamber the distances to the exit slit would be larger, resulting in redoing the measurements of the beam inside the chamber. In Figure 3-2 an image of how we performed the later measurement is shown.

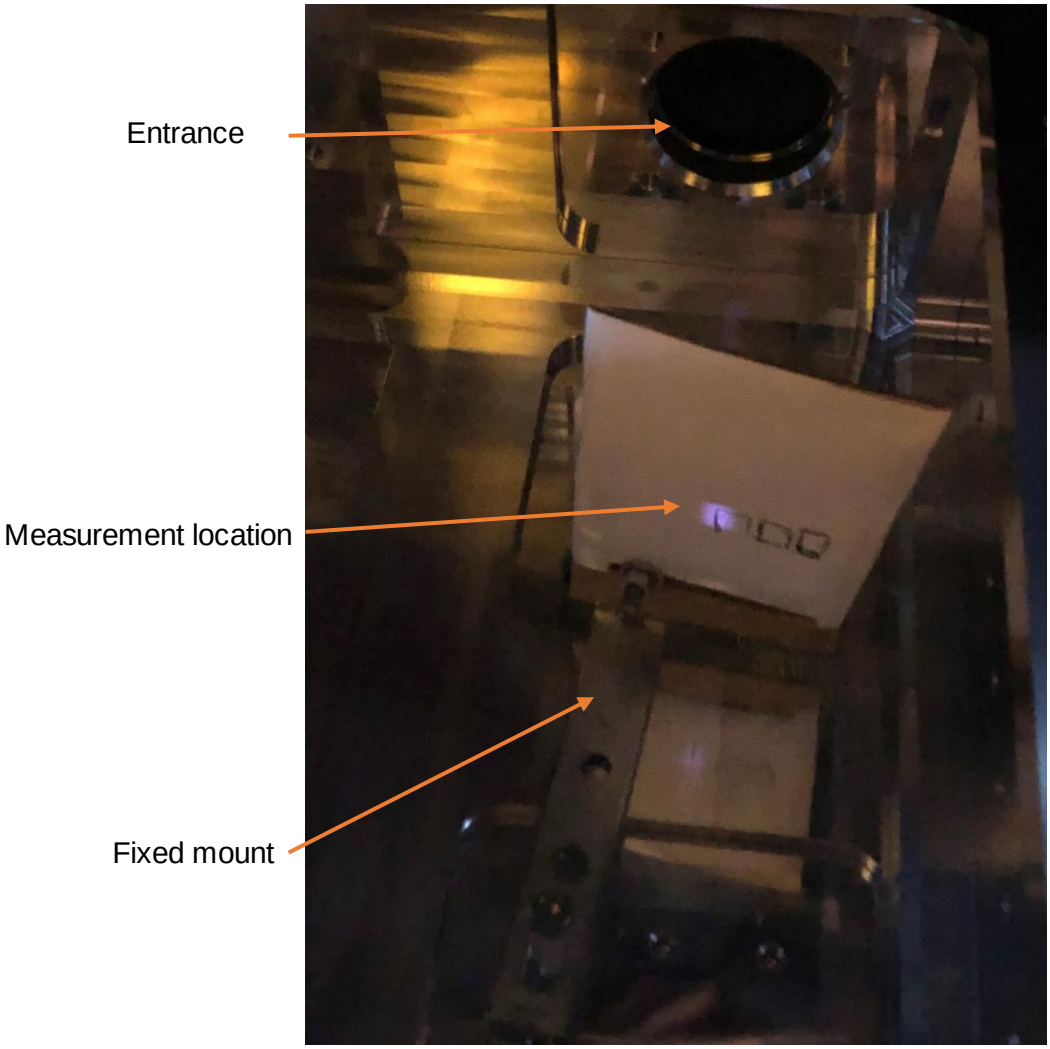

Figure 3-2: Image showing the measurement of the beam size. Where we put the monochromator in full reflection mode and used a fixed piece of paper to trace the cross-section of the beam. The measurement was done multiple times for the same location.

We are working between two extremes, the first is when the beam diverges to much the beam will cover too much area for the light sensor. This means the light sensor must be placed closer to the sample. And in the extreme case this could result in possibly not detecting photons. We could solve this by designing an array of sensors covering a larger cross-section of the beam.

Second, when the beam converges the light sensor must be places further from the sample, such that the beam will be wide enough for the surface matrix of the light sensor to be covered by the beam and not have one hotspot. Placing the light sensor further from the sample brings the difficulty of support from the rotational manipulation point at the feedthrough.

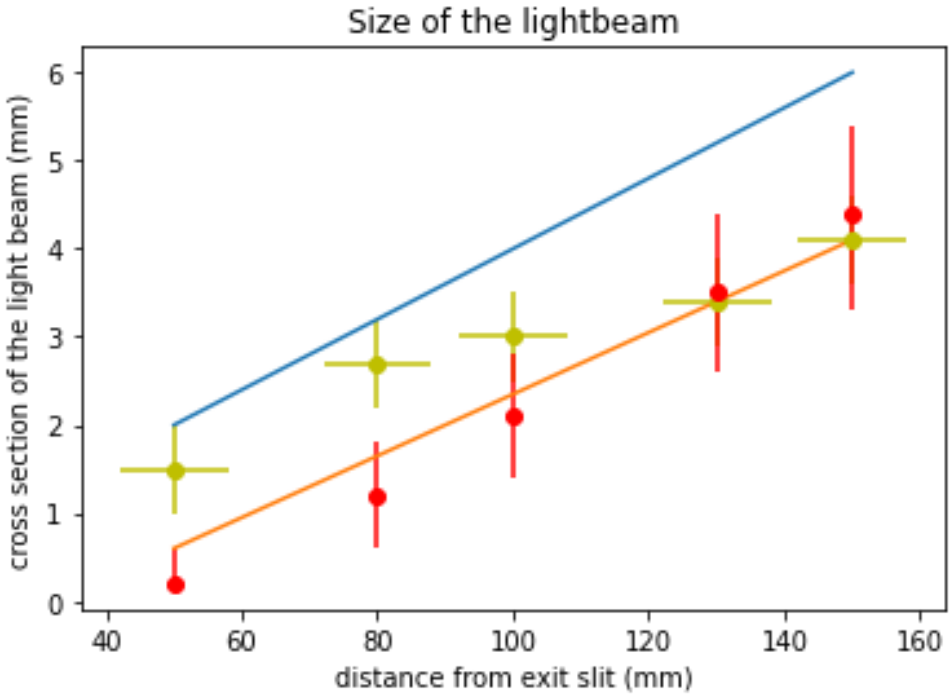

Figure 3-3: The width of the beam measured (yellow) and calculated (red). From the highest measured errors, a liner line (blue) is projected which will be used as the width of the beam. For a sense of idea on the rise angle on the calculated points, a fit of those points was plotted (orange).

The blue line from Figure 3-3 will be used to look at the size of the sample. This line is chosen because it is larger than the biggest measured or calculated point. From the measurements and calculations, it was found that our setup was in the diverging region. Being in this region brought the challenge of designing the sample holder and light sensor holder in such a way they are close to the monochromator and close to each other, without losing the rotational freedom to set the angle of incidence. The measurement data for the larger distances can be found in Appendix B. From these later measurements we found the size of the beam to be $7\ [\mathrm{mm}]$ at a location of $126\ [\mathrm{mm}]$ from the exit slit. All measurements were done with the exit sit of the monochromator opened to its maximal slit size.

Figure 3-4 shows how this beam of light would hit a schematic representation of the sample. Using a script, the maximum angles to which the sample can rotate before part of the beam misses the sample is calculated. Here it is important that the sample is large enough to maintain rotational freedom in reference to the beam, but small enough so it will lose its rotational freedom in reference to the sample chamber. Because of these analyses and calculations, it was decided for ease of calculation to place the face of the sample tangent to the line in the rotation centre.

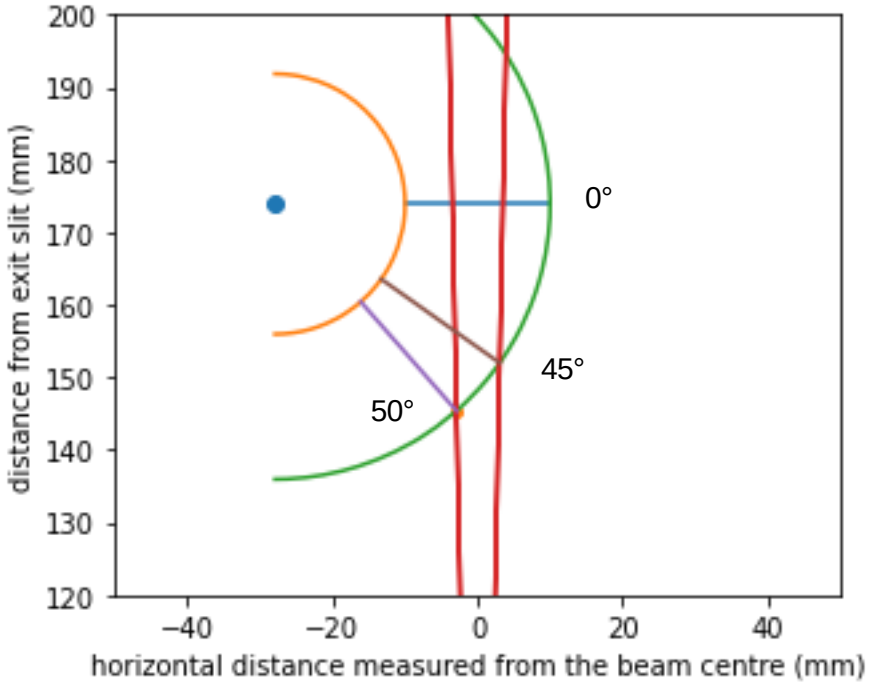

Figure 3-4: The face of the sample drawn in three different positions, to find the most extreme rotation angle before part of the beam starts missing the sample.

From these analyses, it was found that the optimal width of the sample face should be around $3\,[\mathrm{cm}]$. This left enough rotation to go from a full transmission measurement to a reflective measurement, with a maximal angle of $45°$ for the reflective measurements. Information about the beam, the centre of rotation, and the maximum width of the sample now become design restrictions and constrain the design in section 3.3.

3.2 Heat transfer capability calculations

Before even looking at a new design for the sample holder, some back off the hand calculation must be made to get a better understanding of the thermal conductivity. In a previous project it was decided to make the sample holder from copper [40], but the material for the sample mount was still free to choose. The easiest material would be PTFE because the workshop had it on stock. We also investigated TORLON which is a polyamide-imide, because of its thermal properties and performance in vacuum. What we needed to know is which of these materials would be able to thermally isolate the sample holder from the feedthrough as mentioned in section 2.4. And if the isolation is not good enough how we would implement thermal isolating geometry.

A quick and easy indication into the thermal properties of both materials is, to calculate how long it takes to cool down the sample mount. We start with the sample at $-100\,℃$ and the sample chamber at $20\,℃$, and the sample only increasing its temperature 4 degrees Celsius. These constrains led to the following calculations, starting with the internal heat Q.

$$Q = V \cdot \rho \cdot C_p \cdot dT \tag{4}$$

The copper on the cold side has a volume $V = 1.8 \cdot 10^{-5}\,[\mathrm{m}^3]$, and may only change $dT = 4\,[\mathrm{K}]$, it has a heat capacity $C_p = 0.39\,[\mathrm{KJ}/(\mathrm{kg\,K})]$, and a density of $\rho = 8940\,[\mathrm{kg}/\mathrm{m}^3]$.

Using equation (4) together with the properties of copper we find we can store $251\ [\mathrm{J}]$ of heat in the copper sample holder.

We then look at the thermal conductivity, the temperature gradient for the sample mount is $dT = 120\ ℃$ from $-100\ ℃$ to $20\ ℃$. The heat must travel a distance of $dx = 0.06\ [\mathrm{m}]$ through a cross-section area of $A = 1.77 \cdot 10^{-4}\ [\mathrm{m}^2]$. The different properties and results for PTFE and TORLON will be given in Table 1

Table 1 The material properties of both PTFE and TORLON as well as some results from the calculations.:

	PTFE	TORLON
Thermal conductivity (k)	$0.25\ [\mathrm{W/(m\,K)}]$	$0.36\ [\mathrm{W/(m\,K)}]$
Density (ρ)	$2.16 \cdot 10^3\ [\mathrm{kg/m^3}]$	$1.6 \cdot 10^3\ [\mathrm{kg/m^3}]$
Heat flux (q)	$0.09\ [\mathrm{W}]$	$0.14\ [\mathrm{W}]$

Using equation (5) to calculate how much energy can flow through both materials, the results can be found in Table 1. We can lose the minus sign in the equation because we already considered the direction of heat flow. So, we calculate the heat flux q using:

$$q = \frac{dQ}{dt} = -\frac{dT}{dx} \cdot k \cdot A \tag{5}$$

And then a simple calculation as shown in equation (6) to calculate how long it takes to max out the heat storage on the copper with the two different thermal conductivities.

$$t = \frac{Q}{q} \tag{6}$$

This gives us that the TORLON can isolate the sample holder for 30 minutes and 44 seconds, while the PTFE can do it for 44 minutes and 16 seconds. This is way longer than we need from the material. Therefore, we will not need any complicated geometry for thermal isolation and only the material itself will suffice.

3.3 Sample holder design

The next big part of this experimental setup will be the position, way of mounting, and rotationally manipulating the samples to be measured. Next to the constraining requirements mentioned in 1.3.1.2 and the temperature constraint introduced by the rotary feedthrough and pressure sensor. The placement and way of manipulation is mostly determined by the beam of light and its properties. The light beam generation, way of filtering the light, and oxygen-free environment for the sample are decided upon. These three points make how the light enters the sample chamber and can be used to decide the position and placement of the sample holder and light sensor array.

The starting point of the sample holder design is built on a design off Jeroen van den Borgh a student working together with Dr. Tina Pollmann before my project. The designs from that project form the basis for our VUV experiment. That same project already found copper to be the best material for the sample holder thermal and vacuum properties, therefore we will not investigate this further.

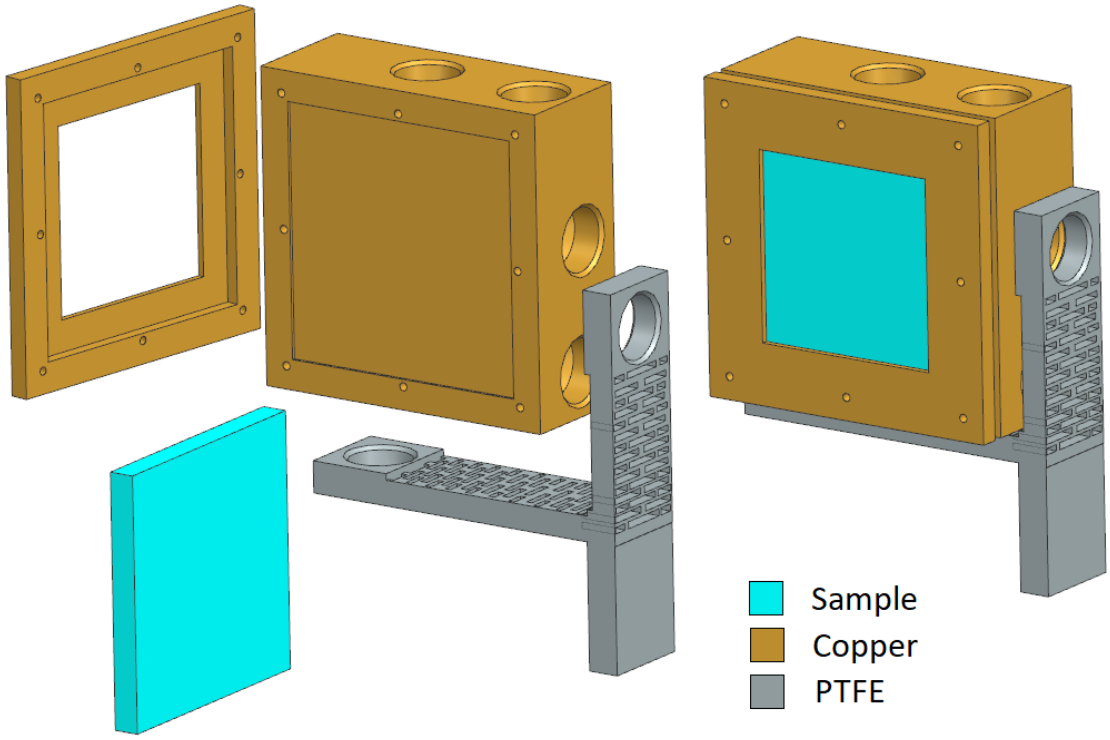

Figure 3-5:Sample holder design from Jeroen van den Borgh, the basis for the designs of the sample holder and the sample holder mount thermally isolating the sample from the chamber [40].

His design did consider the thermal isolation, but he did not investigate this property in detail. And therefore, used a complicated geometry, which we will try to simplify. Furthermore, was this design for accepting different sample thicknesses over complicated in use, prone to making mistakes, and therefore not adhering to the ease of access and simplicity requirement of the overall setup.

So, the points on which his design must be improved are, having space for two samples instead of one, investigation into thermal properties is done to simplify the design of the sample holder mount connecting the sample holder to the sample chamber, and simplify the system for different sample thicknesses.

To simplify the calculations and measurements for future checks and changes, the new design will also have a relocated position for the face of the sample. In the new design the face of the sample will always be along the normal of the rotary feedthroughs centre point, see section 3.1. This way there will be no offsets or weird corners when calculating on rotations and angles of incidence of the sample face.

With the design as shown in Figure 3-5, the orientation of the sample holder and the detectors is shown in Figure 3-6.

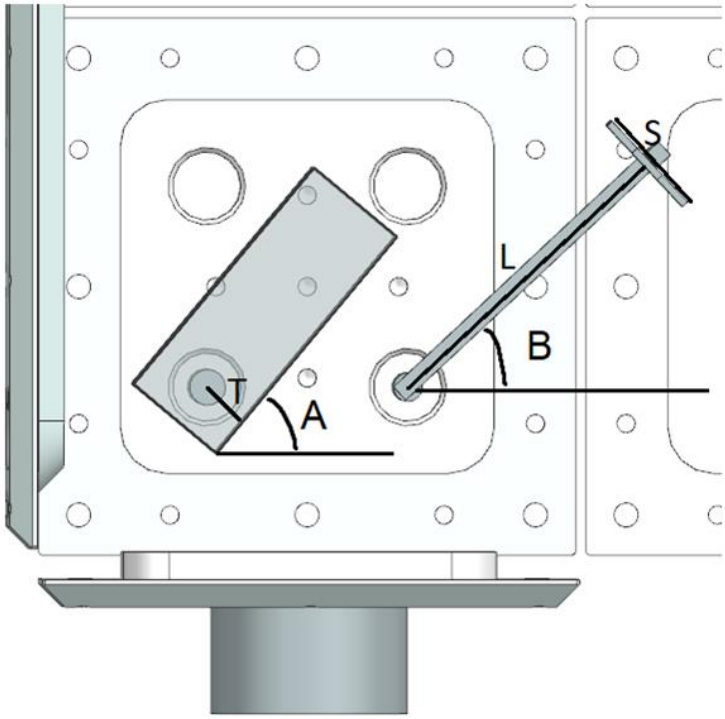

Figure 3-6: Sample holder and detector array orientation as per the old design. Were the sample holder is placed in the bottom left corner, and the light sensor array is place in the bottom right [40].

The first adjustment of making the holder suitable for two samples can become a simple copy and paste, mirroring the current design about its rotational axis. This larger sample holder needs to be moved to a different feedthrough, to prevent the sample holder from colliding with the sample chamber walls. The light sensor arm will also be moved, this such that the path length of the light will stay the same in both the reflection and transmission measurement. This will give the best chance of the same size beam at both measurement positions. This non-collision requirement we just introduced, will require a minimum arm length for the light sensor array, section 3.4. This leads to the orientation in Figure 3-7.

This doubled design, the restriction of space, and the size of the sample from section 3.1. Give that the sample holder must be $46\ [\mathrm{mm}]$ wide. To facilitate the bolts to clamp the sample to the holder. The thickness of the bottom part of the sample holder is given by the screw point to connect the sample holder to the mount. Making the final dimensions of the sample holder $92\ [\mathrm{mm}]$ long, $40\ [\mathrm{mm}]$ high and with a thickness of $18\ [\mathrm{mm}]$. See Appendix C for technical drawing. These dimensions will both be used in the design of the sample holder as well as the sample mount. And with these dimensions' samples of $3\ [\mathrm{cm}]$ by $3\ [\mathrm{cm}]$ can be installed.

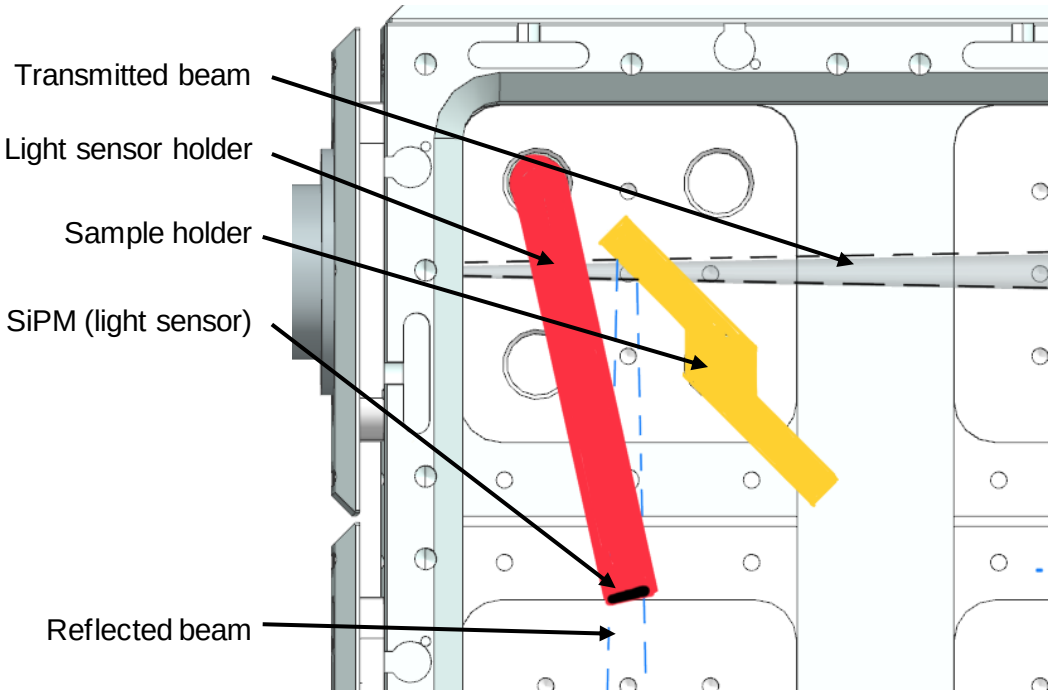

Figure 3-7:The orientation of the different objects within the sample chamber as per the new design. Placing the sample holder on the feedthrough as far as possible from any wall, as well as the light sensor holder having an equally good reach to both the reflective and transmissive measurement.

Next the simplification of the connection between the sample and sample holder will be designed for ease of access. But the design will also have to make sure the face of the sample where the light hits is always the same distance from the light source. This is an important requirement to ensure no other parameter than the thickness of the sample will change when we switch the sample to a sample with a different thickness.

And lastly the mount, which will thermally isolate the sample holder from the sample chamber. Instead of copying this intricate grated design, the decision was made to look more closely into the thermal properties of the system as liquid nitrogen will be used in future experiments. The specific calculations and assumptions can be found in section 3.2. It was found that the material of choice was good enough to thermally insulate the sample holder from the sample chamber. Therefore, the design is simplified by using the materials in their factory fabricated forms, not introducing any difficult geometries.

Looking at the simplification any further raises the question if it is needed for the mount to have a certain shape or form. This is an interesting piece of information, given that the workshop has only rod-shaped material in stock. So, to reduce the time needed for the workshop too manufacture these parts, the design will keep as many as possible parts rod-shaped.

This led to the design of the sample mount having a simpler structure on its connection to the sample chamber, but because of the face of the sample always being on the normal the top will have a more complex shape. Material and time wise it was favoured to fabricate these two parts separate and connect them together using poly-amide screws. This also introduced an extra boundary in favour of the thermal isolation.

Figure 3-8: The sample holder mount fabricated, assembled, and adjusted to fit the sample chamber.

The simplification of the sample mount left it still too thick for the feedthrough. This was fixed by shaving it down a few extra millimetres. See Figure 3-8 for an image of the assembled sample mount.

If we look at the requirements in section 1.3.1 the sample holder will need an easy way of mounting samples, the sample holder needs to house two samples this has be explained before, and it needs to cool the sample. These requirements together with the re-locating of the sample face location led to the new design as seen in Figure 3-9.

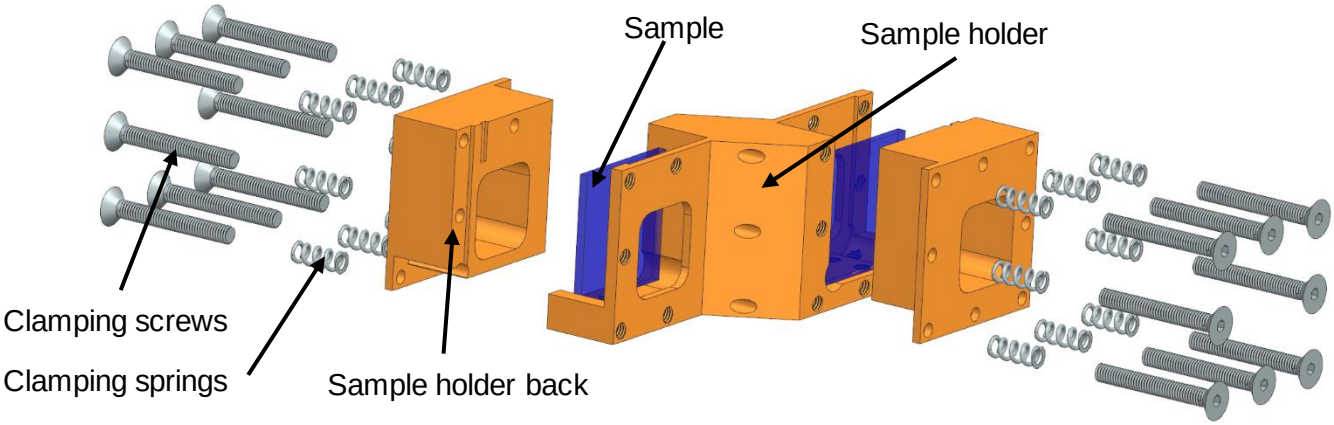

Figure 3-9: Exploded view of the sample holder design. With all the parts, screws, springs, backplate, and sample visible.

The requirement of cooling the sample was implemented by using a big copper block. This way the sample holder would have enough thermal mass to cool the sample. We cannot use any grease to improve the thermal contact between the sample and the copper. Therefore, the sample is clamped against the sample holder using springs. This ensures that if the sample changes size due to the lower temperatures the springs keep pressure on the sample ensuring a good as possible contact. We figured the best way of figuring out the correct spring, would be to test different strengths. Because the spring may not interfere with the easy installation of the sample but is needs to ensure a good contact between the sample and the copper. We therefore we acquired two types, one set with a spring force of $2\ [\mathrm{N}]$, and a second set with a spring force of $17.3\ [\mathrm{N}]$. The difference between the two is significant, with the goal of getting a better understanding of this method for clamping the sample. In this clamping we also decided to notch out a slit for one of the temperature sensors, this way it can be pressed against the sample giving a better insight into the temperature of the sample. This clamping also made the installation of a sample into the holder easier, with more space to do so.

Having a sample holder mount and a design for a sample holder, we need to check the accessibility. We will test if placing the sample holder assembly inside the sample chamber is possible. And if the sample holder will leave enough room for operators to uses their hands to manipulate tools and screws with enough ease that the assembly will be workable inside the sample chamber. Using a mock- up of the sample holder assembly it was found that the design as is, left enough room for hands and tools to work on the sample holder. This resulted in the fabrication by the workshop, the final product can be seen in Figure 3-10.

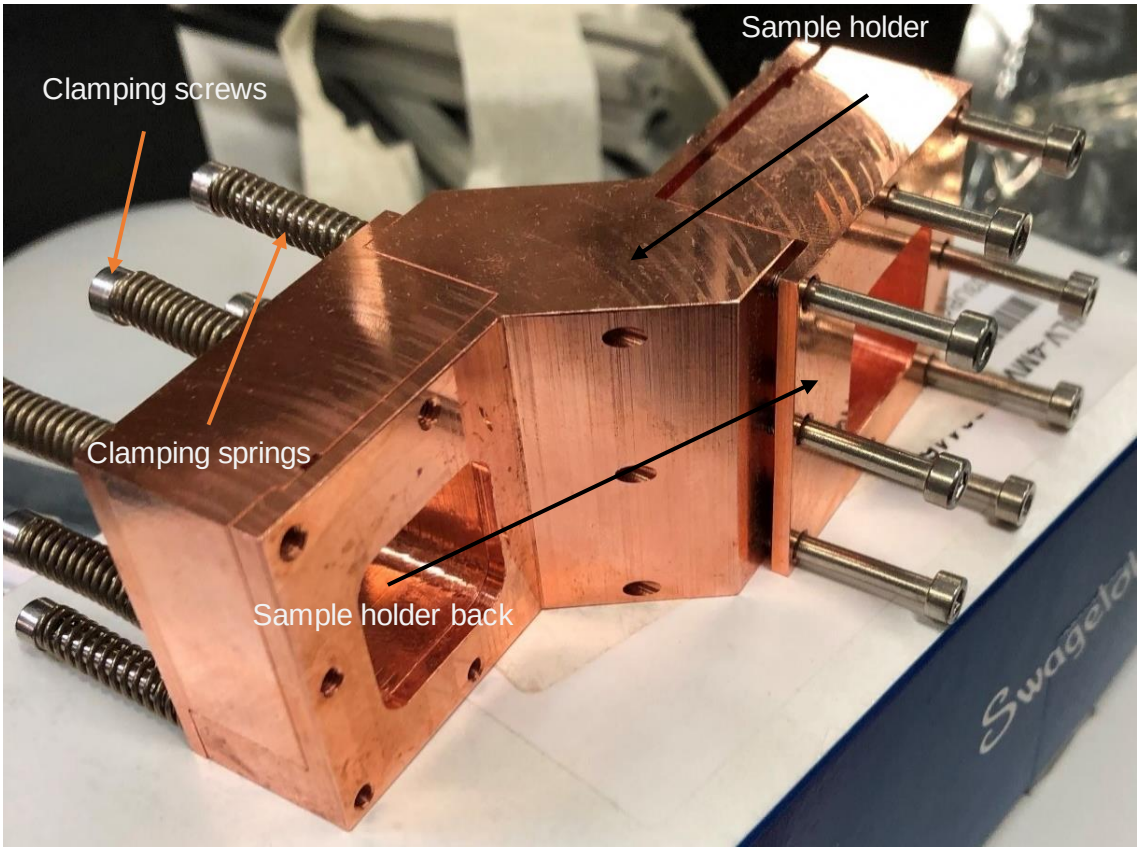

Figure 3-10: The sample holder fabricated and assembled without mount, one side with springs, one side without.

3.4 Light sensor holder

As was mentioned in 1.3.1 we need to be able to measure absorption and reflection of light on a sample. And in 1.3.2 I already briefly touched upon our biggest challenge will be the placement of the light sensor. We need to measure two different things, transmission and reflection, and the way the experiment is build these characterization measurements need to happen in two different places. Next to these two places we also want to be able to measure the diffuse reflection as a function of the angle. The easy solution is placing multiple light sensors in both locations, and the easy answer is that light sensors are too expensive. So, we need to be able to swivel the light sensor from one to the other locations, this was already in Jeroen his design Figure 3-6.

Unfortunately, we cannot rely completely on the design from Jeroen. With redesigning the sample holder, we moved the sample holder to another position. In Jeroen his design the arm holding the light sensors never need to cross the point where feedthrough connects to the sample holder, but in my design it does. The only way of crossing is by going over the sample holder with the arm. This way we would keep our flexibility of moving the light sensors while there is a vacuum using the feedthrough.

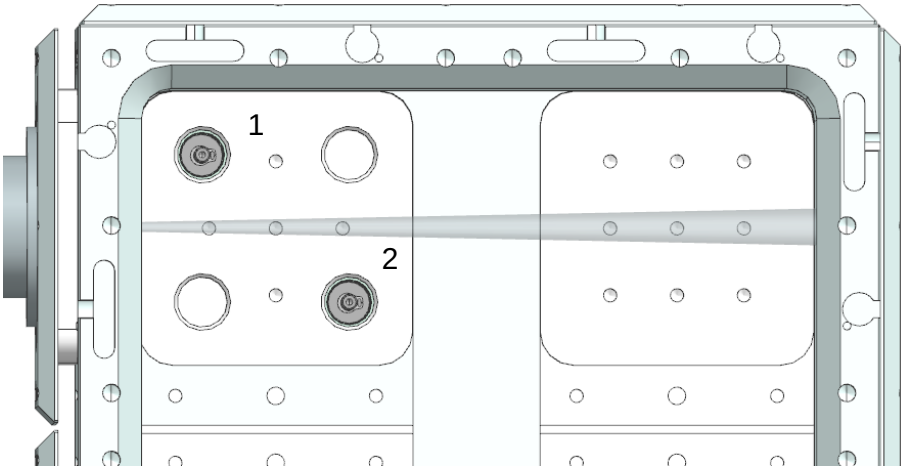

Figure 3-11: Schematic drawing of the sample chamber. The two rotary feedthroughs which will connect to the light sensor (1) and sample holder (2) are visible. Also visible is a mock-up of the light beam from which we calculated the width.

The schematic shown in Figure 3-11 is used to find the width of the beam at certain positions in the chamber. This is important because of the limited photosensitive area of the light sensor described in 2.4. And we want to capture as much of the beam as possible to make sure as little as possible photons miss the light sensor. Due to low light intensity and having light that is easily absorbed by other materials, we are measuring on a photon counting level. Therefore, it is important we can measure every possible photon that travels in the direction of the light sensor.

Measuring in the sample chamber with light from the deuterium lamp and calculating the width gave us an average beam with of $7.4\ [\mathrm{mm}]$ at the face of the sample, see Appendix B. And we have a photosensitive area of $3\,x\,3\ [\mathrm{mm}]$. So, we need to think of a convenient way to place multiple light sensors together, this would also be the case with the larger $6\,x\,6\ [\mathrm{mm}]$ model. The light is supposed to be a limiting factor but in the current configuration we cannot comply to this, therefore the only limit will be in the freedom of rotation.

Because the light sensors are so expensive and fragile, I need to make sure that no matter what the position of the sample holder, it will never collide with the light sensor holder. This was easily solved by measuring the length between the rotation centre of the light sensor holder and the sample holder and find the highest value. Making sure the senor arm is longer than that maximum value ensures a free movement of the light sensor, this will be the lower limit of the light senor arm and was found to be $130\ [\mathrm{mm}]$. And because we want to keep the light sensors as close as possible to the sample, we use the $130\ [\mathrm{mm}]$ with an extra $5\ [\mathrm{mm}]$ off safety margin.

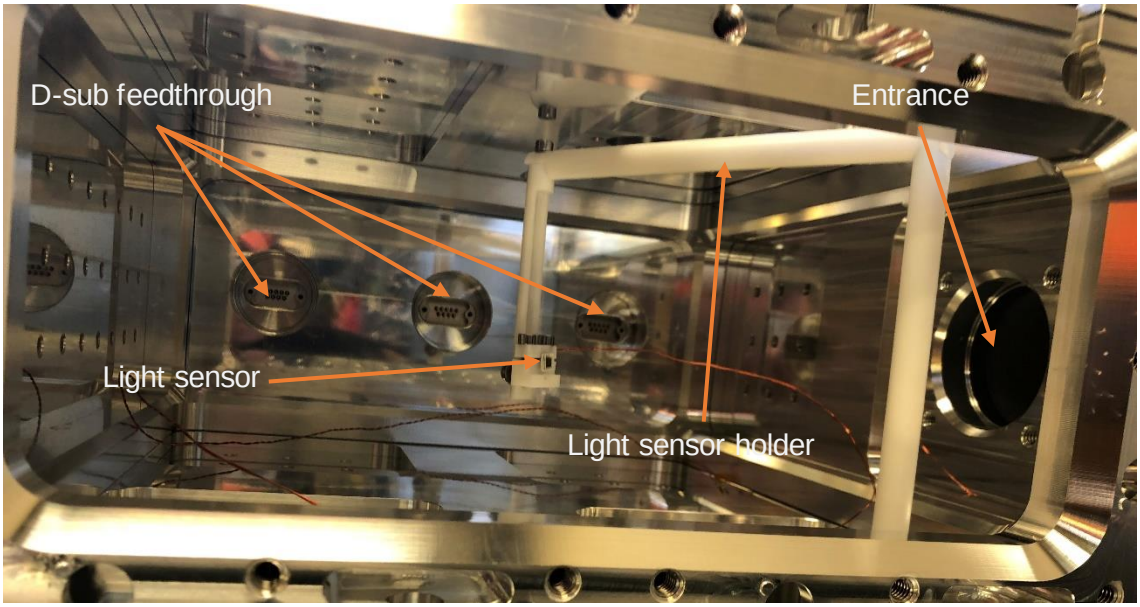

Figure 3-12: The sample holder as designed in Appendix A. The light sensor holder is installed in the sample chamber equipped with a light sensor (SiPM).

Knowing that the amount and geometry of the light sensors placed in the experiment will change in the future. Thus, this holder was designed in such a way individual parts can be replaced to accommodate such changes in the future. Taking time into account we decided to try and make the system work with one light sensor. And because of testing we want to be able to easily place and take out the light sensor. The time and testing argument made me look at this design problem different than all the previous designs, instead of think what do I want with this design and then what do I need for it, I started with what we have available. The workshop had some $10\ [\mathrm{mm}]$ PTFE rod, and I decided to design my light sensor holder around that $10\ [\mathrm{mm}]$ rod, see Appendix A for the design drawings.

3.5 Table

The experimental setup has been designed around being modular. The table that will house the experiment should therefore also be modular, such that any changes to the experiment in the future do not lead to a new table. It was clear early in this process that the table would have to be designed and assembled by ourselves. We had seen in other projects this standardized table/ cabinet building sets. Here we would design the table with the materials available from the manufacturer and they would deliver everything cut to the correct length with the correct fasteners. This resulted in the design as seen in Figure 3-13. It was order at ITEM, a company suppling these premanufactured parts.

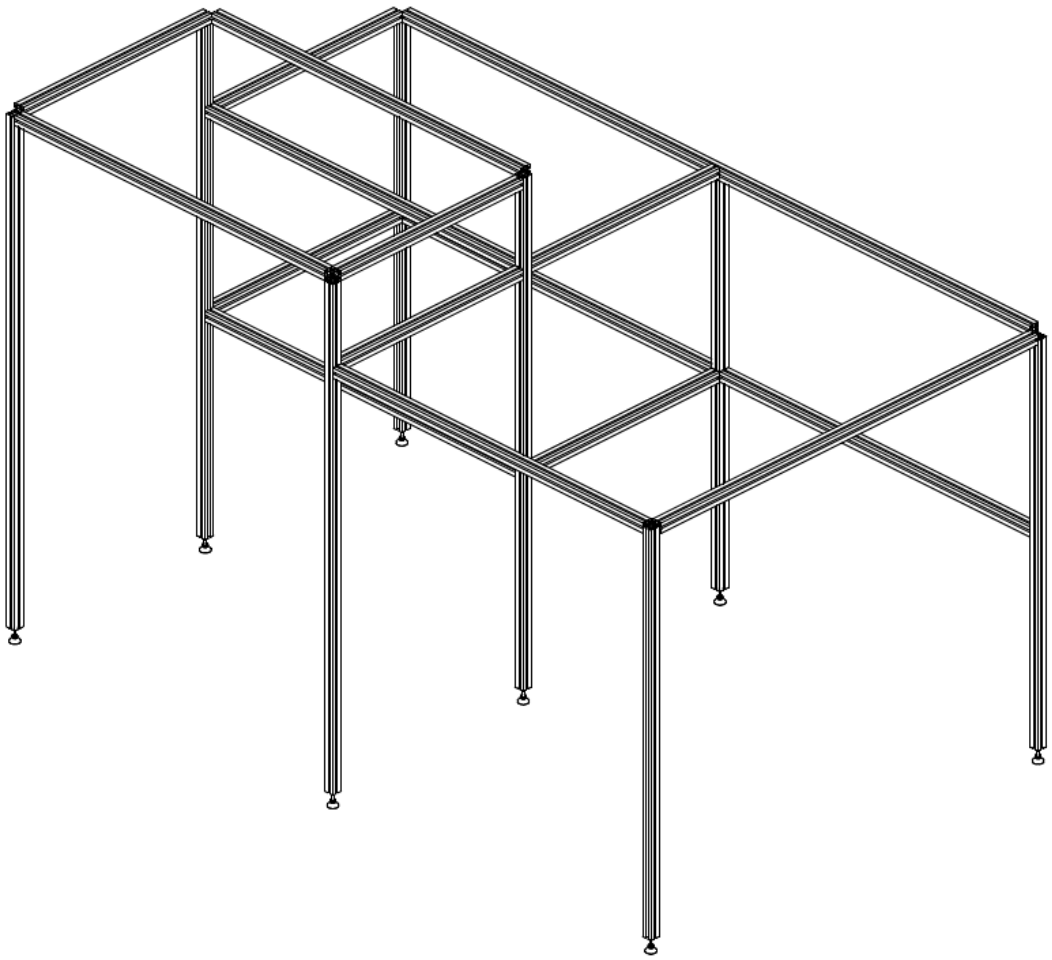

Figure 3-13: The table for the experimental setup as designed per our requirements with premanufactured standardized materials.

Having multiple options for the thickness of the beams we asked advice with the ITEM sales team on what we would need in our setup. Due to the weight and size of our experiment the advice was profile 5 with the cheapest corner fasteners. This was the cheapest, easiest, and most modular table we could find. The profile 5 is a $20\ x\ 20\ [\mathrm{mm}]$ beam and the cheap fasteners were of a kind we had not seen before, see Figure 3-14 and Figure 3-15.

Figure 3-14: The profile 5 beams of $20\ x\ 20\ [mm]$ with the original fasteners. In the image is visible how this looks like when all is installed.

Figure 3-15: The table fully assembled as per design with all the original parts.

After the table was assembled, we concluded that it was not sufficient to support the experiment. Appling a sideways force, as one would by hitting the table on accident, would result in extreme wobbling off the table. Fixating the tabletop to the frame did not solve the wobbling problem and the decision on fixing this frame or go for a completely new table with a larger profile size had to be made. It was decided that a new table would be too big of a project expense. Therefore, we added corner supports and additional beams to improve the rigidness of the table. In the outermost corners we added large bookshelf supports, making the outermost table legs sturdy. Also, extra small 90° brackets were added on all other corners, often replacing one of the original connections. This gave the frame enough stiffness to stop the wobbling and pass the health and safety inspections. See Figure 3-16 for the final assembly of the table.

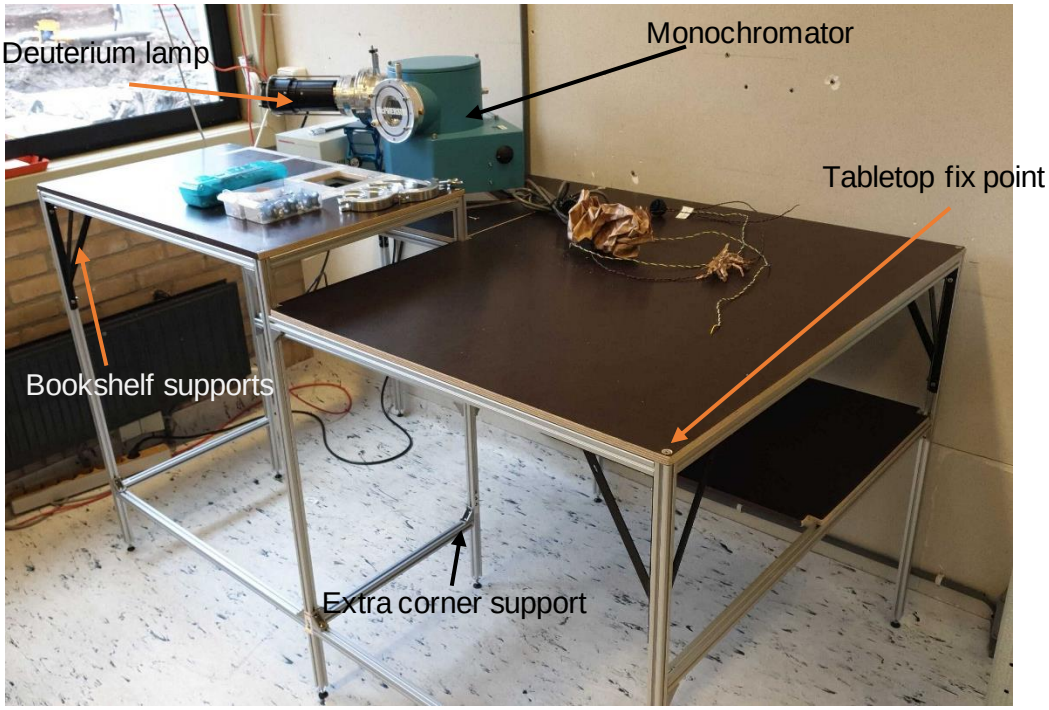

Figure 3-16: The final table assembly with all the extra supports installed. The monochromator has been put on the table to see how it would behave with extra weight added to the assembly.

3.6 Electronics

In the electronics department of our experiment, we decided not to try and reinvent the wheel. Dr. Pollmann had done a similar experiment at the Technische Universität München (TUM) with Andreas Leonhardt. We use a similar lamp, a similar monochromator, but different light detectors. The part we wanted to use from the TUM setup is the use of a Raspberry Pi together with an Arduino to control the monochromator to set the wavelength [41]. With having a Raspberry Pi in our setup, we decided to use this same device for data acquisition. This gave us the electronics as schematically seen in figure.

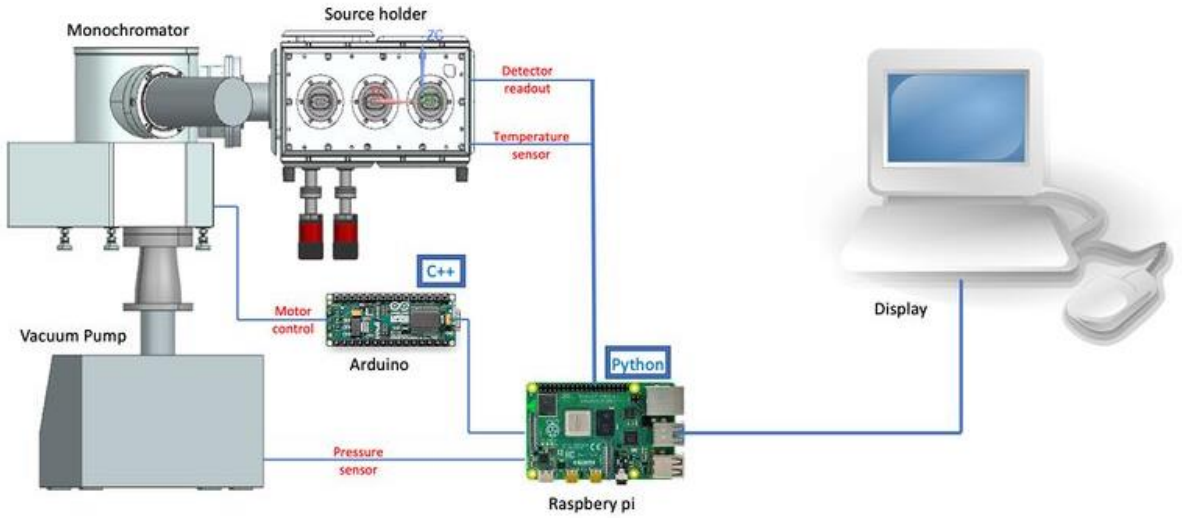

Figure 3-17: A schematic representation of the electronics in the VUV experiment. The Raspberry Pi will be used for both data acquisition and controlling the wavelength.

The Raspberry Pi used in the setup is a model 4 B 4GB with Wi-Fi and Bluetooth [42]. The Arduino used is an Arduino Nano 3.0 Atmega328 5V 16 MHz [43]. To control a stepper motor as installed in the monochromator you need a stepper motor driver. With this driver the Arduino can communicate to the motor. Using the manuals available to us with some research on the workings of stepper motors we managed to connect the build in stepper motor to the driver. To make future changes to the system easier we labelled all the cabling. The final assembly of the motor control can be seen in Figure 3-18.

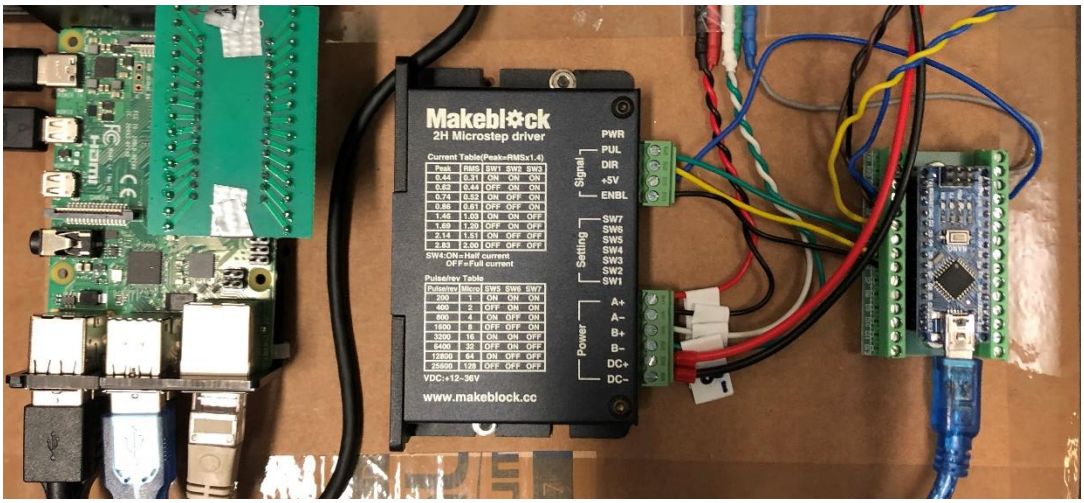

Figure 3-18: The electronics for the motor control with on the left the Raspberry Pi, in the middle the motor driver, and on the right the Arduino.

The motor driver we used is the MB 2H MICROSTEP, which is a 2-phse hybrid stepper motor driver. It was selected because we need a supply of $24\ [\mathrm{V}]$ to the stepper motor and the MB 2H MICROSTEP has a range of 12 to $36\ [\mathrm{V}]$ [44].

Using a Raspberry Pi to read out the sensors required a bit of investigation. The Raspberry has only digital connections, so compatibility solutions for the analogue sensors needed to be investigated. As mentioned in 2.5 the pressure sensor used is from Pfeiffer, the temperature sensors are PT100s and the light sensors Hamamatsu SiPMs. All having different ways of supplying the signal.

The Pfeiffer MPT 200 AR is programmed to send all its information using the USB protocol. Using the converter cables supplied by Pfeiffer the MPT 200 AR can be connected to the Raspberry Pi using USB, and the data values can be called upon but still need conversion into understandable pressure values.

To read out he PT100s we use a little voltage divider together with an analogue-to-digital converter (ADC). The ADC is needed for the Raspberry Pi to read the signal, because it only reads digital input and the ADC used is the Grove 4 channel 16 bit ADC [45]. The signal received by the Raspberry Pi represents the resistance value of the PT100 and using the standardized table for the PT100 resistance to temperature conversion we get a temperature value. See Figure 3-19 for the Raspberry Pi connected to the ADC.

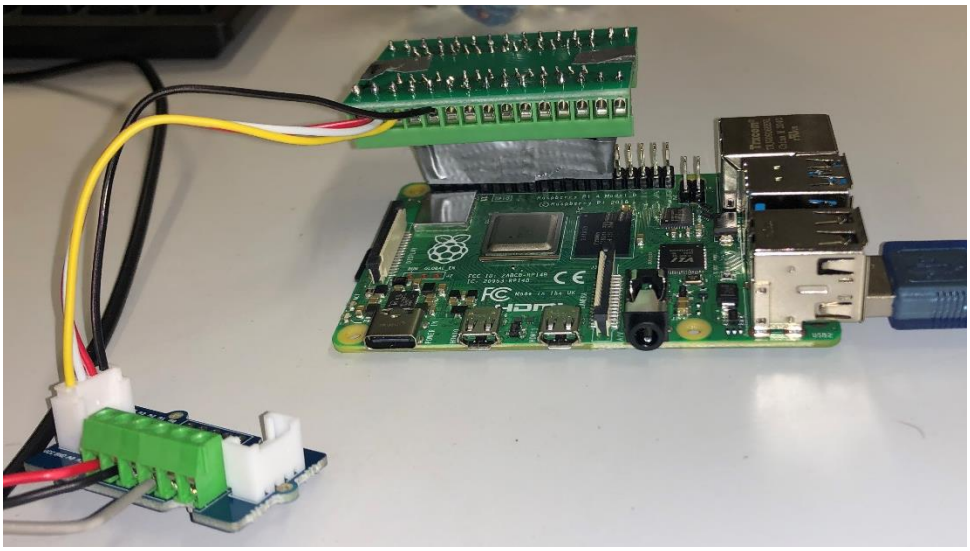

Figure 3-19: The Raspberry Pi connected to the ADC testing the signal received and accuracy of the converted temperature.

The Hamamatsu SiPMs have a somewhat similar connection as the PT100s. Due to the possibility of noise and figuring out the shape and speed of the signal we used an oscilloscope, Tektronix TDS 3034, to register the signal. The electronics surrounding the SiPMs is a bit more intricate, a high voltage supply is needed to reverse bias the SiPM, a low pass high pass filter combination to improve the signal, an amplifier, and data acquisition electronics. At first, we wanted to use the Arduino combined with the Raspberry Pi, but the speed of the Arduino is too low to be able to register the signals. During all the testing we therefore decided to keep using the oscilloscope.

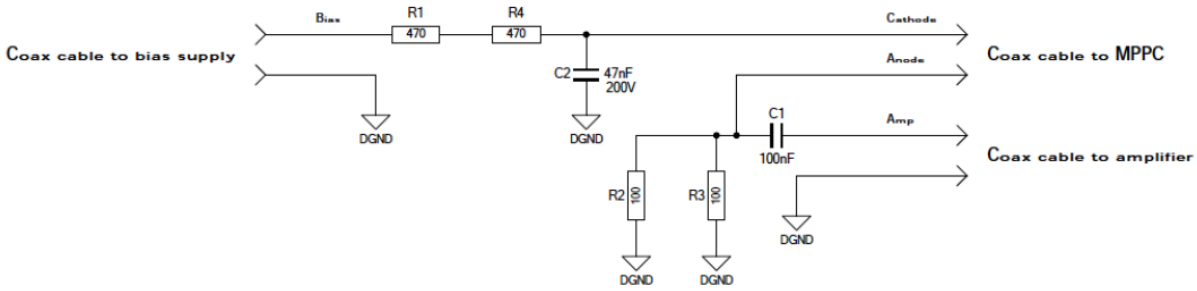

Figure 3-20: The filter circuit as used in the XAMS experiment in combination with SiPMs [46].

The filter shown in Figure 3-20 was designed by the colleagues of the XAMS experiment when they started to use the SiPMs. The high voltage power supply used is a Keithley 2410. For amplification we used what we had lying around in the lab, the mini circuit ZHL-32A+ voltage amplifier [47]. In Figure 3-21 the test setup is show, with the inside of the dark box shown in Figure 3-22.

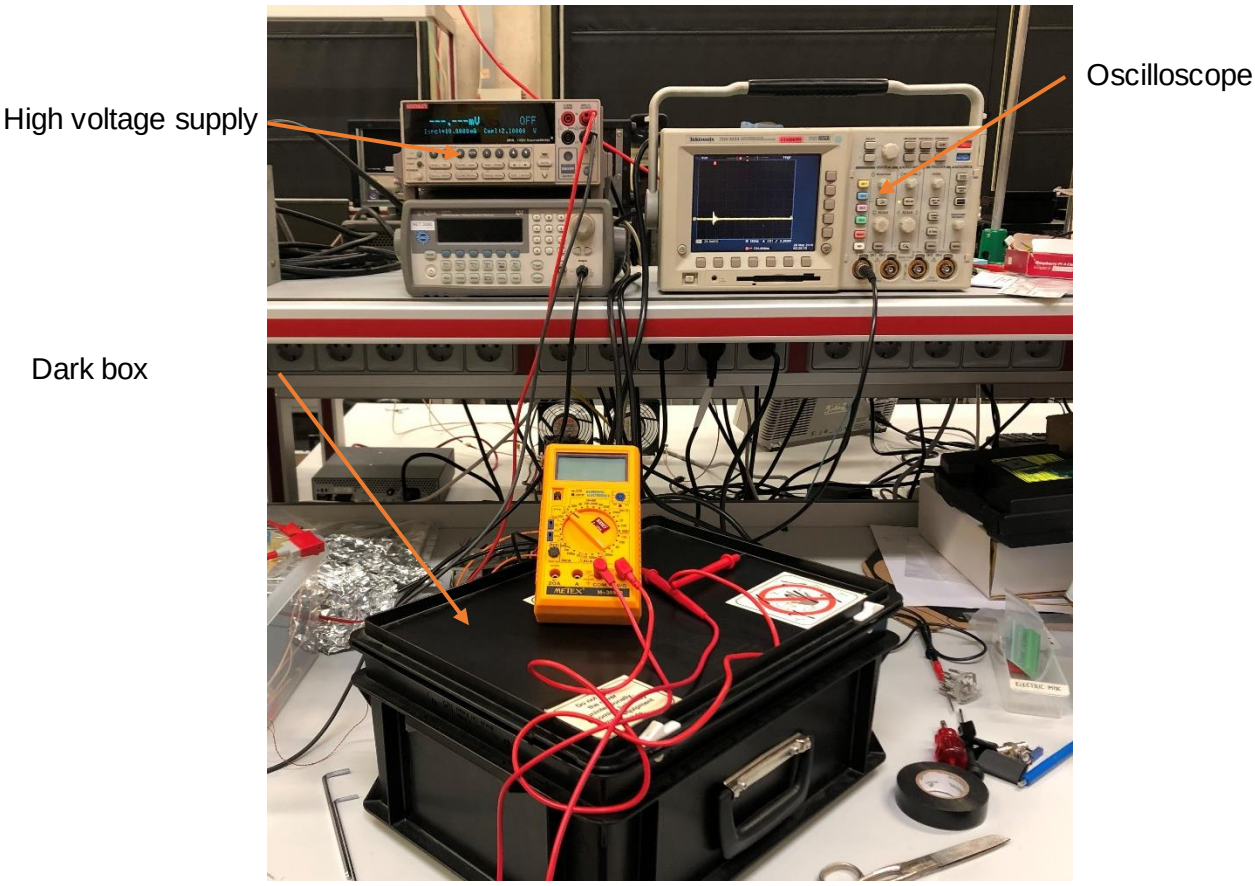

Figure 3-21: The test setup for the SiPMs, were we use a Keithley high voltage supply to bias the SiPM a mini circuit amplifier to amplify the resulting signal which will be detected using a Tektronix oscilloscope.

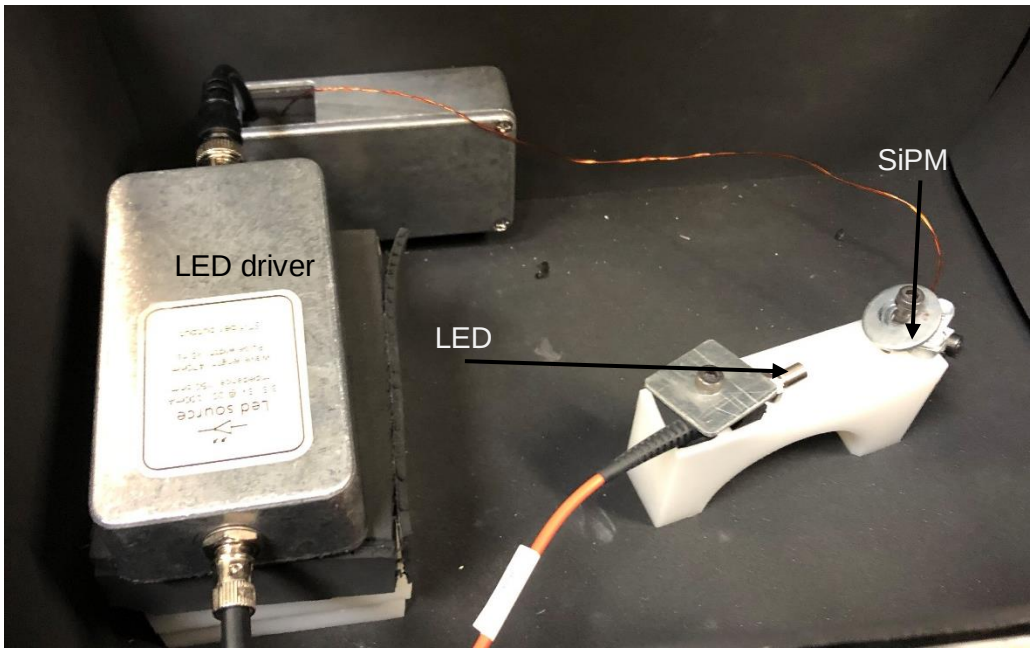

Figure 3-22: The inside of the dark box from Figure 3-21 in which we test the SiPM. Seen in the image a LED source to trigger the SiPM.

Connecting all the different sensors to the data acquisition turned out more difficult than originally anticipated. The first sensor to connect is the pressure sensor, this being the most straight forward connection with all its cabling already delivered from the factory. The RS-485 cabling with an RS-485 to USB converter plug into the vacuum pumping station and the Raspberry Pi.

The temperature sensors and SiPMs must cross the vacuum barrier. Taking requirement 7 in consideration from 1.3.1.1, all the cables inside the vacuum will be made from vacuum proof Kapton coated wire. And as a connector to the D-sub feedthrough 2.6 we use D-sub female pins, see Figure 3-23 for such a wire soldered to a PT100. Outside the vacuum we will use normal solid core copper wire on a D-sub connector, see Figure 3-24.

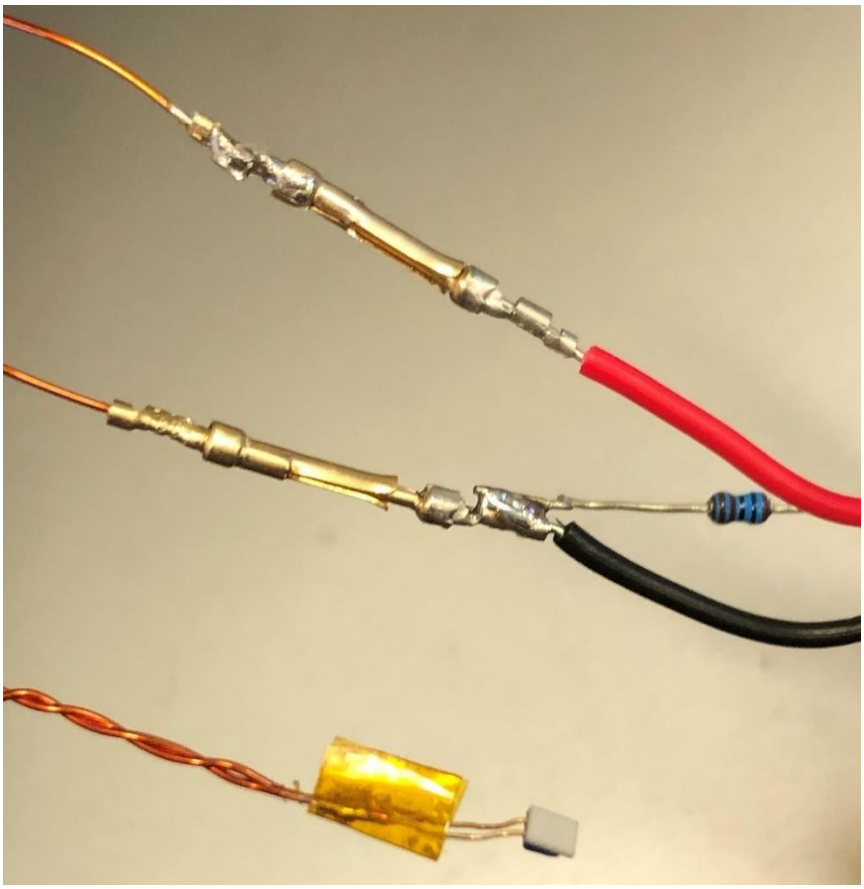

Figure 3-23: Kapton wire soldered to a PT100 sensor with D-sub female connectors. The connectors are connected to a test circuit to verify the cables are working.

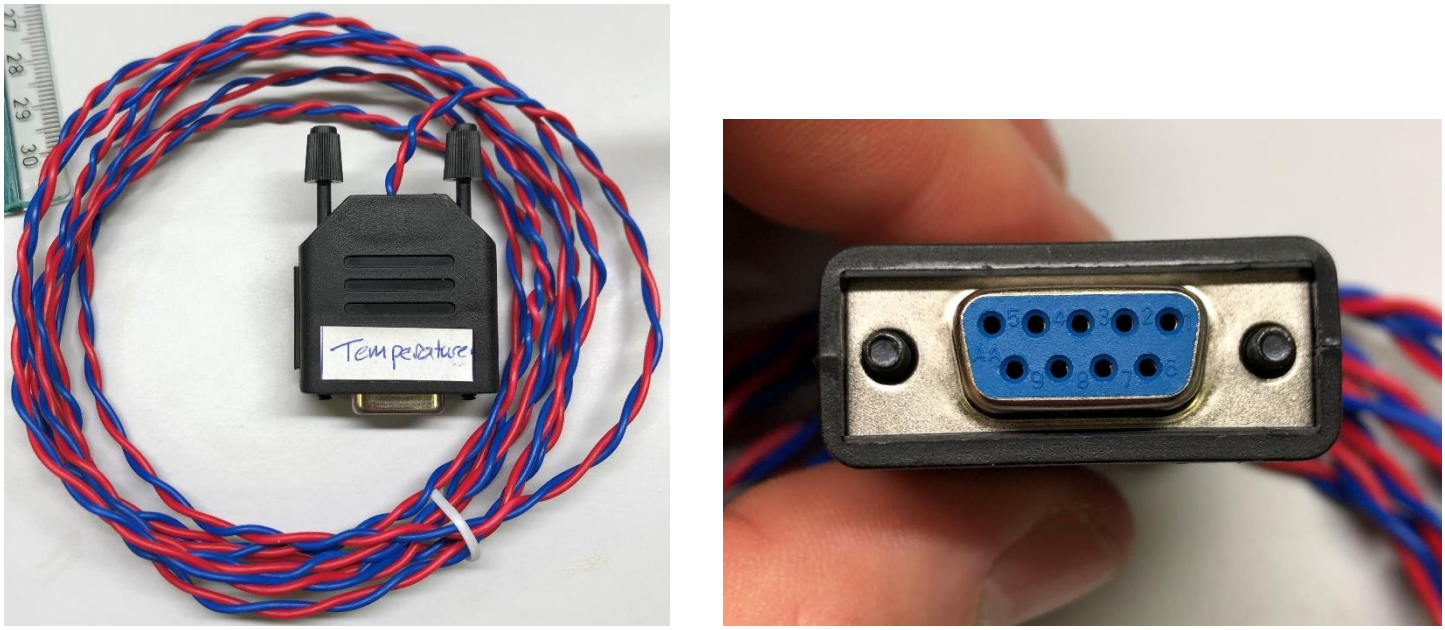

Figure 3-24: The fabricated cables as used outside of the vacuum. On the left an overall view of the twisted pair cable, and on the left a zoomed picture of what the connector looks like.

With the temperature sensors we do twist the wires, but not because of noise reasons. Twisting the wires creates a neater workspace around the experiment and with more sensors in the future with each a set of cables reducing clutter is a nice incidental.

With the SiPMs we started off on the same course as with the temperature sensors. Creating a Kapton wire for inside the vacuum and a normal wire for the outside, see Figure 3-24. But due to an impedance mismatch explained in section 4.2, we changed all the cables connected to the SiPM to be Kapton wire.

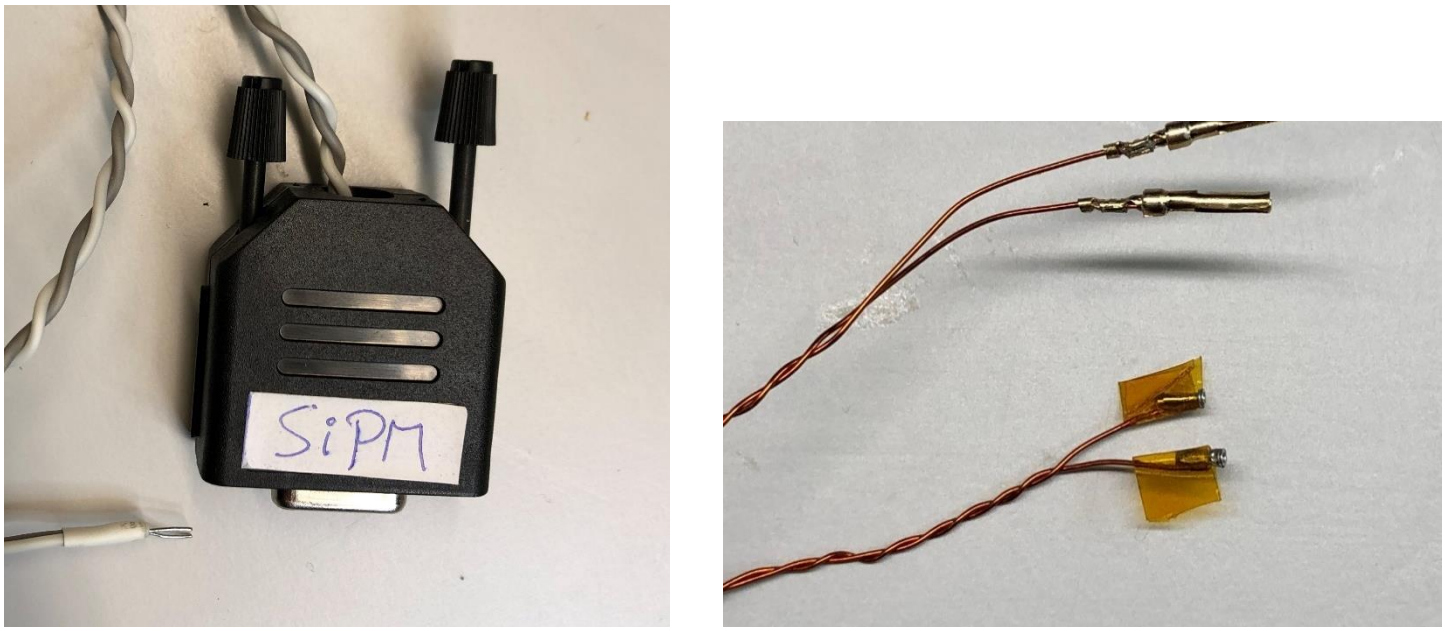

Figure 3-25: The initial set of wires for the connection of the SiPM to de data acquisition. On the left the connector and wire for outside the vacuum, and on the right the wire for inside the vacuum.

3.7 Redesigning prefabricated parts

As mentioned in the scope of the research 1.3.2, we do not know if prefabricated parts will be good enough for our modular setup. One of the mismatches between products was between the standardized KF standard on the vacuum chamber from Ideal vacuum and the nonstandard connection on the McPherson monochromator. Here McPherson custom fabricated an adapter, which unfortunately had to be adjusted by our own workshop to fit the O-ring seal. The original adapter without the grove for the O-ring is shown in Figure 3-26.

Figure 3-26: The original adapter made by McPherson. This adapter will enable us to connect their in-house nonstandard flange to the standardized KF flange on the vacuum chamber.

Considering requirement 4 in chapter 1.3.1.1 we want ease of access to the sample chamber. This way the swapping of samples will so less of time, such that we can change samples and do a characterization measurement on the same day. To enable this, we ordered prefabricated hinges from Ideal vacuum, these unfortunately did not work with all the adapter plates we installed to make our setup modular. Hence, we had to redesign the hinges to compensate for the extra space added by the adapter. To save time we decided to disassemble the hinges and remake only one side, this was easy because both sides of the hinges are mirror images of each other and therefore would always fit one of the two sides. The original hinge can be seen in Figure 3-27, the fabricated part can be seen next to the part it is modelled after in Figure 3-28.

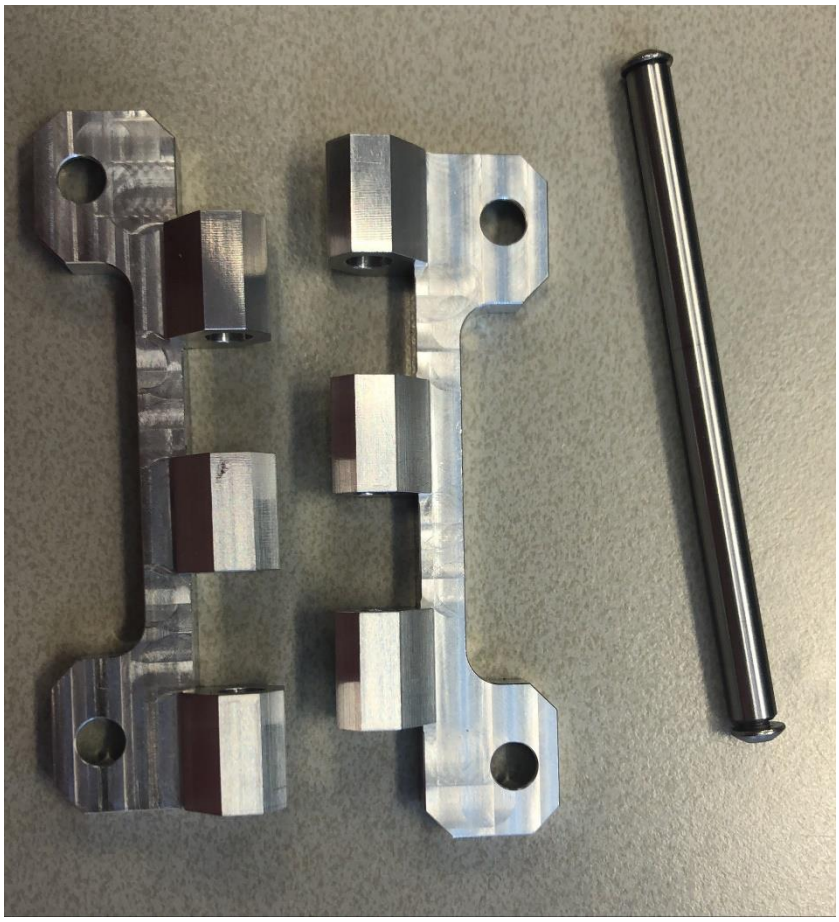

Figure 3-27: The original hinge as fabricated by Ideal vacuum. disassembled to test if we can remake only one side of the hinge.

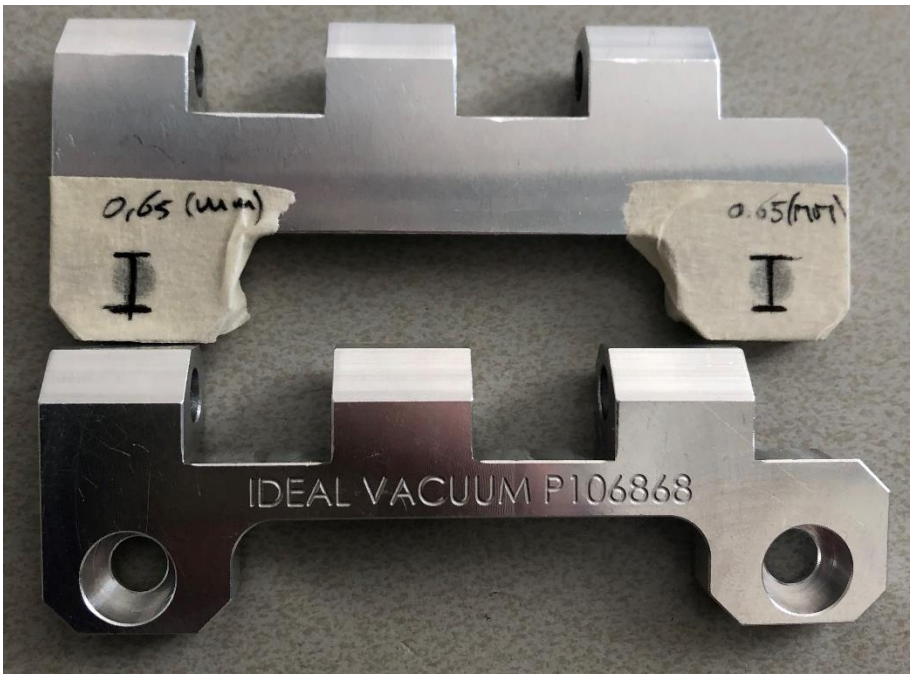

Figure 3-28: The remade hinge part next to the original hinge part of which our modified part has be based.

3.8 The pre-assembly cleaning of the vacuum system

Having a good vacuum starts with the proper cleaning of all the individual parts. The removal of oil residues reduces outgassing and a wipe down of the seals results in a better seal reducing the changes of a leak. Using an ultrasonic soap cleaning bath to remove the oil from all the metal and plastic parts. After this bath the parts are rinsed with demi water to remove any soap residues. And finally, the parts are baked in an oven to evaporate any water from small holes and nocks. After which the parts are wrapped in a thick aluminium foil to keep them clean until installation. The cleaning process can be seen in Figure 3-29, Figure 3-30, and Figure 3-31.

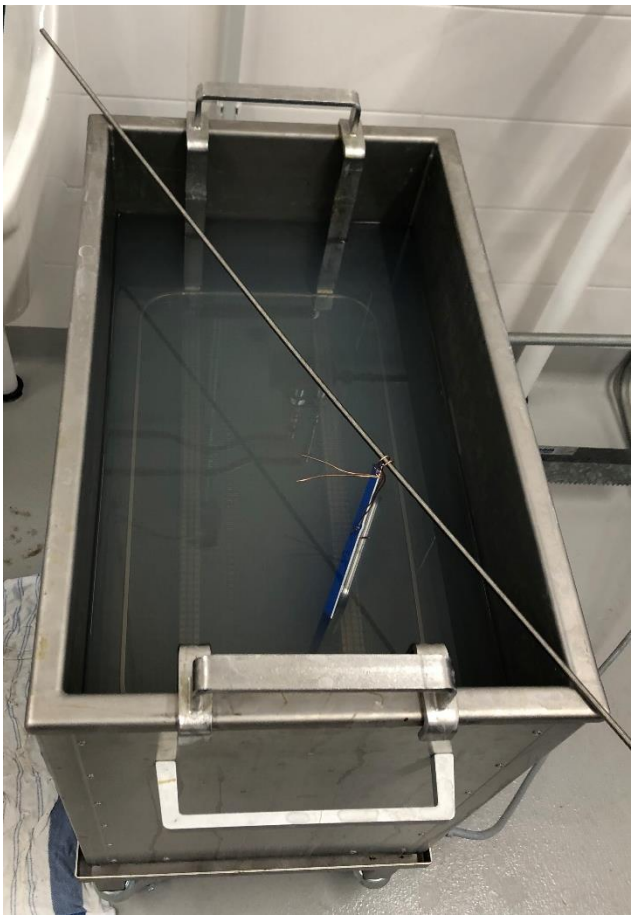

Figure 3-29: The ultrasonic soap bath used for cleaning all the plastic and metal parts of the VUV experiment. This cleaning was done in the workshop of NIKHEF.

Figure 3-30: The rinsing of the ultrasonically cleaned parts with demi water, to remove any soap residue left on the parts after the cleaning process.

Due to the renovations on the workshop at NIKHEF the ultrasonic bath with demi water was unavailable. This was solved by rising of the parts with demi water above the sink as a quick fix solution to refrain the project from delay. We gathered that using enough water with the addition of isopropanol for spots that were missed after drying it would be cleaned well enough for parts that came sealed from the factory.

During the baking process the door of the oven was kept ajar, that way the air in the oven would not saturate with moisture eventually slowing down this part of the process. After backing some of the soap residues became visible, isopropanol was used to clean those spots off.

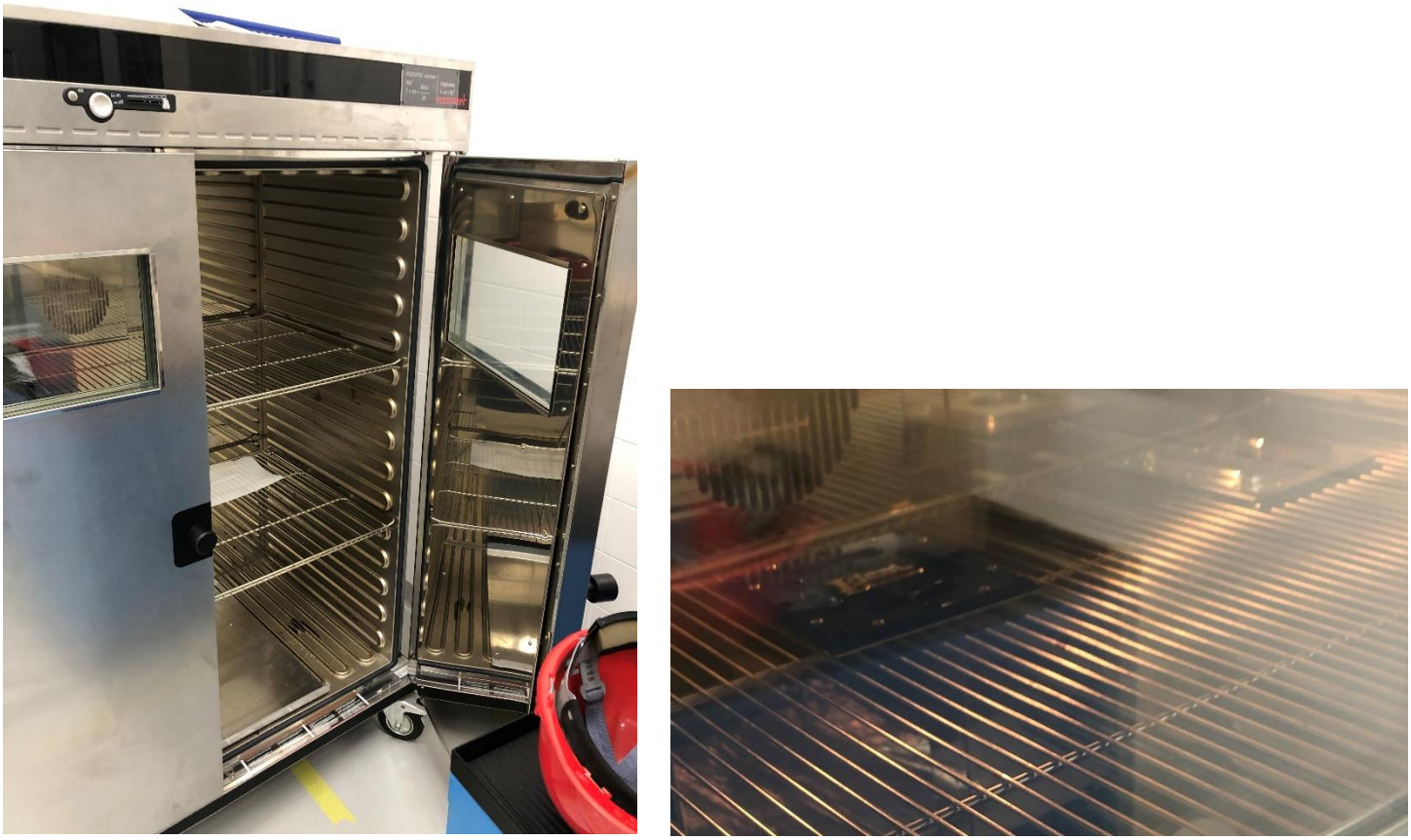

Figure 3-31: On the left an outside view of the oven used to bake the parts, on the right an image of parts being baked.

Figure 3-32: All the parts for the VUV experiment cleaned and sealed ready for assembly.

4 Results

During this thesis multiple different systems have been installed and need to be commissioned to make sure they work as per the set requirements in 1.3.1. The individual systems will be discussed resulting in multiple subchapters of results.

4.1 The vacuum system

To consider the vacuum system working properly it is required the system can maintain a pressure in the order $1 \cdot 10^{-5}$ [mbar]. This will fulfil requirement 2 in providing an environment without the oxygen absorbing light in the VUV region. The pumping of the vacuum was favoured to be as quick as possible, such that the time between switching on the pump and starting the first characterization measurement would not take significantly longer than 24 hours.

After assembling all the clean parts and double checking all the seals we got down to a pressure of $1.2 \cdot 10^{-4}$ [mbar], too high for any characterization measurement. A final check of all the screws and seals was done without disassembling the setup which resulted in a pressure of $7.9 \cdot 10^{-5}$ [mbar]. Looking at our requirements that is still not a good enough vacuum for a characterization measurement but good enough to commission the SiPMs, this was a decision necessary to keep the project going. The last pressure reading of a pump down run can be seen in Figure 4-1. The time it takes for the system to reach this low pressure is 31 hours, this is fast enough to barely fulfil the pumping time requirement.

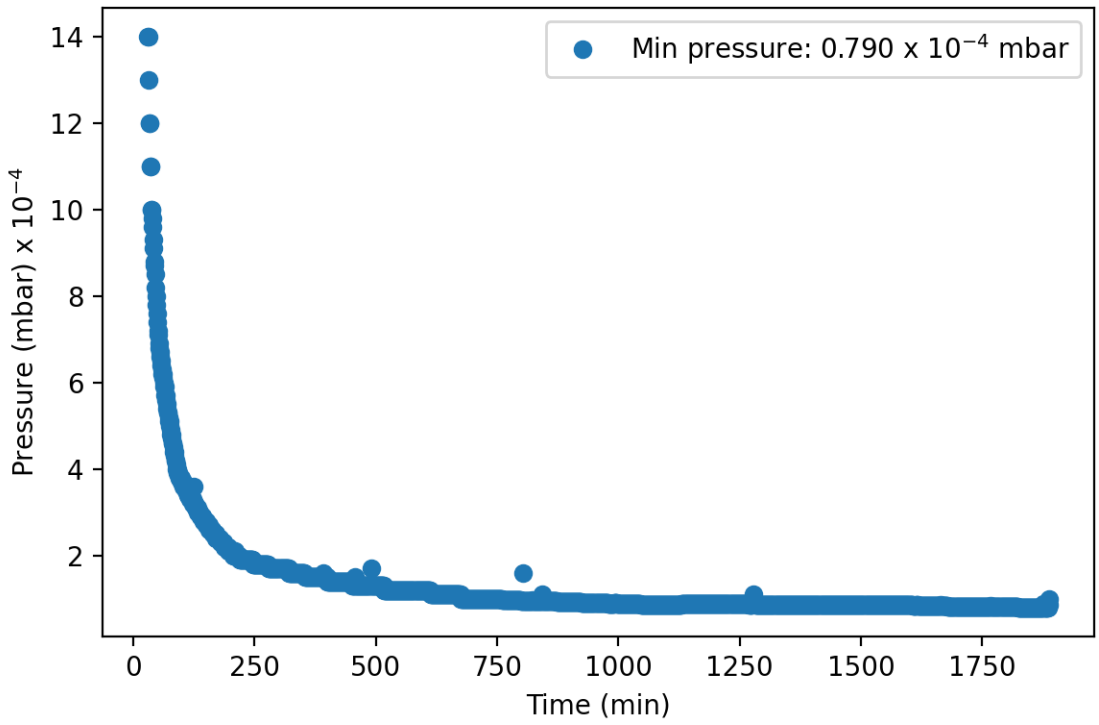

Figure 4-1: A recording of the pressure during the last commissioning run. Here we see the system can reach a vacuum of $7.9 \cdot 10^{-5}$ [mbar] in around 1875 minutes.

4.2 The sensors and their cables

Using the designed light sensor holder, chapter 3.4, and putting the monochromator in to full reflection mode. In full reflection mode the monochromator reflects all the wavelengths which means also all the light in the visible spectrum. This enables us to align the light sensor with the beam of light, see Figure 4-2.

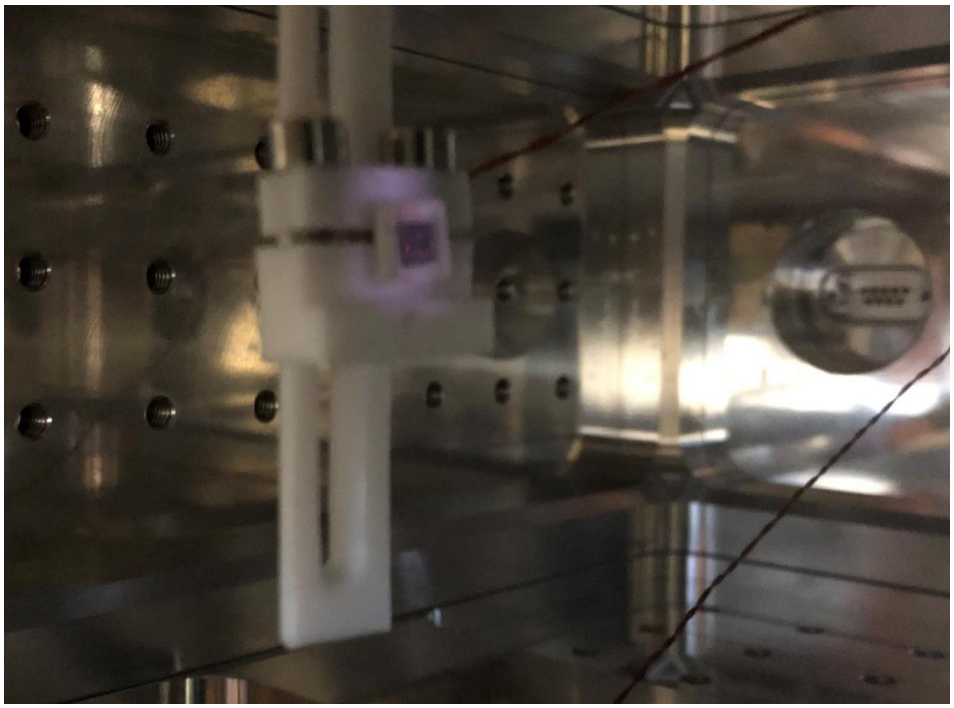

Figure 4-2: The light sensor is placed in the beam of light, using all the height adjustment slit on the light sensor holder. The light is visible on the sensor because the monochromator is in full reflective mode, reflecting every wavelength.

Unfortunately, the same combination of wires we used for the temperature sensor were not working for the SiPMs. The noise visible on the scope was of significant proportions and completely overshadowed the signal from the light sensor. Making even the dark count, chapter 2.5, not visible, see Figure 4-3. We think the peaks not following the periodicity of the input are signals from the light sensor but with this noise it is incomparable with the signals from the manual, Figure 2-16. Meticulosity following the current by plugin and unplugging different parts of the circuit we found that the problem was in the cabling.

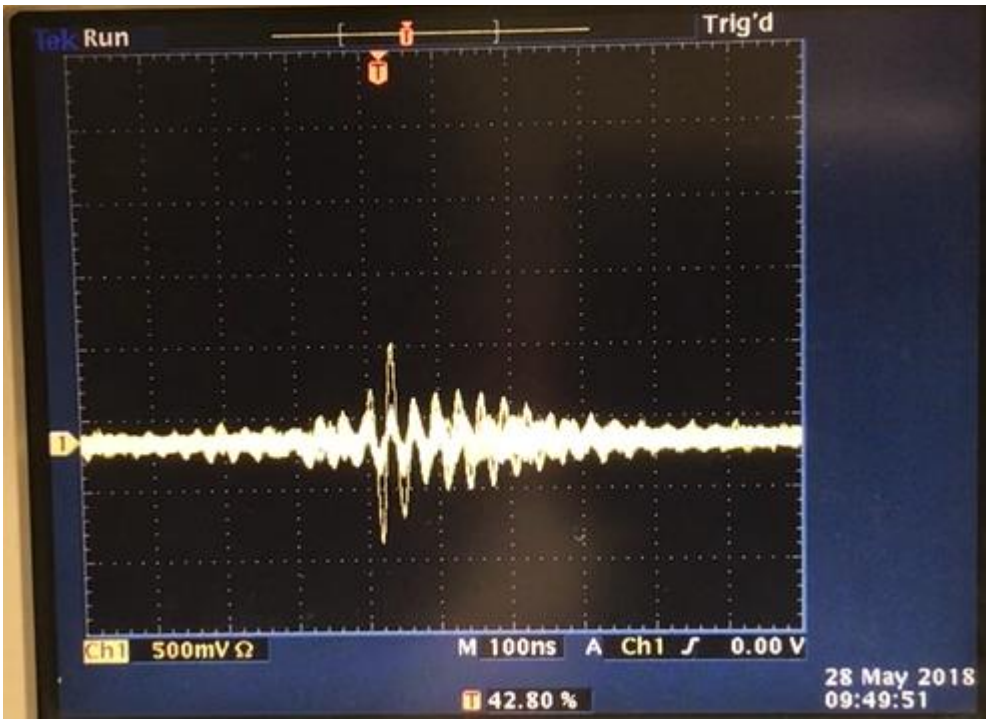

Figure 4-3: The signal from the SiPM. The noise on the signal is significant enough that we cannot make out the difference between noise and signal.

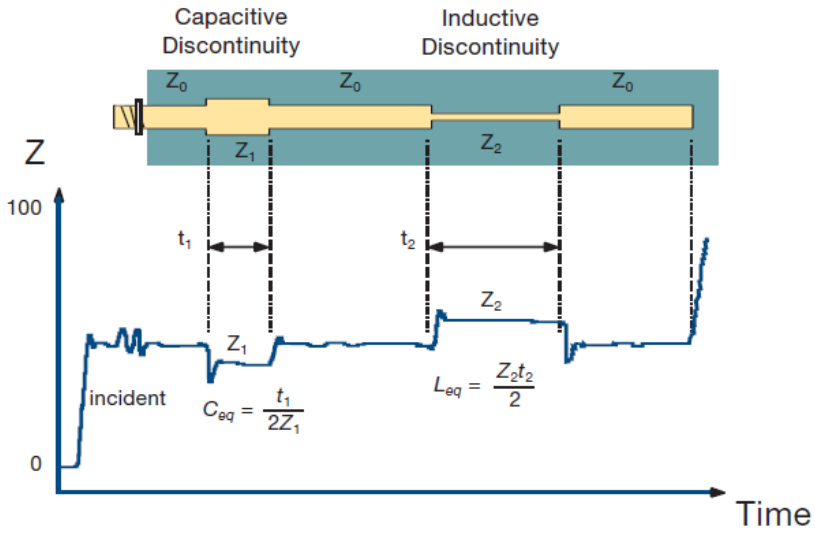

Figure 4-4: A schematic representation of a TDR measurement [48].

We therefore decided to perform Time Domain Reflectometer (TDR) measurement to find if any of our cable problems could be caused by impedance mismatch, see Figure 4-4 for a schematic representation of a TDR measurement. In the test setup we had been working with prefabricated lab cables rated at $50\ [\Omega]$ impedance, but now we were using our own made cables. In this TDR measurement we connect our fabricated cables to a cable which has been rated at $50\ [\Omega]$ and see if the connection will create any reflections at the connection point.

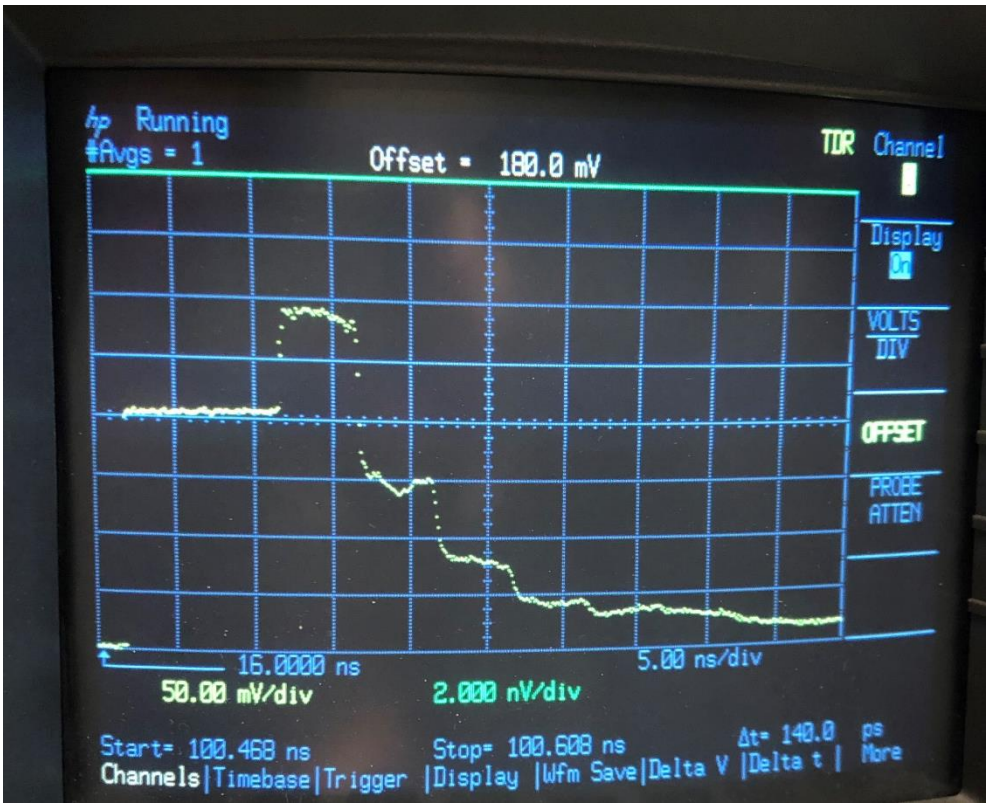

Figure 4-5: the TDR measurement of the grey and white SiPM cable for outside the vacuum seen in Figure 3-25 left. The first section of the plot shows the behaviour from the standardized lab cable at $50\ [\Omega]$*. Halfway in the third division from the left the graph jumps up meaning there is a reflection and therefore an impedance mismatch.*

The measurement of the grey and white SiPM cable from Figure 3-25 left can be seen in Figure 4-5. And it is clearly visible that there is an impedance mismatch between the two cables by the jump seen in division column three. The mismatch of this cable is of such a significance we cannot use this cable in a system designed around $50\ [\Omega]$.

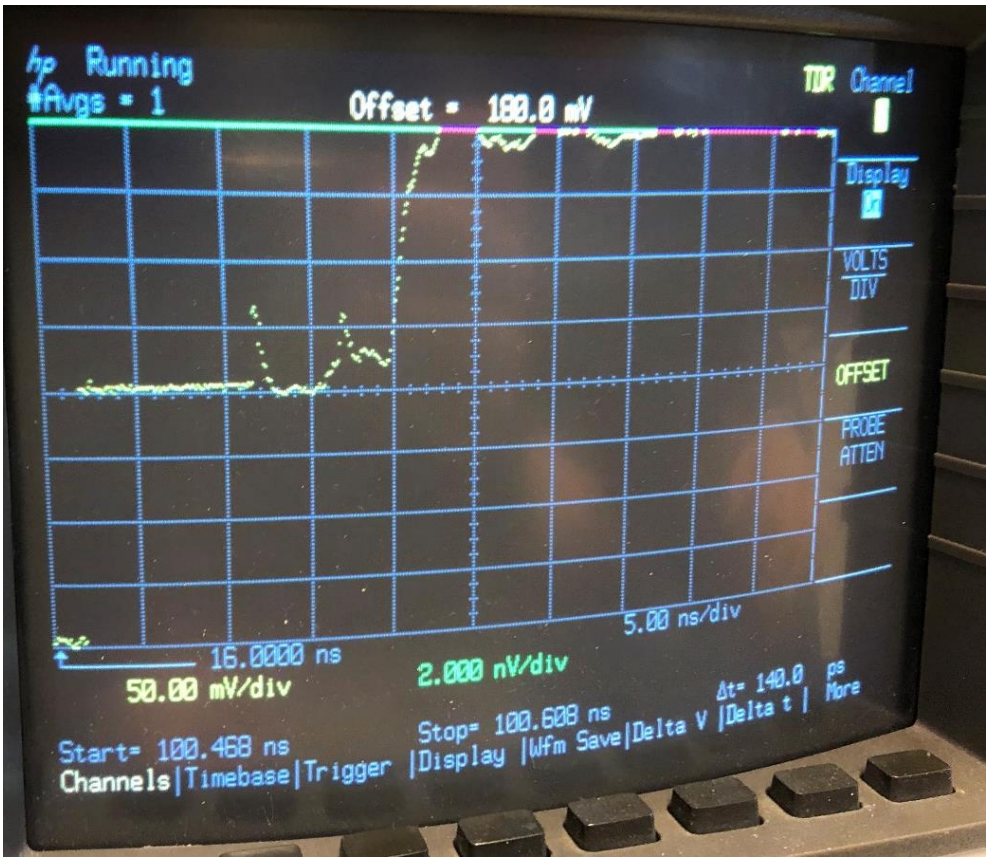

Figure 4-6: TDR measurement of the Kapton wire for inside the vacuum seen in Figure 3-25 right. Some peaks caused by a mismatch are visible but most of the cable is trying to follow the $50\ [\Omega]$ *impedance.*

In Figure 4-6 we see the TDR measurement of the Kapton wire shown in Figure 3-25 right. There is a clear difference in the behaviour of the cables shown in Figure 4-5 and Figure 4-6. The Kapton cable in the latter image tries to stay close to the $50\ [\Omega]$ line with a few peaks as an exception. The Kapton cable was made into a twisted wire pair and the peaks visible in the TDR measurement correspond to locations where the wire twisting was bad. Pressing the two cables together removed the peaks to a level where it was safe to rate the cable $50\ [\Omega]$.

These two TDR measurements made us decide to use the Kapton wire on both the in- and outside of the sample chamber for the SiPMs. That way we know for sure there in no impedance mismatch in the system and all the parts and cables in the system work on the $50\ [\Omega]$ impedance.

Fixing the impedances unfortunately did not fix all the noise problems. Having so much electrical components connected to the same wall socket. We therefore decided to let the oscilloscope perform a Fast Fourier Transform (FFT) on the signal coming back from the SiPM, see Figure 4-7 for FFT results.

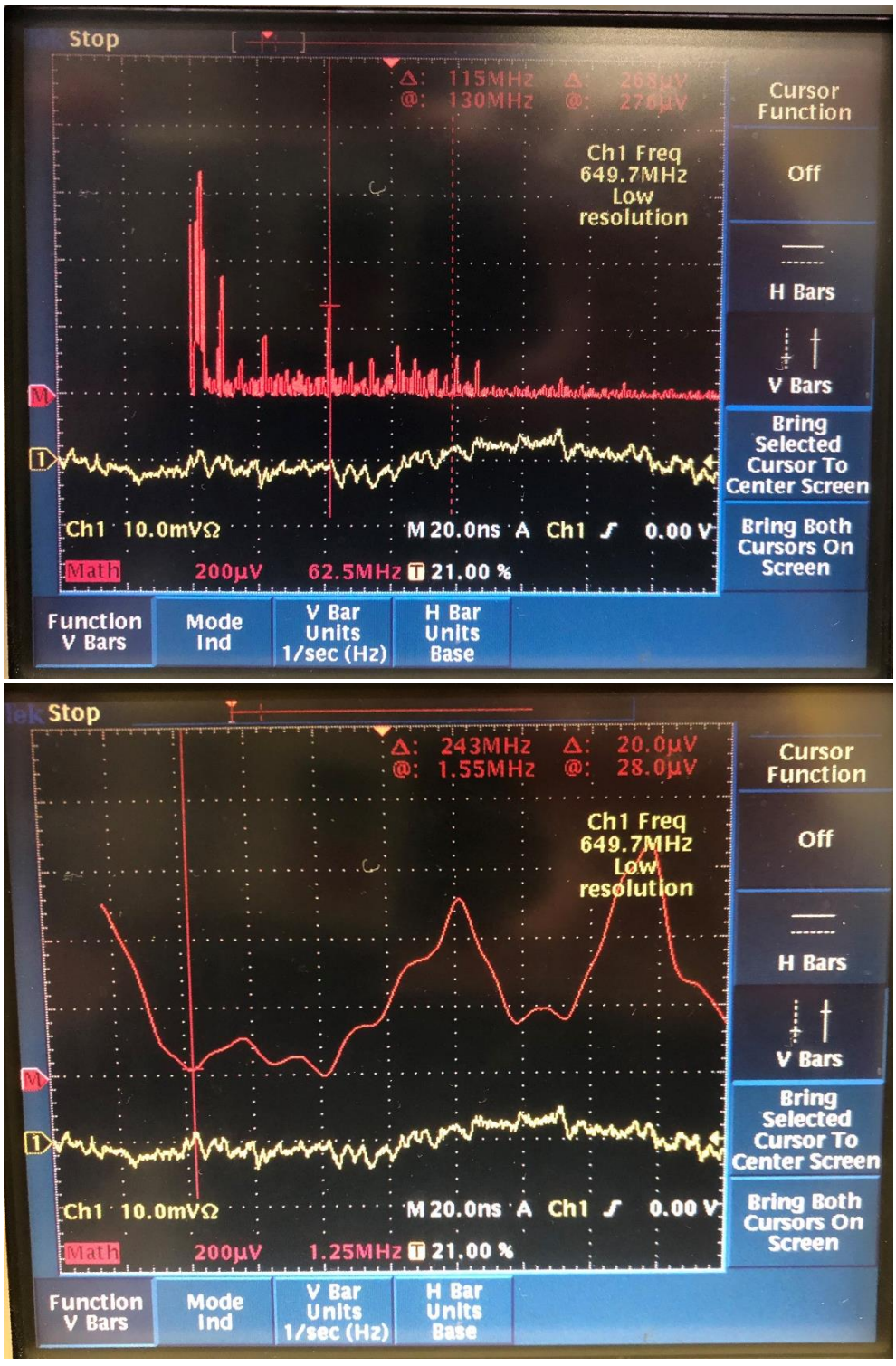

Figure 4-7: The FFT analyses, top being original zoom, bottom being zoomed in on the lower frequencies. The FFT of the signal (red) showing us which frequencies are most common. The original signal (yellow) is visible in a triggered snap.

From the FFT analyses we see that the most prominent frequencies are, $< 1.45\,[\mathrm{MHz}]$, $6.38\,[\mathrm{MHz}]$, $10\,[\mathrm{MHz}]$, $13.6\,[\mathrm{MHz}]$, $30\,[\mathrm{MHz}]$, $70\,[\mathrm{MHz}]$, and $130\,[\mathrm{MHz}]$. The frequencies below $1.45\,[\mathrm{MHz}]$ are most likely the ones from the other machines but should not cause the signal to be undistinguishable. We could not find a connection between a specific piece of equipment and one of these frequencies. We therefore looked at a Ferrite bead for the higher frequencies. A Ferrite bead is a ring designed to be an electromagnetic interference suppressor at high frequencies. We borrowed on of the rings from the XAMS lab used to reduce the noise on the same SiPMs in their experiment [49]. We also borrowed a ring from the R&D lab where our experiment is located. This way we have two rings specific for noise specific for our location in the building, we did not make any calculations and just tried these rings to see if they would make any difference.

With the Ferrite beads, the wires all selected on the correct impedance and all noise generating equipment isolated on a different wall socket we managed to get a signal from the SiPM in the dark box test setup. In Figure 4-8 we see the signal shape as we expect from the manual. it is safe to assume that with the frequency the small peaks appear, those will be the dark count 1 pe signals. This also means that the larger peak in the middle means the SiPM is detecting a lot of photons, and our dark box is not light tight.

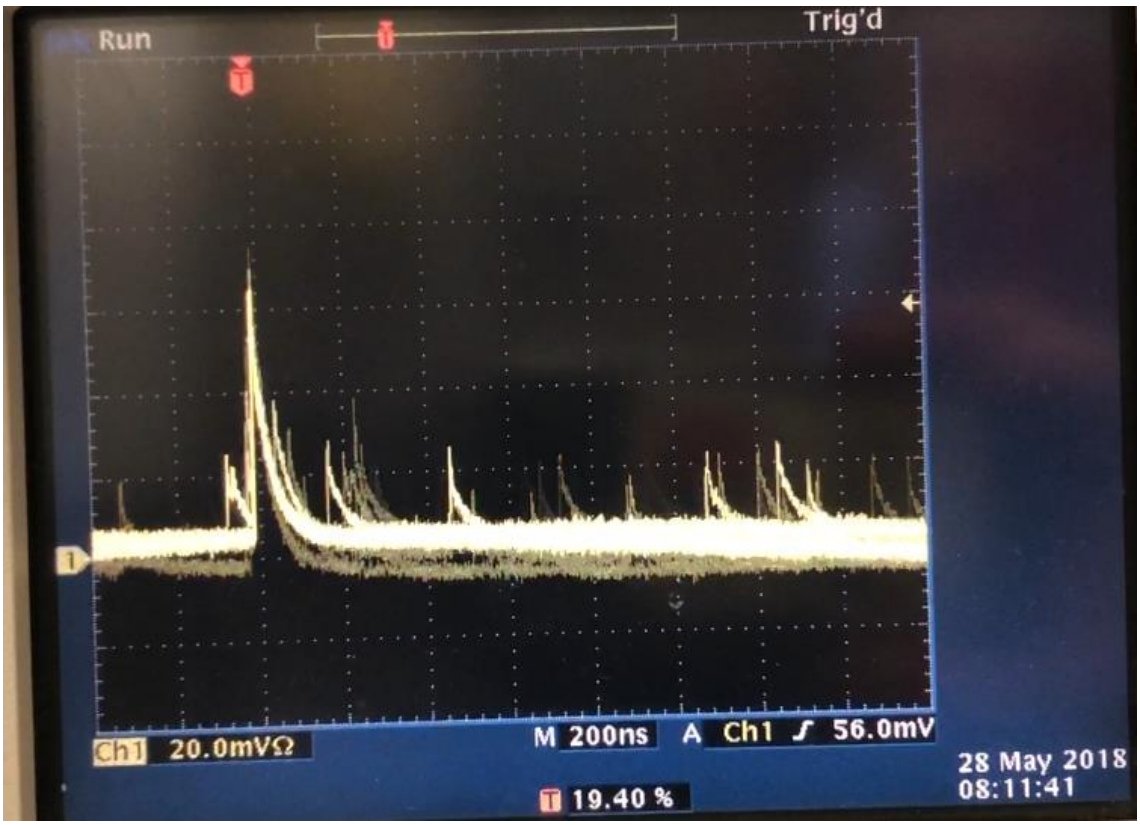

Figure 4-8: The signal from the SiPM as expected. Lots of dark count 1 pe signals and a larger 3 pe signal which indicates the SiPM is detecting a lot of photons.

Unfortunately, I was not able to recreate this signal within our experimental setup. There is a source of noise or a faulty cable which I did not manage to find in the time I had.

4.3 Controllers and Data acquisition

As mentioned in section 3.6 we looked at the TUM experimental setup to design our wavelength motor control. After which we also decided to do as much data acquisition as possible using the same system. In the design of the motor control and data acquisition I was helped a lot by other members of the VUV group, mainly with programming.

The wavelength motor control is handled by an Arduino Nano, when the data acquisition for a certain characterization measurement is finished, the Raspberry Pi will send a target wavelength. With that signal the Arduino knows it can change to that wavelength and the data collection can start again. That way we have a setup which can do an array of characterization measurement at different wavelengths without a controller present.

It starts with figuring out the motor, how does it work, what do we need and how can we prevent this motor from breaking any of the delicate parts in the monochromator. We have a connector on the back, but the manual does not describe pin functions, see Figure 4-10. So, we investigate the information we did have from the manual together with tracing cables. Using the continuity function on a multimeter we found the wiring for the limit switches. The limit switch could now be implemented into the system as safety precautions to shut the system down when the motor would turn the system to wavelengths it was not made for. The cabling for the light sensor was not investigated any further due to time and no need for an automatic reset, we always want an operator present when the system needs to be reset.

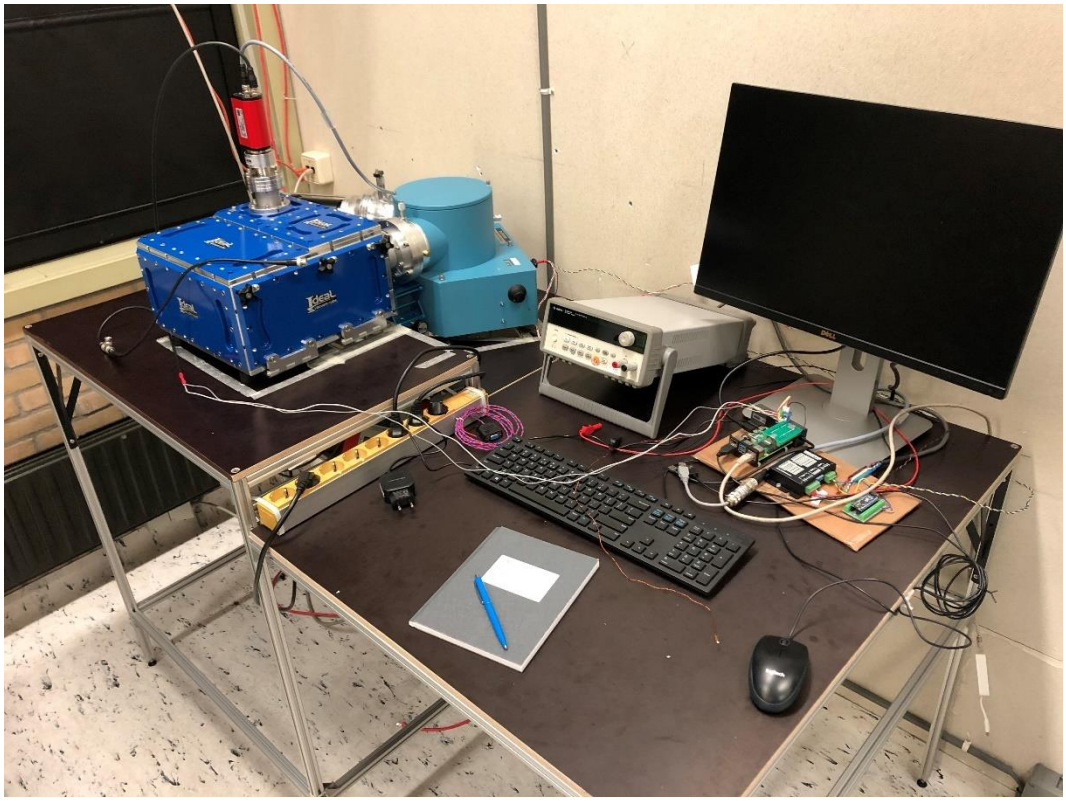

Figure 4-9: The fully installed data acquisition system, except for the SiPMs.

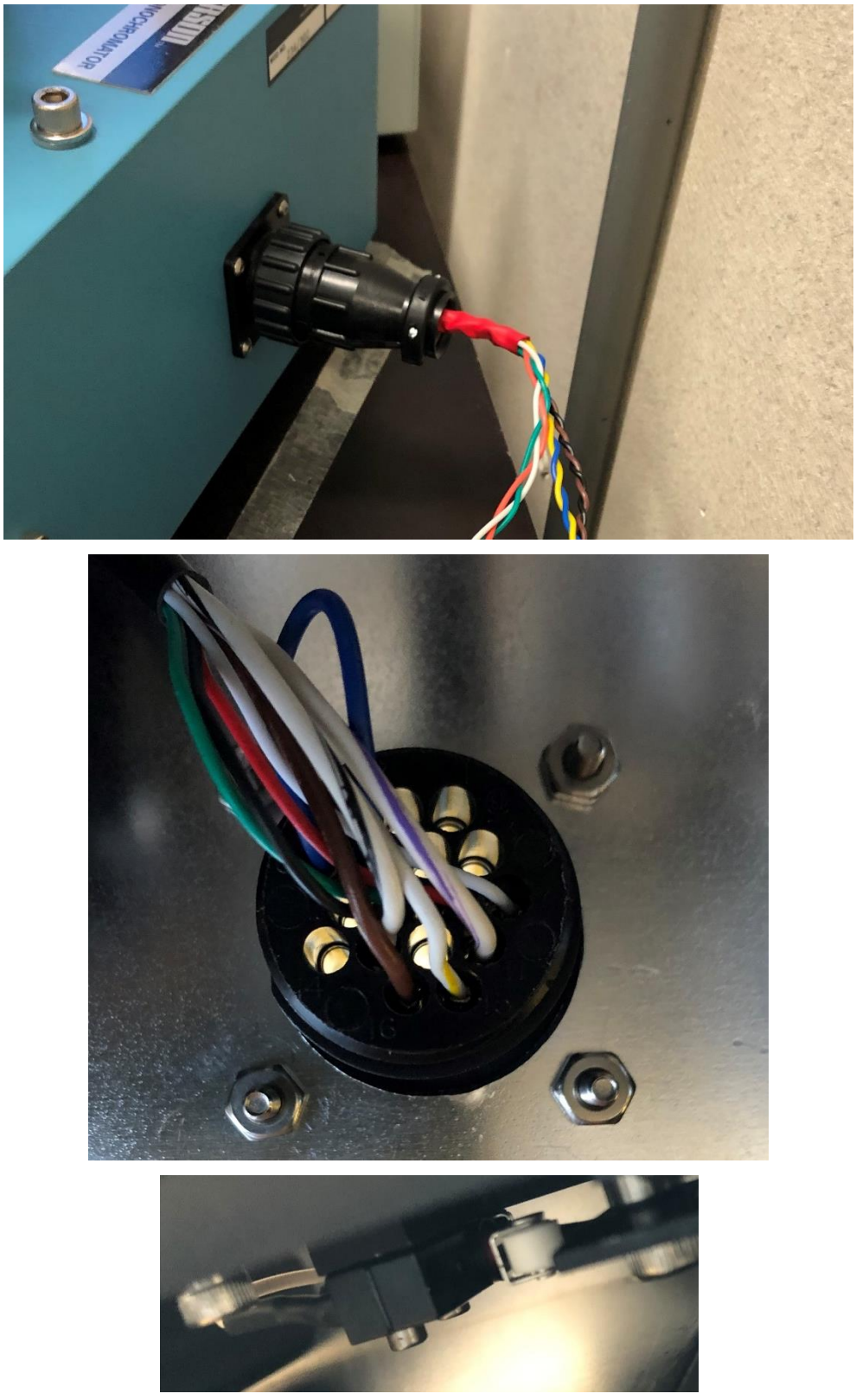

Figure 4-10: Output connector for the McPherson monochromator, connecting to limit switches and a light sensor to reset the wavelength. Top is the outside connector which we made to connect the limit switches to the Arduino. Middle is the inside view of the connector where the search started. Bottom is a picture of a limit switch where we had to use a camera to see the colours.

The next step was connecting the wires from the motor to the motor driver, according to the wiring schematic from the motor manual. Using the motor controller program from the TUM project together with the motor driver we managed to get the motor running. The motor can control the wavelength up to one Ångström, which is more accurate than we need. The limit switches have been tested so, when no operator is present the system will stop before it breaks. The motor control part is working as was required and designed.

For the data acquisition we needed all the signals to be read by the Raspberry Pi. For the pressure this was easy using the factory-made cabling to USB. The received value had to be converted according to a conversion given by Pfeiffer and the pressure data was added to the program to be stored. For the temperature we needed an ADC unit, section 3.6, which would convert the voltage to a digital signal for the Raspberry Pi. Testing the temperature sensor with the standardized PT100 conversion table made us able to measure $0\,℃$ on a little block of ice. We did not have a $100\,℃$ source and could therefore not test a second known temperature. The temperature measurement was added to the data acquisition code.

As we were working on the sensors and their cabling, we noticed the Arduino we planned for data acquisition of the SiPMs was not sufficiently fast. The amount of dark count signals from the SiPM is $1 \cdot 10^6$ counts per second. The width of the signal will be $20\,[\mathrm{ns}]$ and the timing between different signals is unknown. We know the Arduino has a pin check speed of 10000 times per second and a clock speed of $16\,[\mathrm{MHz}]$. Extra electronics, which is fast enough to register peaks and only send the peaks we are interested in, to the Raspberry Pi is needed. Due to time, I was not able to buy or build this and therefore I was not able to finish the data acquisition of the SiPMs. The code for the motor control and data acquisition will be accessible in a GitHub repository.

5 Discussion

We set the goal of designing an optical characterization experiment in the VUV region. The results indicate that most of the design follows the specifications required for a working optical characterization experiment. We did not want to reinvent the wheel and therefore used all the good design aspects of previously done experiments at NIKHEF and TUM. The final design will show we have made significant alterations to comply better with the requirements and specifications. The results provide new insight into the workings of these optical characterization experiments but considering some of the commissioning was not done more investigation is needed to fully understand this setup. That also concerns some of the designing which was done for reasons beyond the scope of this study.

Using the prefabricated vacuum components because we needed to have a vacuum of at least $1 \cdot 10^{-5}[\mathrm{mbar}]$ in a short amount of time being modular, showed to be a good decision. With the combination of parts chosen, we were able to reach a maximal vacuum of $7.9 \cdot 10^{-5}\ [\mathrm{mbar}]$. The data suggests that we will be able to reach the minimal requirement for our vacuum. However, this still needs additional investigation, because the vacuum goal was not reached in the most basic configuration of the setup. And the specifications indicate the pump can reach a vacuum of $1 \cdot 10^{-7}\ [\mathrm{mbar}]$ in a $10\ [\mathrm{L}]$ chamber in $557\ [\mathrm{s}]$. The pressure we reached in the time we did suggest there is still a significant leak present. Even though the tests provide insight into the quality of the current vacuum it does not contribute to the solution. The quality of the vacuum is therefore mostly limited by the time available for leak testing. Further research is needed to establish the quality of the different vacuum seals to improve the vacuum.

The data acquisition and control electronics have been mostly based on research done by projects at the TUM. Our study demonstrates that control electronics can be reproduced from the TUM experiment, the precision of the control system was beyond the scope of this research. With the control setup we can control the monochromator to its designed accuracy of $0.1\ [\mathrm{nm}]$. We decided to only automate the wavelength selection, this leaves further automation for future projects to investigate. The system in not tested and commissioned. So, to make sure the wavelength indicated by the monochromator is the wavelength at the sample, further test and investigation is needed.

The final design of the light sensor holder met all the requirements. However, some design choses have been made for reasons other than going for the most optimal light sensor holder. The design provides an insight into the importance of being in close contact with the workshop. Due to this contact the design was altered to the materials in stock, as well as keeping the shapes of the light sensor holder as original as possible to reduces fabrication time. This reduced the limitation of time for the commissioning of the actual light sensor. I would suggest more investigation into what the light sensor holder design requires is needed for better results.

The light sensor itself (SiPM) was connected to the system using knowledge from the XAMS experiment. The results show that following their wiring diagram will result in readable signals. However, the signals cannot be registered by the Arduino or Raspberry Pi. The data contributes a clearer understanding of this incompatibility. Due to the too superficial investigation into the speed of the electronics we were planning to use for the data acquisition, we cannot confirm the SiPM will work in the experimental setup as planned. The results do provide a new insight into what is needed for the light sensor to communicate with the electronics. For further research on this system, I advise an electronic circuit called a peak detector. This circuit will only send out a

signal when a certain peak threshold is reached. A solution for peaks quickly recuring after one another needs to be researched still.

The sample holder design was based of previously done research at NIKHEF. Making the needed adjustments to the design resulted in a sample holder as per requirements. In the process of designing, we found a lot of challenges in screw sizes and overall size of the holder. The only restriction that was created by this design, was the restriction of the sample size. We could not investigate the thermal behaviour of the copper, because this is beyond the scope of this research. But I think that investigating the thermal behaviour could give some interesting insights, also concerning the size of the sample holder. Because of the operating temperature of the feedthroughs and pressure sensor. We use springs to clamp samples in the sample holder. We could not test the concept of this clamping other than a quick fit test. I therefore advise to investigate this method of securing the sample further. To see if the idea is feasible and how much force is needed to clamp a sample.

The final assembly of the VUV setup show that the different prefabricated part work together. And in the experiment any changes and alterations to these parts were limited by the imagination. This resulted in very creative solutions for problems we did not foresee with prefabricated parts.

6 Conclusion

This research aimed to design, commission and build an experimental setup for measuring the optical properties of detector materials. The VUV experiment is aimed at the region of scintillation light produced by liquid xenon, $178\ [\mathrm{nm}]$. The information on these properties helps the larger dark matter liquid xenon experiments to improve. The most important restriction will be the VUV region in which the measurements have to take place. In the process of designing the different parts of the experiment it was most important to keep thinking outside the box and not follow the designs already available.

Analyses of digital CAD drawing of the design helped us investigate the different aspects important to the design. This resulted in a sample chamber reaching a vacuum of $7.9 \cdot 10^{-5}\ [\mathrm{mbar}]$, this is not good enough for performing an optical characterization measurement but will be good enough for testing and commissioning the SiPMs in the VUV region. Based on these conclusions, future project members should leak test the setup using a helium leak tester.

The controller to semi-automate the experimental setup works as designed and required. It can control the wavelength of the monochromator at the level of accuracy of the monochromator $0.1\ [\mathrm{nm}]$. We did decide not to use the position sensor inside the monochromator enabling the same starting point whenever a characterization measurement is started.

The final design of the sample holder was designed with very few requirements, but other aspects of the setup became restrictions. The beam of light resulted to be the biggest design restriction on the sample holder. Also, the limit size of the vacuum chamber and the location of the feedthroughs would limit the sample holder more than the initial requirements. Analysing the beam inside the sample chamber resulted in the dimensions of the sample holder. The method of clamping the sample is tested at room temperature and works as required. Further investigation into this clamping method at lower temperatures is needed.

The final design for the light sensor holder was based on readily available parts in the workshop. This together with the time constrained the project was on for commissioning the light sensors, resulted in a working bare bone design. For future projects I would advise more investigation in the requirements of the light sensor holder. There will be a lot to gain concerning materials and size. The light sensor holder was used for testing the sensors within the sample chamber.

We worked on commissioning the SiPM light sensors. Using previously done research by the XAMS experiment at NIKHEF. Using the electronics from XAMS we managed to perform a test on the SiPM and investigating the characteristics of the signal in our electronic system. With the knowledge of the shape and timing of the signal, we worked on the acquisition of the signals. The result of this little test is that the electronics used in the VUV experiment are not fast enough to handle the signals from the SiPM at $1 \cdot 10^6$ counts per second and a signal width of $20\ [\mathrm{ns}]$. For future research it will be an interesting investigation what electronics will be needed to make the SiPM compatible with the data acquisition electronics of the VUV experiment.

Appendices

Appendix A. Design of the sensor holder

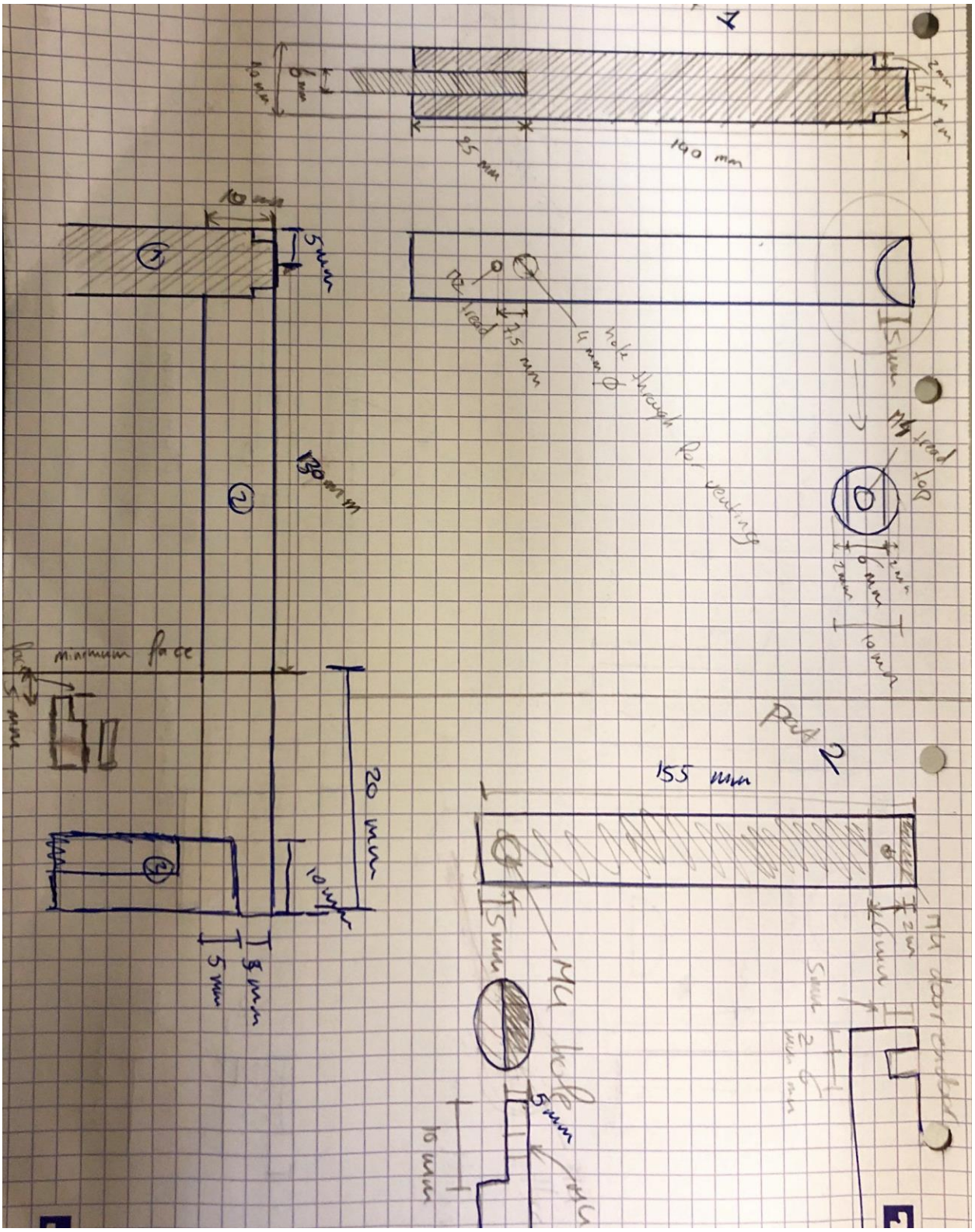

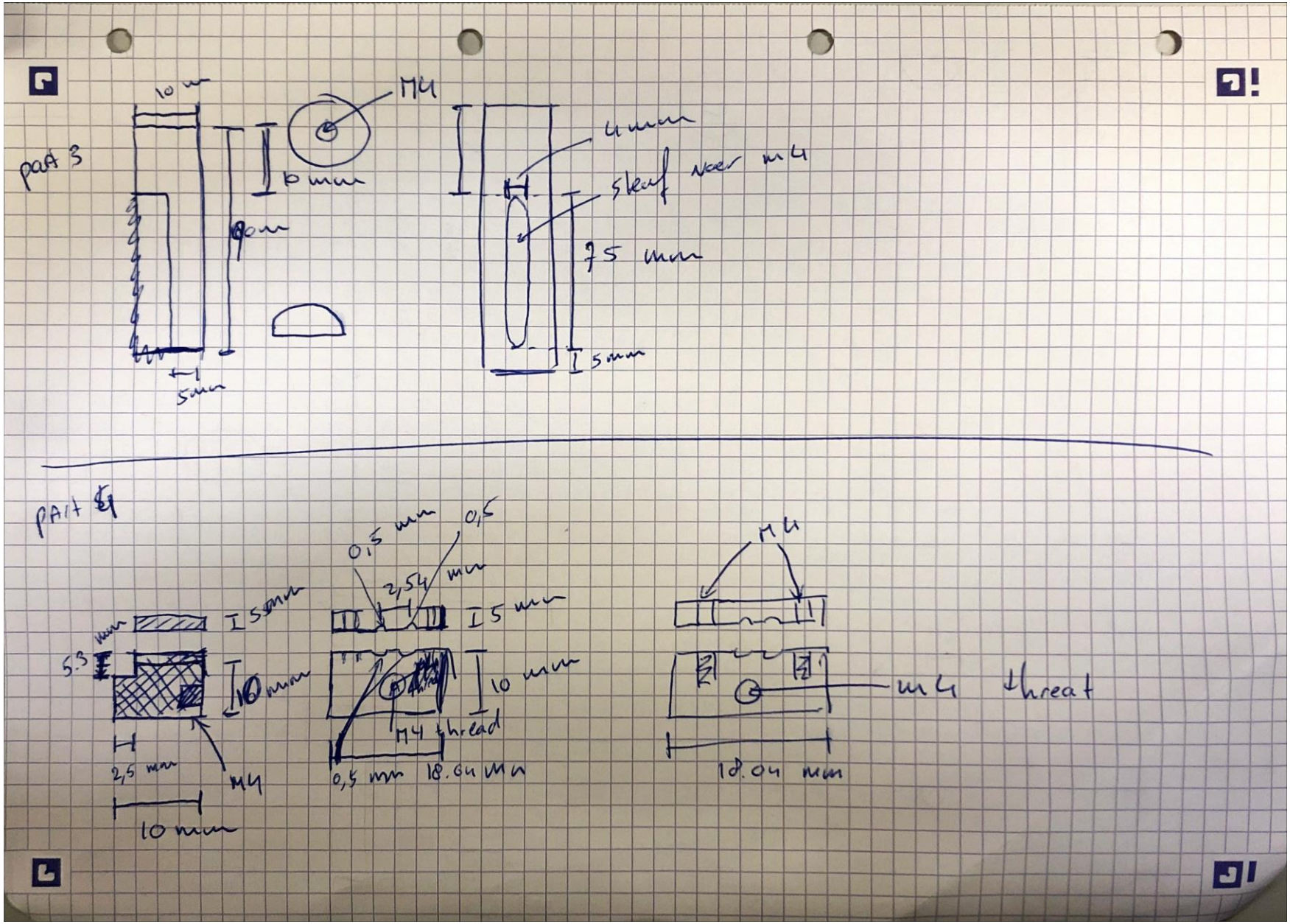
part 3
10 mm
M4
5 mm
4 mm
sleef near M4
75 mm
5 mm
part 4
5 mm
5.5 mm
10 mm
2,5 mm
M4
10 mm
0,5 mm
0,5
2,54 mm
5 mm
10 mm
M4 thread
0,5 mm
18.04 mm
M4
M4 threat
10.04 mm

Appendix B. Beam width measurements

Table 2: Measurements of the size of the beam inside the sample chamber.

Measurements Entrance 3.05(mm) Exit 1.65 (mm)			
Distance (mm)	Measurer	Horizontal (mm)	Vertical (mm)
103 ± 1	Casimir	6.8 ± 0.2	9.1 ± 0.2
	Emily	7.7 ± 0.2	9.5 ± 0.2
	Marjolein	7.7 ± 0.2	9.5 ± 0.2
	Average	**7.4 ± 0.2**	**9.4 ± 0.2**
126 ± 1	Casimir	7.5 ± 0.2	9.9 ± 0.2
	Emily	6.9 ± 0.2	10.4 ± 0.2
	Marjolein	6.5 ± 0.2	12.1 ± 0.2
	Average	**7.0 ± 0.2**	**10.9 ± 0.2**
162 ± 1	Casimir	7.0 ± 0.2	12.3 ± 0.2
	Emily	8.9 ± 0.2	12.7 ± 0.2
	Marjolein	8.1 ± 0.2	12.0 ± 0.2
	Average	**8.0 ± 0.2**	**12.3 ± 0.2**
175 ± 1	Casimir	9.1 ± 0.2	11.4 ± 0.2
	Emily	8.8 ± 0.2	11.7 ± 0.2
	Marjolein	6.8 ± 0.2	13.7 ± 0.2
	Average	**8.2 ± 0.2**	**12.3 ± 0.2**
232 ± 1	Casimir	10.9 ± 0.2	18.0 ± 0.2
	Emily	10.6 ± 0.2	15.9 ± 0.2
	Marjolein	13.7 ± 0.2	14.9 ± 0.2
	Average	**11.7 ± 0.2**	**16.3 ± 0.2**
251 ± 1	Casimir	10.8 ± 0.2	18.2 ± 0.2
	Emily	11.6 ± 0.2	15.2 ± 0.2
	Marjolein	12.8 ± 0.2	16.6 ± 0.2
	Average	**11.7 ± 0.2**	**16.7 ± 0.2**

Appendix C. Technical drawing sample holder

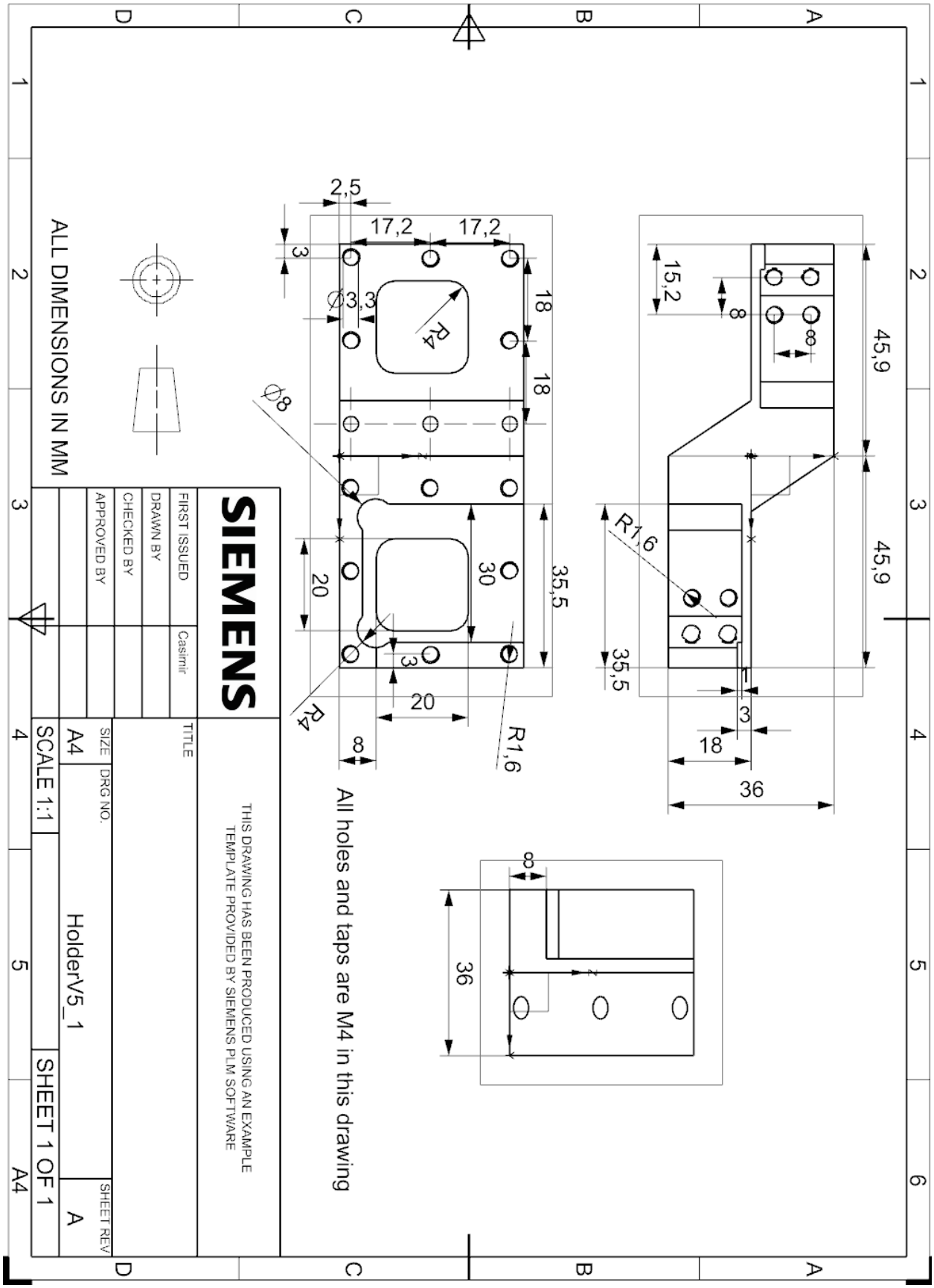

Bibliography

[1] F. Zwicky, “Die Rotverschiebung von extragalaktischen Nebeln,” *Helv. Phys. Acta*, vol. 6, pp. 110–127, 1933.

[2] G. Bertone and D. Hooper, “History of dark matter,” *Rev. Mod. Phys.*, vol. 90, no. 4, pp. 1–88, 2018.

[3] “Gravitational lensing of distant star-forming galaxies (schematic).” [Online]. Available: https://www.eso.org/public/images/eso1313b/. [Accessed: 07-Mar-2022].

[4] “The Bullet Cluster.” [Online]. Available: https://www.esa.int/ESA_Multimedia/Images/2007/07/The_Bullet_Cluster2. [Accessed: 07-Mar-2022].

[5] D. Clowe, A. Gonzalez, and M. Markevitch, “Weak-Lensing Mass Reconstruction of the Interacting Cluster 1E 0657−558: Direct Evidence for the Existence of Dark Matter,” *Astrophys. J.*, vol. 604, no. 2, pp. 596–603, 2004.

[6] “Planck and the cosmic microwave background.” [Online]. Available: https://www.esa.int/Science_Exploration/Space_Science/Planck/Planck_and_the_cosmic_microwave_background.

[7] G. Bertone, D. Hooper, and J. Silk, “Particle dark matter: Evidence, candidates and constraints,” *Phys. Rep.*, vol. 405, no. 5–6, pp. 279–390, 2005.

[8] T. M. Undagoitia and L. Rauch, “Dark matter direct-detection experiments,” *J. Phys. G Nucl. Part. Phys.*, vol. 43, no. 1, 2015.

[9] C. W. Walter, “The super-kamiokande experiment,” *Neutrino Oscil. Present Status Futur. Plans*, pp. 19–43, 2008.

[10] E. Andres, “The AMANDA Neutrino Telescope: Principle of Operation and First Results,” vol. 97, pp. 1–36, 1999.

[11] M. Aguilar *et al.*, “The Alpha Magnetic Spectrometer (AMS) on the International Space Station: Part I - results from the test flight on the space shuttle,” *Phys. Rep.*, vol. 366, p. 331, 2002.

[12] M. de Naurois, “Status and current sensitivity of the CELESTE experiment,” pp. 540–543, 2003.

[13] M. Casolino and N. De Simone, “The pamela cosmic ray space observatory: Detector, objectives and first results,” *Frascati Phys. Ser.*, vol. 47, no. SPEC. ISS., pp. 19–48, 2008.

[14] J. D. Lewin and R. F. Smith, “Review of mathematics, numerical factors, and corrections for dark matter experiments based on elastic nuclear recoil,” vol. 6, no. 96, pp. 87–112, 1996.

[15] M. Schumann, “Direct detection of WIMP dark matter: Concepts and status,” *J. Phys. G Nucl. Part. Phys.*, vol. 46, no. 10, 2019.

[16] J. Billard, E. Figueroa-Feliciano, and L. Strigari, “Implication of neutrino backgrounds on the reach of next generation dark matter direct detection experiments,” *Phys. Rev. D - Part. Fields, Gravit. Cosmol.*, vol. 89, no. 2, 2014.

[17] C. Savage, G. Gelmini, P. Gondolo, and K. Freese, “Compatibility of DAMA/LIBRA dark matter detection with other searches,” *J. Cosmol. Astropart. Phys.*, vol. 2009, no. 4, pp. 1–45, 2009.

[18] “International Atomic Energy Agency (IAEA) Nuclear Data Services. Livechart - Table of Nuclides - Nuclear structure and decay data.” [Online]. Available: https://nds.iaea.org/relnsd/vcharthtml/VChartHTML.html. [Accessed: 25-Mar-2022].

[19] E. Aprile and T. Doke, “Liquid xenon detectors for particle physics and astrophysics,” *Rev. Mod. Phys.*, vol. 82, no. 3, pp. 2053–2097, 2010.

[20] C. Thorn, “Catalogue of liquid argon properties.” [Online]. Available: http://microboone-docdb.fnal.gov:8080/cgi-bin/ShowDocument?docid=412. [Accessed: 25-Mar-2022].

[21] D. S. Akerib *et al.*, “Tritium calibration of the LUX dark matter experiment,” *Phys. Rev. D*, vol. 93, no. 7, 2016.

[22] Y. Meng *et al.*, “Dark Matter Search Results from the PandaX-4T Commissioning Run,” *Phys. Rev. Lett.*, vol. 127, no. 26, pp. 1–11, 2021.

[23] D. S. Akerib *et al.*, “The Large Underground Xenon (LUX) experiment,” *Nucl. Instruments Methods Phys. Res. Sect. A Accel. Spectrometers, Detect. Assoc. Equip.*, vol. 704, pp. 111–126, 2013.

[24] D. Y. Akimov *et al.*, “The ZEPLIN-III dark matter detector: Instrument design, manufacture and commissioning,” *Astropart. Phys.*, vol. 27, no. 1, pp. 46–60, 2007.

[25] E. Aprile *et al.*, “Projected WIMP sensitivity of the XENONnT dark matter experiment,” *J. Cosmol. Astropart. Phys.*, vol. 2020, no. 11, 2020.

[26] P. Di Gangi, “The xenon road to direct detection of dark matter at lngs: The xenon project,” *Universe*, vol. 7, no. 8, 2021.

[27] “Hamamatsu L11798 specifications, Doc. Ref. TLSZ1014E06.”

[28] “McPHERSON 200mm f.l. Vacuum Monochromator 234/302.” [Online]. Available: https://www.mcphersoninc.com/pdf/234302.pdf. [Accessed: 31-Jul-2022].

[29] “McPHERSON 234/302 user manual.”

[30] “Ideal vacuum Cube user manual, Doc. Ref. IdealCUBE-6x121416.”

[31] “Pfeiffer vacuum HiCube Eco, Doc. Ref. pt0553BEN.”

[32] “Pfeiffer vacuum MPT 200 AR, Doc. Ref. PTR40141.”

[33] “Heraeus 1Pt100 KN1510 datasheet,Doc. Ref. 20003959235.”

[34] “TE PTF Pt100 datasheet, Doc. Ref. A3-775357.”

[35] “Hamamatsu photonics VUV-MPPC datasheet, Doc. Ref. KSX-I50133-E_VUV-MPPC_b.”

[36] “characterizations Id (Diode Current) - Vd (Diode Voltage) IN4728A.” [Online]. Available: https://electronics.stackexchange.com/questions/392997/characterizations-id-diode-current-vd-diode-voltage-in4728a. [Accessed: 17-Mar-2022].

[37] “Hamamatsu photonics MPPC Technical note, Doc. Ref. KAPD9008E01.”

[38] “Pfeiffer vacuum Magnetically Coupled Rotary Feedthrough, Doc. Ref. 420MRM016.”

[39] “Pfeiffer vacuum D-sub feedthrough, Doc. Ref. 120XSD040-9.”

[40] J. Van Der Borgh, “Designing the sample chamber for vacuum ultraviolet reflection measurements,” Universiteit van Amsterdam; Vrije Universiteit Amsterdam, 2021.

[41] A. Leonhardt, “Characterization of Wavelength Shifters for Rare-Event Search Experiments at Low Temperatures,” no. June, 2021.

[42] “Raspberry Pi model 4.” [Online]. Available: https://www.bitsandparts.nl/Raspberry-Pi-4-Model-B-4GB-WiFi-BT-p1885648. [Accessed: 24-Mar-2022].

[43] “Adrduino Nano 3.0.” [Online]. Available: https://www.bitsandparts.nl/Arduino-Nano-3.0-Atmega328-5V-16-MHz-(compatible-clone)-p122093. [Accessed: 24-Mar-2022].

[44] “MB 2H MICROSTEP.” [Online]. Available: https://www.reichelt.com/de/en/makeblock-me-2h-microstep-driver-v1-mb-2h-microstep-p202132.html. [Accessed: 24-Mar-2022].

[45] “Analog-to-Digital Converter.” [Online]. Available: https://www.kiwi-electronics.nl/nl/grove-4-channel-16-bit-adc-ads1115-w-programmable-amplifier-gain-10046?language=nl-nl&currency=EUR&gclid=CjwKCAjwhOyJBhA4EiwAEcJdcTfUpZkdXxZ-mLxQoDJyjJ7FhaKx7OEIrv7UBmOT53kx1qGrDlZj1xoCJeoQAvD_BwE. [Accessed: 24-Mar-2022].

[46] A. A. L. Villalpando, “Characterization of Silicon Photomultipliers for Event Position Reconstruction in a Dual-Phase Xenon Time Projection Chamber,” University of Amsterdam, Vrije Universiteit Amsterdam, 2019.

[47] “Mini Circuits, ZHL-32A+.” [Online]. Available: https://www.minicircuits.com/pdfs/ZHL-32A+.pdf. [Accessed: 25-Mar-2022].

[48] “How TDR impedance measurements work.” [Online]. Available: https://www.protoexpress.com/blog/tdr-impedance-measurements/. [Accessed: 27-Mar-2022].

[49] M. E. Flierman, “Calibration of SiPMs in a dual phase xenon TPC.”